USGS
science for a changing world

Prepared in cooperation with the National Park Service

Simulated Effects of Sea-Level Rise on the Shallow, Fresh Groundwater System of Assateague Island, Maryland and Virginia

Scientific Investigations Report 2020–5104

U.S. Department of the Interior
U.S. Geological Survey

Cover. Aerial view of Assateague Island, looking north. Ocean City, Maryland, is visible in the far distance at top. Photograph by Susanne Bledsoe, U.S. Army Corps of Engineers.

Simulated Effects of Sea-Level Rise on the Shallow, Fresh Groundwater System of Assateague Island, Maryland and Virginia

By Brandon J. Fleming, Jeff P. Raffensperger, Phillip J. Goodling, and John P. Masterson

Prepared in cooperation with the National Park Service

Scientific Investigations Report 2020–5104

U.S. Department of the Interior
U.S. Geological Survey

U.S. Geological Survey, Reston, Virginia: 2021

Suggested citation:
Fleming, B.J., Raffensperger, J.P., Goodling, P.J., and Masterson, J., 2021, Simulated effects of sea-level rise on the shallow, fresh groundwater system of Assateague Island, Maryland and Virginia: U.S. Geological Survey Scientific Investigations Report 2020–5104, 62 p., https://doi.org/10.3133/sir20205104.

Associated data for this publication:
Fleming, B.J., and Raffensperger, J.P., 2021, MODFLOW-NWT model with SWI2 used to evaluate the water-table response to sea-level rise and change in recharge, Assateague Island, Maryland and Virginia: U.S. Geological Survey data release, https://doi.org/10.5066/P9AJOLRK.

ISSN 2328-0328 (online)

Acknowledgments

The authors gratefully acknowledge support for this study provided by the National Park Service. Eric Sherry and Brian Sturgis of the National Park Service and Chris Lewis, Steve Curtin (retired), and Deb Bringman of the U.S. Geological Survey (USGS) are thanked for assistance with data collection and quality assurance. Chris Langevin, Glen Carleton, and Paul Misut (USGS) are thanked for technical discussions throughout the model development process, and Mark Nardi (USGS) is thanked for assisting with vegetation-based water-level observations used in model calibration.

Contents

Figures

Tables

Conversion Factors

International System of Units to Inch/Pound

Multiply	By	To obtain
	Length	
meter (m)	3.281	foot (ft)
kilometer (km)	0.6214	mile (mi)
meter (m)	1.094	yard (yd)
	Area	
square meter (m^2)	0.0002471	acre
square kilometer (km^2)	247.1	acre
square meter (m^2)	10.76	square foot (ft^2)
square kilometer (km^2)	0.3861	square mile (mi^2)
	Volume	
cubic meter (m^3)	264.2	gallon (gal)
cubic meter (m^3)	0.0002642	million gallons (Mgal)
cubic meter (m^3)	35.31	cubic foot (ft^3)
cubic meter (m^3)	1.308	cubic yard (yd^3)
cubic meter (m^3)	0.0008107	acre-foot (acre-ft)
	Hydraulic conductivity	
meter per day (m/d)	3.281	foot per day (ft/d)

U.S. customary units to International System of Units

Multiply	By	To obtain
	Length	
foot (ft)	0.3048	meter (m)
mile (mi)	1.609	kilometer (km)
yard (yd)	0.9144	meter (m)
	Area	
acre	4,047	square meter (m^2)
acre	0.004047	square kilometer (km^2)
square foot (ft^2)	0.09290	square meter (m^2)
square mile (mi^2)	2.590	square kilometer (km^2)
	Volume	
gallon (gal)	0.003785	cubic meter (m^3)
million gallons (Mgal)	3,785	cubic meter (m^3)
cubic foot (ft^3)	0.02832	cubic meter (m^3)
cubic yard (yd^3)	0.7646	cubic meter (m^3)
acre-foot (acre-ft)	1,233	cubic meter (m^3)
	Hydraulic conductivity	
foot per day (ft/d)	0.3048	meter per day (m/d)

Temperature in degrees Celsius (°C) may be converted to degrees Fahrenheit (°F) as follows: °F = (1.8 × °C) + 32.

Temperature in degrees Fahrenheit (°F) may be converted to degrees Celsius (°C) as follows: °C = (°F – 32) / 1.8.

Datum

Vertical coordinate information is referenced to North American Vertical Datum of 1988 (NAVD 88).

Horizontal coordinate information is referenced to the North American Datum of 1983 (NAD 83).

Altitude, as used in this report, refers to distance above the vertical datum.

Supplemental Information

Specific conductance is given in microsiemens per centimeter at 18 degrees Celsius (µS/cm at 18 °C).

Concentrations of chemical constituents in water are given in milligrams per liter (mg/L).

Abbreviations

asl	above sea level
bls	below land surface
css	composite scaled sensitivity
dss	dimensionless scaled sensitivity
ET	evapotranspiration
NOAA	National Oceanic and Atmospheric Administration
NPS	National Park Service
NWIS	National Water Information System
SC	specific conductance
SLR	sea-level rise
USGS	U.S. Geological Survey

Simulated Effects of Sea-Level Rise on the Shallow, Fresh Groundwater System of Assateague Island, Maryland and Virginia

By Brandon J. Fleming, Jeff P. Raffensperger, Phillip J. Goodling, and John P. Masterson

Abstract

The U.S. Geological Survey, in cooperation with the National Park Service, developed a three-dimensional groundwater-flow model for Assateague Island in eastern Maryland and Virginia to assess the effects of sea-level rise on the groundwater system. Sea-level rise is expected to increase the altitude of the water table in barrier island aquifer systems, possibly leading to adverse effects to ecosystems on the barrier islands. The potential effects of sea-level rise were evaluated by simulating groundwater conditions under sea-level-rise scenarios of 20 centimeters (cm), 40 cm, and 60 cm. Results show that as sea level rises, low-lying areas of the island originally represented as receiving freshwater recharge in the baseline scenario are inundated by saltwater. This change from freshwater recharge to saltwater decreases the overall amount of freshwater recharging the system. As the water table rises in response to the higher sea levels, freshwater flow out of the system changes, with more freshwater leaving as submarine groundwater discharge and less freshwater leaving as seeps and evapotranspiration. At the current land-surface altitude, as much as 50 percent of the island may be inundated with a 60-cm rise in sea level, and the low-lying marshes may change from freshwater to saltwater.

Groundwater levels at 32 wells were monitored for as long as 12 months between October 2014 and September 2015 on Assateague Island. Results from objective classification analysis of 14 shallow monitoring wells show two dominant processes affecting groundwater levels in two different settings on the island. On the western side of the island, between the primary dune and the inland bays, water levels clearly respond to precipitation events. This side of the island is more protected from ocean tides and typically is more vegetated than the eastern side. On the eastern side of the island, between the Atlantic Ocean and the primary dune, water levels clearly respond to tidal events. Specific conductance was measured at four wells, two on the western part of the island and two on the eastern part of the island. Specific conductance values in the two wells west of the primary dune show episodic decreases, coinciding with precipitation events. Specific conductance values in the two wells on the eastern side of the primary dune show episodic increases, coinciding with high-tide events. These high frequency monitoring data are intended to aid in designing a monitoring network that can document both short-term and long-term hydrologic processes on Assateague Island National Seashore.

This study uses a modeling approach consistent with models developed for Gateway National Recreation Area, Sandy Hook Unit (New Jersey) and Fire Island National Seashore (New York). Combined, these models are meant to improve the regional capabilities for predicting climate-change effects on barrier islands and provide resource managers with a common set of tools for adaptation and mitigation of potentially adverse effects of sea-level rise.

Introduction

Assateague Island is a barrier island complex on the Atlantic coast of Maryland and Virginia (fig. 1). Assateague Island National Seashore, managed by the National Park Service (NPS), was established in 1965 and covers most of Assateague Island within Maryland. The Maryland Department of Natural Resources manages a 3-kilometer (km) long area known as Assateague State Park. The Virginia section of the island is managed by the U.S. Fish and Wildlife Service as Chincoteague National Wildlife Refuge (Schupp, 2013). The island is surrounded by the Atlantic Ocean to the east and by Sinepuxent and Chincoteague Bays to the west. Assateague Island is characterized by low topographic relief with a mean altitude of about 2 meters (m) and maximum dune altitude of about 15 m above mean sea level (as defined by the North American Vertical Datum of 1988). The effect of climate change and sea-level rise on Assateague Island is expected to include changes in erosion rates, island morphology, marsh health, and groundwater flow.

The areas within Assateague Island that are considered to be most vulnerable to sea-level rise are those with the highest occurrence of overwash and the highest rates of shoreline change (Pendleton and others, 2004; Schupp, 2013). However, in addition to increased erosion and surface inundation from rising sea level, the groundwater-flow system can be

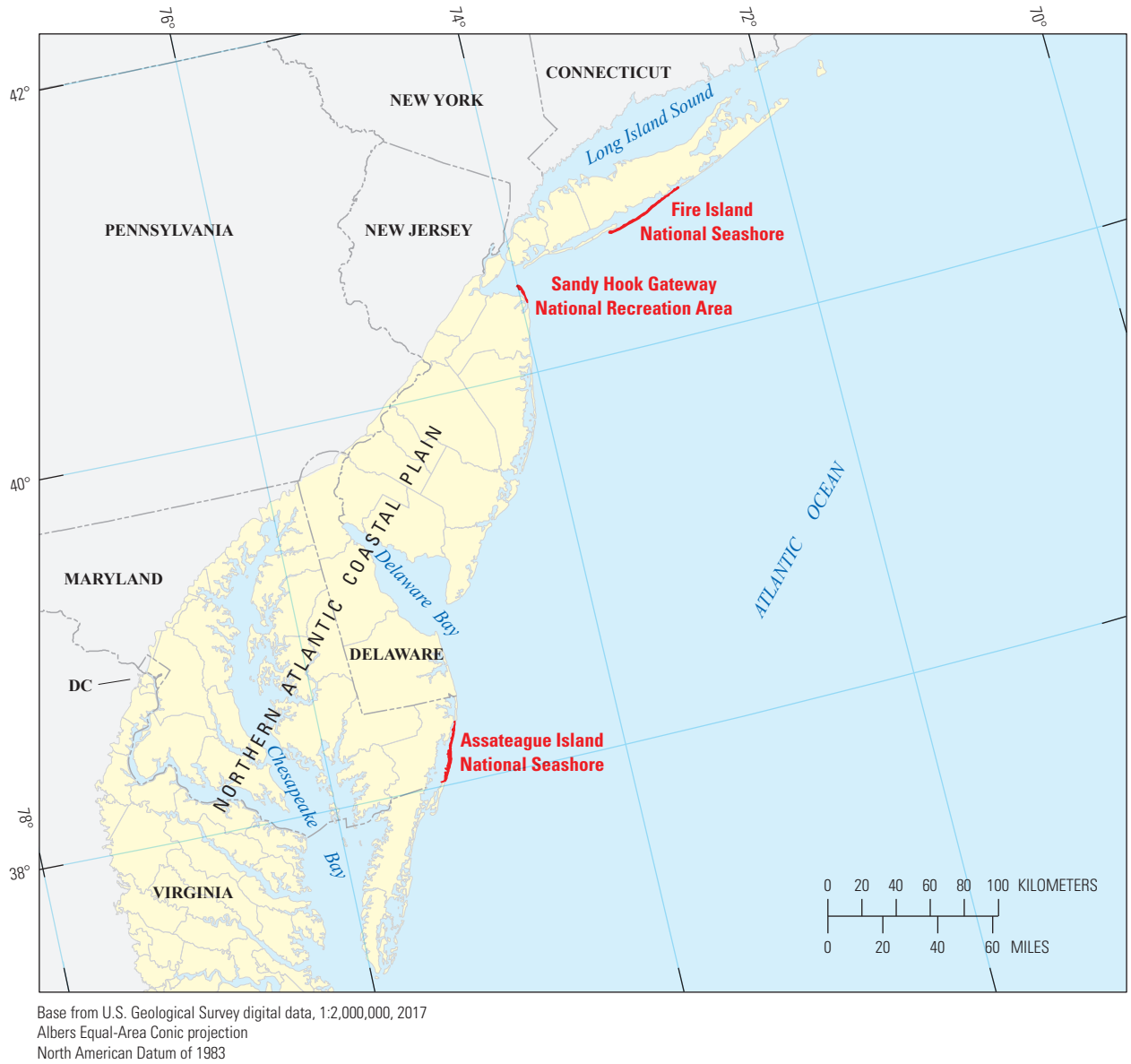

Figure 1. Locations of Assateague Island National Seashore, Maryland and Virginia (the current study area); Sandy Hook Gateway National Recreation Area, New Jersey; and Fire Island National Seashore, New York.

substantially affected by increased water-table altitude, subsurface flooding of low-lying areas, and the potential for saltwater intrusion (Masterson and Garabedian, 2007; Masterson and others, 2014). Understanding how sea-level rise may affect groundwater hydrology in shallow, unconfined coastal systems such as Assateague Island is important for assessing the potential effects of sea-level rise on the sustainability of federally listed endangered species, such as piping plovers. To address these concerns, the U.S. Geological Survey (USGS) in cooperation with the NPS conducted a study to improve the understanding of sea-level rise and climate change on barrier island groundwater systems in the northeastern United States. This study is one of three investigations conducted at national seashore barrier island systems in the Northeast using similar modeling approaches. The companion investigations are at Sandy Hook Gateway National Recreation Area in New Jersey and Fire Island National Seashore in New York. These three studies were developed to improve NPS resource managers' ability to adapt and mitigate potentially adverse effects of sea-level rise on the national seashores in the northeastern United States.

Purpose and Scope

This report describes the potential response of the groundwater system on Assateague Island, Maryland and Virginia, to increases in sea level of up to 60 centimeters (cm). The report includes discussions of (1) the groundwater response (specifically the depth to the water table) to

sea-level-rise scenarios of 20 cm, 40 cm, and 60 cm using a newly developed groundwater-flow model, (2) the possibility of groundwater response to future changes in recharge, and (3) the potential water level and water quality monitoring strategies available to meet NPS resource managers' needs. Groundwater level and specific conductance data are summarized in appendix 1. Water-level and specific conductance data are available through the U.S. Geological Survey (USGS) National Water Information System (NWIS) database (USGS, 2017). The groundwater-flow model development, calibration, sensitivity analysis, and goodness of fit is described in appendix 2 and in Fleming and Raffensperger (2021).

Background and Previous Investigations

Several studies describe the hydrology near Assateague Island. Dillow and others (2002) describe the groundwater-flow paths in the surficial aquifer that discharge to Chincoteague and Sinepuxent Bays. Nitrate loads from groundwater to the inland bays were estimated by Dillow and Greene (1999). For the nearby Virginia Eastern Shore, Richardson (1994) developed a three-dimensional groundwater-flow model using the SHARP code (Essaid, 1990) to represent variable-density groundwater flow. Later, Sanford and others (2009) simulated the same area of the Virginia Eastern Shore using the coupled groundwater flow and mass transport code SEAWAT (Langevin and others, 2003) to represent variable-density groundwater flow. A regional model of the Delmarva Peninsula (Sanford and others, 2012) was developed to estimate groundwater travel times to discharging streams.

The potential effects of sea-level rise on coastal groundwater systems have been evaluated in various studies on the east coast of the United States and elsewhere. Langevin and Zygnerski (2013) evaluated the effects of sea-level rise in southeastern Florida. For Cape Cod, Massachusetts, Masterson and Garabedian (2007) and Walter and others (2016) developed or expanded groundwater-flow models with sea-level-rise scenarios. For Fire Island, New York, Schubert (2010) analyzed the shallow groundwater-flow system. Gingerich and others (2017) used the SUTRA code (Voss and Provost, 2002) to model variable-density groundwater flow for a Pacific Island atoll. Michael and others (2013) evaluated the global effects of sea-level rise on coastal groundwater systems and identified two types of coastal aquifer settings: recharge limited and topography limited.

For Assateague Island, a groundwater-flow model was developed previously (Masterson and others, 2013) and used to explore the effects of sea-level rise (Masterson and others, 2014). Banks and others (2012) describe the installation of a groundwater-monitoring network, and Fienen and others (2013) applied Bayesian networks to extract results from groundwater-flow models to provide information for decision support. A hydrogeomorphic map (Krantz, 2009) was developed to understand the relation between morphology and hydrology on Assateague Island. Various approaches have been taken to describe coastal groundwater systems. This study is a companion study to the Sandy Hook, N.J., and Fire Island, N.Y., studies, designed using the same modeling approaches and sea-level scenarios to provide resource managers with a common set of tools for determining ways in which to adapt to the potentially adverse effects of sea-level rise.

Hydrogeologic Framework

The study area is underlain by a series of confined and unconfined aquifers collectively known as the Northern Atlantic Coastal Plain aquifer system (Trapp and Horn, 1997). The regional confined aquifer system in the study area is generally overlain by younger sediments ranging in age from Tertiary to Quaternary. These sediments were deposited in a variety of environments, including alluvial, tidal marsh, back barrier, and marine marginal, and form an unconfined, surficial aquifer. The groundwater hydrology of Assateague Island is controlled largely by the landforms of the island (Krantz, 2009).

The water table in the shallow, unconfined aquifer system generally follows the local topography, and water levels can range from land surface to as deep as 15 m below land surface (bls). However, the water table often is less than 1 m bls (Dillow and others, 2002). The only surface-water features on the island are a limited number of groundwater-fed ponds, which represent surface-water expressions of the water table. As a result, the groundwater hydrology, including the distribution of fresh and brackish water in the shallow aquifer, and the geometry of the fresh groundwater lens beneath the island, affects the distribution of plant communities and habitat for a diverse community of invertebrate and vertebrate wildlife (Krantz, 2009).

Simulation of the Shallow Groundwater-Flow System

Groundwater flow on Assateague Island was simulated to evaluate the effects of sea-level rise and changes in recharge on the depth to freshwater below the land surface, changes in freshwater discharge, and the depth of the freshwater/saltwater interface. The conceptual model used to design the groundwater-flow model is described in the section "Conceptual Model." and a detailed description of the groundwater-flow model is given in appendix 2. The USGS groundwater modeling code MODFLOW-NWT (Niswonger and others, 2011) with the Seawater Intrusion (SWI2) Package (Bakker and others, 2013) is used to simulate variable-density flow. The model is based on a previous groundwater-flow model developed for Assateague Island (Masterson and others, 2013) and shares the same extent as the earlier model. The model domain includes parts of the mainland west of Chincoteague and Sinepuxent Bays, and Sinepuxent Neck in the northern extent of the model (fig. 2).

Conceptual Model

The conceptual model describes the geometry of the system and boundary conditions that control the movement of groundwater. It synthesizes available information about the groundwater-flow system, including the hydrogeologic framework, hydraulic properties, recharge, evapotranspiration, and the nature of the freshwater/saltwater interface. This conceptual model forms the basis for the construction of the numerical groundwater-flow model.

The model includes an unconfined barrier island aquifer system on top of the layered Coastal Plain aquifer system. The bottom of the barrier island aquifer is considered an impermeable clay confining unit (Richardson, 1994). Recharge and evapotranspiration vary spatially, depending on the ground cover and vegetation on the island surface. Saline surface-water bodies are represented as head-dependent flux boundaries. A wave-overheight boundary, representing mounding of groundwater near the shoreline caused by wave runup and tidal infiltration and seepage (tidal pumping) is included along the Atlantic Ocean coastline. The lateral boundaries were simulated as no-flow boundary conditions that extend beyond the maximum limit of the freshwater system on Assateague Island.

Baseline Scenario

A simulation produced using the calibrated hydraulic properties and initial boundary conditions is referred to as the baseline scenario. The baseline scenario uses a sea-level boundary equal to the 1983–2001 mean sea level at Ocean City, Md. (−0.109 m, NAVD 88; National Oceanic and Atmospheric Administration, 2016) and calibrated model parameters described in appendix 2. The baseline scenario model estimates water-table altitude, depth to water below land surface, and the position of the 50-percent freshwater/saltwater interface. Results from subsequent scenarios with different boundary conditions representing sea-level stages are compared to the baseline scenario as difference maps.

Recharge and Discharge Areas

Flow into the fresh groundwater system occurs in areas assigned as recharge and along the Atlantic coast because of the wave-overheight boundary. Flow out of the fresh groundwater system occurs as evapotranspiration from vegetation, seeps (discharge to the land surface), or submarine groundwater discharge. Groundwater discharge as evapotranspiration (ET; fig. 3) occurs where the water table is above the estimated extinction depth for ET, the depth at which the roots of the vegetation group reach below land surface to take up freshwater. For the baseline scenario, coastal inflows and recharge contribute water into the system, whereas evapotranspiration and surface seeps are discharges. (table 1).

Depth to Water

Much of the land area of Assateague Island is less than 1 m above sea level (asl), especially along the bay side. In these areas, the water table is between 0 and 1 m asl (fig. 4). Most of the island has a water table within 1 m of land surface, with the exception of the primary dune complex, which spans the entire ocean side of the island (fig. 4). The primary dune, which is the topographic high, separates the vegetated and non-vegetated parts of the island. Depth to water can be as much as 6 m along the dune, whereas the water table is above land surface at several enclosed depressions. The highest water-table altitudes, 1 m or more asl, coincide with higher altitudes near the primary dune and topographic high on the southern part of Assateague Island (fig. 5). Overall, water-table altitudes range from 0 to about 3 m asl on the island.

Freshwater/Saltwater Interface

The altitude of the freshwater/saltwater interface for the baseline scenario is shown in figure 6. The numerical modeling code used to simulate steady-state groundwater flow on Assateague Island, MODFLOW-NWT (Niswonger and others, 2011) with SWI2 (Saltwater Intrusion) package (Bakker and others, 2013), simulates the freshwater/saltwater transition zone as a sharp interface with a concentration of 50-percent seawater. The aquifer contains freshwater to the base of the aquifer in much of the island. Areas along the bay have an interface position approximately −10 m or less below the North American Vertical Datum of 1988 (NAVD 88).

Steady-State Simulation for Scenarios of Sea-Level Rise and Varying Recharge

The baseline scenario model was used as a starting point to develop sea-level-rise scenarios. The altitude of the saline water bodies was increased by 20 cm, 40 cm, and 60 cm for three different sea-level-rise scenarios to be consistent with the companion studies as Sandy Hook, N.J., and Fire Island, N.Y. Land-surface cells at altitudes less than the respective sea-level boundary for each scenario were reassigned as saline-water-body boundary conditions. Associated land-surface model boundary conditions, including drains, recharge, and evapotranspiration, were turned off for those “inundated” cells for each sea-level-rise scenario. Each sea-level-rise model run was allowed to run for 100 years, a period sufficient for a steady state to be achieved.

Recharge and Discharge Areas

The sea-level-rise scenarios cause many low-lying areas that receive recharge in the baseline scenario to be inundated and therefore converted to saltwater. Inundation reduces the

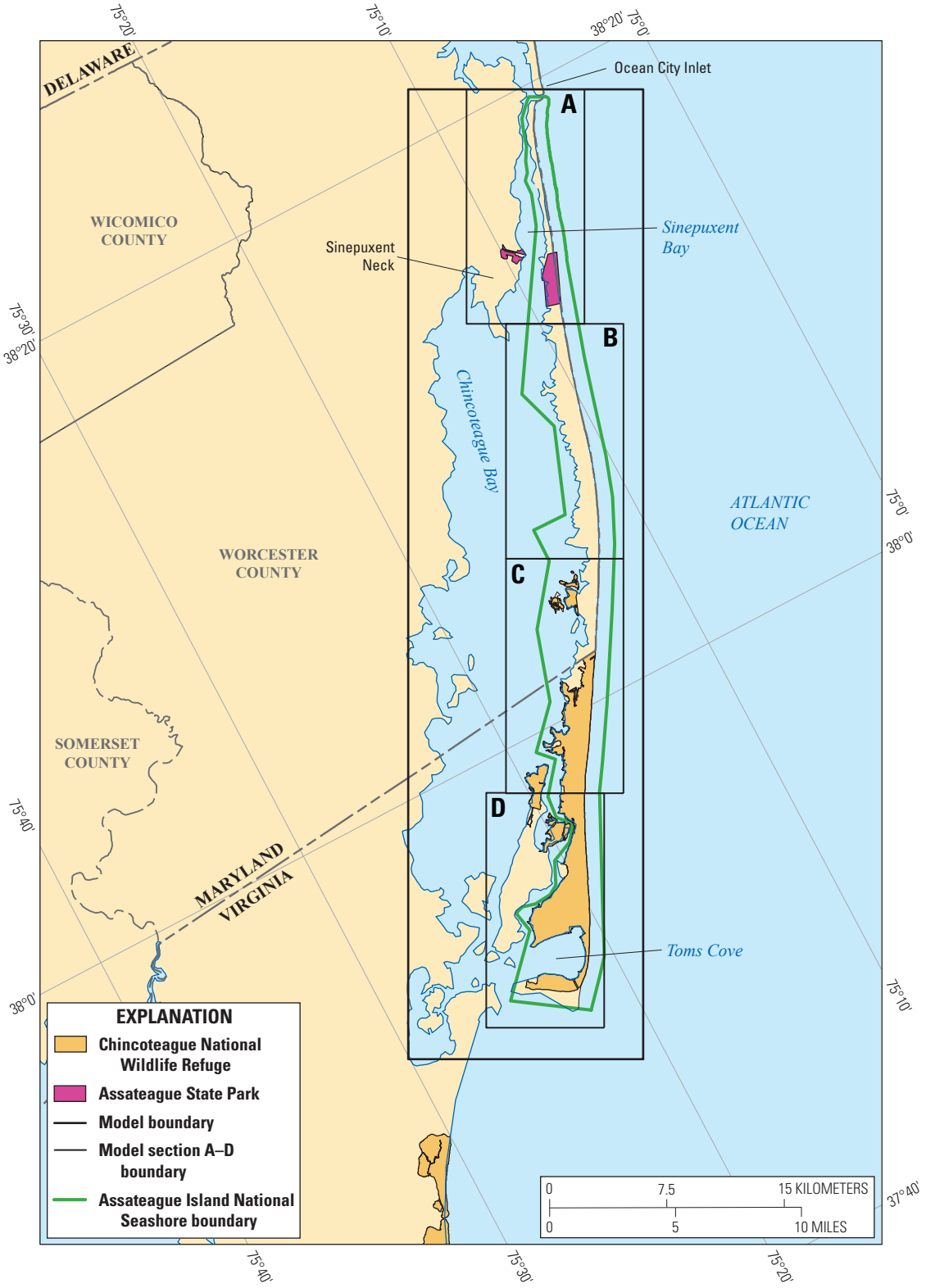

Base from U.S. Geological Survey 1:2,000,000-scale
State boundary digital line graph, Albers Equal-Area Conic Projection
North American Datum of 1983 (NAD 83)

Figure 2. Study area and the model grid extent with sections A through D, Assateague Island, Maryland and Virginia.

Table 1. Simulated flow rates to model boundaries for the baseline scenario, 20-, 40-, and 60-centimeter sea-level-rise scenarios, and increased and decreased recharge scenarios, Assateague Island, Maryland and Virginia.

[cm, centimeter; SLR, sea-level rise; m^3/d, cubic meters per day; GW, groundwater; ET, evapotranspiration]

Boundary condition	Baseline	20-cm SLR	40-cm SLR	60-cm SLR	Recharge decreased by 10 percent	Recharge increased by 10 percent	60-cm SLR and recharge increased by 10 percent
Flow into groundwater-flow model from boundary [negative indicated flow out of the fresh groundwater system] (in m^3/d)							
Recharge	4,801,157,632	4,025,190,400	3,508,828,416	3,049,707,776	4,321,041,408	5,281,274,368	3,354,679,296
GW discharge to seeps	−2,880,596,224	−1,819,698,560	−1,407,593,600	−1,029,743,936	−2,635,861,504	−3,149,794,816	−1,189,886,720
GW discharge to evapotranspiration	−2,326,050,560	−1,713,842,304	−1,411,811,584	−1,060,658,176	−2,146,323,584	−2,479,760,128	−1,132,049,408
GW submarine discharge	400,879,616	−493,502,464	−691,023,872	−960,323,584	461,053,952	342,552,576	−1,033,932,800
Percentage of recharge discharging to seeps, ET, and submarine groundwater boundaries (may not equal 100 percent because of rounding errors)							
Seeps	−0.60	−0.45	−0.40	−0.34	−0.61	−0.60	−0.35
Evapotranspiration	−0.48	−0.43	−0.40	−0.35	−0.50	−0.47	−0.34
Submarine groundwater discharge	0.08	−0.12	−0.20	−0.31	0.11	0.06	−0.31
Total flow in and out of groundwater-flow models for each sea level rise scenario							
In	37,901,275,136	46,451,863,552	46,671,962,112	46,715,252,736	37,907,197,952	37,894,627,328	46,712,492,032
Out	37,500,395,520	46,945,366,016	47,362,985,984	47,675,576,320	37,446,144,000	37,552,074,752	47,746,424,832
Head dependent boundary difference	400,879,616	−493,502,464	−691,023,872	−960,323,584	461,053,952	342,552,576	−1,033,932,800

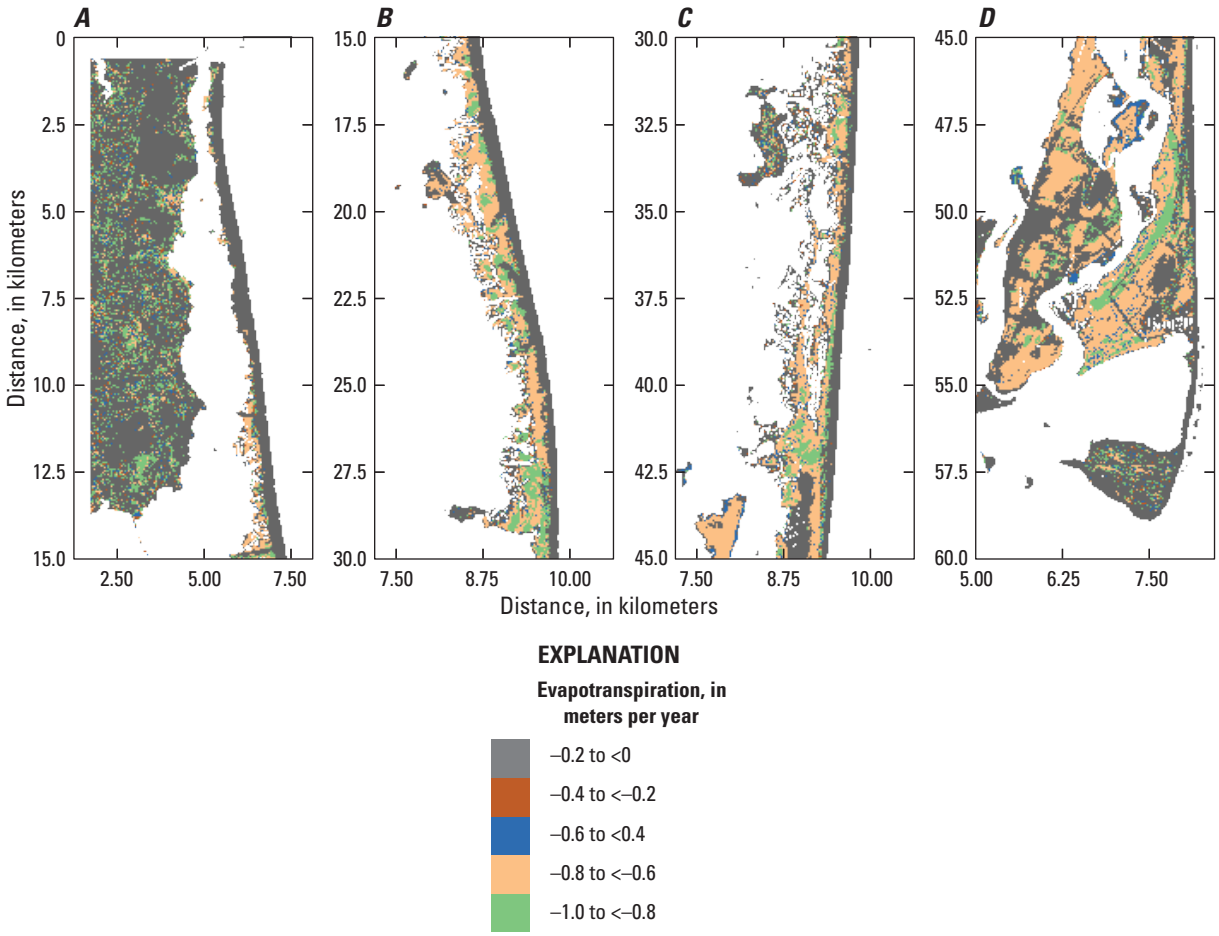

Figure 3. Distribution of evapotranspiration for the baseline scenario for sections A–D, Assateague Island, Maryland and Virginia. (<, less than; note the different scales)

land area that receives recharge and the total volume of freshwater recharge (table 1). The inundation from the sea-level-rise scenarios reduces the number of model cells assigned to account for seepage and evapotranspiration, and with successively higher sea-level positions, the groundwater discharge to seeps and evapotranspiration decreases. At the current land-surface altitude, as much as 50 percent of the island may be inundated with a 60-cm rise in sea level, and the low-lying marshes may change from freshwater to saltwater. In addition to the change in island geometry caused by inundation (table 2), the sea-level-rise scenarios cause a rise in the water table on the rest of the island. This higher water table affects groundwater discharge in the existing areas assigned as seeps and through changes in ET (fig. 7) and submarine groundwater discharge. As the sea level rises, submarine groundwater discharge increases, whereas changes in discharge by seeps and evapotranspiration vary locally.

Changes in recharge of ±10 percent to the baseline scenario were evaluated. The reduced recharge scenario lowered the water table, resulting in decreased discharge to seeps and evapotranspiration, and decreased output to submarine groundwater. In contrast, the increased recharge scenario slightly increased the water table, increasing discharge to seeps and evapotranspiration, and decreasing the input from submarine groundwater. The final scenario was 60-cm sea-level rise with an increase of 10 percent in recharge. These results are slightly different from the 60-cm sea-level-rise scenario in that the increased recharge caused a slight increase in discharge to seeps, evapotranspiration, and submarine groundwater discharge (table 1).

Depth to Water

For the simulation of a 20-cm sea-level rise, the changes in water-table altitude are typically less than 10 cm and occur in areas of the low altitude, marshy, back-bay parts of the island (fig. 8*A*). For the 40-cm sea-level-rise scenario, the increase in water-table altitude encroaches inland from the back bay, with maximum water-table altitudes increasing by as much as 40 cm (fig. 8*B*). For the 60-cm sea-level-rise simulation, the water-table altitude changes encroach further inland

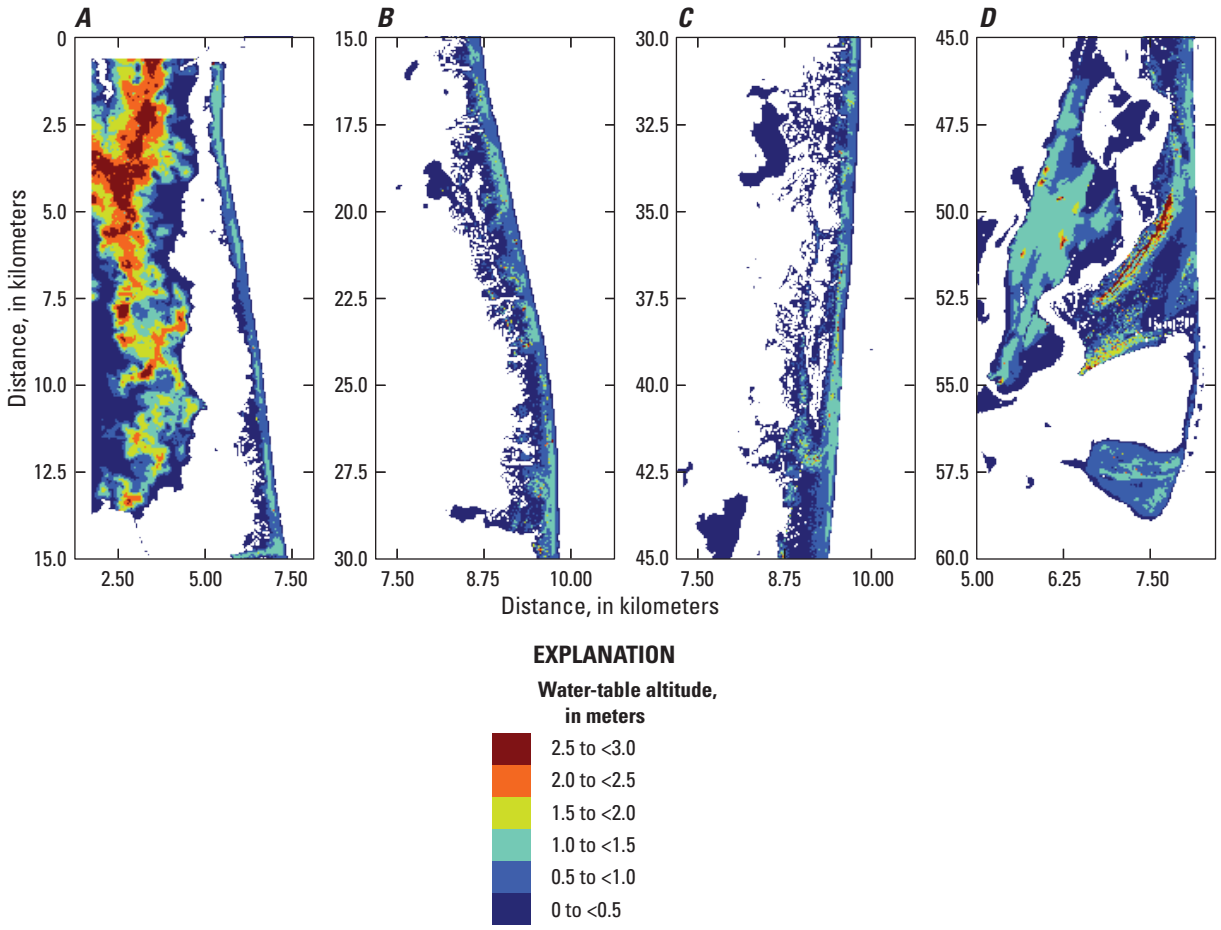

Figure 4. Water-table distribution for the baseline scenario of sections A–D, Assateague Island, Maryland and Virginia. (<, less than; note the different scales)

from the bay side, with the maximum water table increasing by as much as 50 cm (fig. 8*C*). On the northern, narrowest part of the island, 60 cm of sea-level rise is predicted to increase the water table across the island's entire width. Large areas on the southern part of the island near Toms Cove show changes of between 30 cm and 50 cm. At dunes and other higher topographic features, the increased water-table altitude is still well below land surface. However, in lower topographic areas, the water table enters the capture zone for vegetation root systems or discharges to the land surface.

Freshwater/Saltwater Interface

Changes to the altitude of the 50-percent freshwater/saltwater interface are localized, with most of the changes occurring in the southern part of the island (fig. 9). These low-lying areas are affected by inundation, and the freshwater lens present in the baseline scenario is not present in the 60-cm sea-level-rise scenario. Similarly, but to a lesser extent on the northern part of the island, low-lying areas on the bay side are inundated, and parts of the freshwater lens are gone under the 60-cm sea-level-rise scenario.

Results from the sea-level-rise scenarios show an increase in the altitude of the water table, inundation of low-lying areas, and an increase in discharge from seeps and evapotranspiration in non-inundated areas. Boundary conditions change over the low-lying areas of the island in the sea-level-rise scenarios. Inundated areas are converted from recharge, evapotranspiration, and drains with freshwater inputs to specified head with a saltwater source. This decreases the overall flow of freshwater into the model from recharge (fig. 10). In successive sea-level-rise scenarios the subsequent flow out of the model as evapotranspiration and seeps decreases (table 1) whereas freshwater flow to submarine groundwater discharge increases. Changes in recharge of ±10 percent have minor effects on the results of the model.

On the Atlantic coast of North America, groundwater systems of many barrier islands are topographically limited (Michael and others, 2013) in response to sea-level rise. This

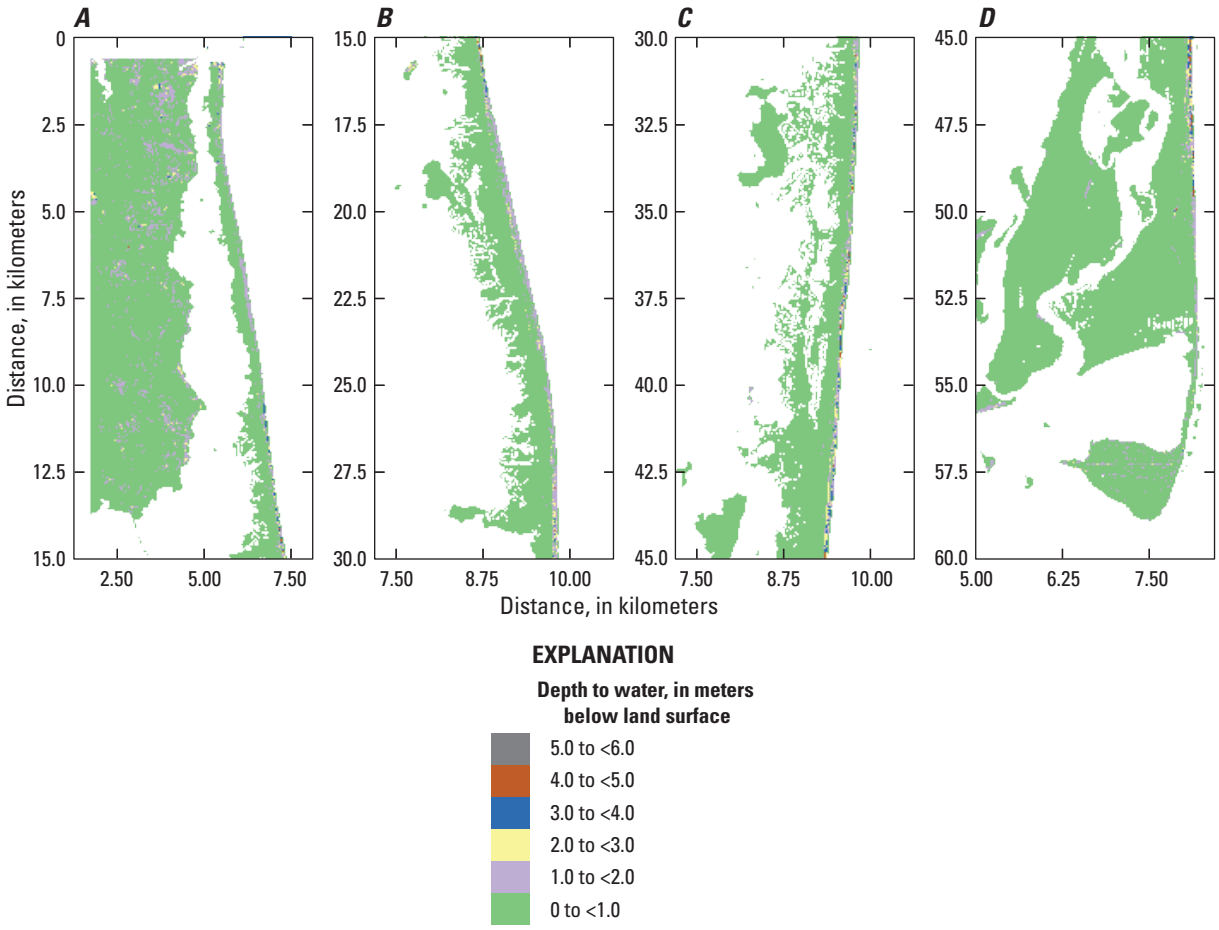

Figure 5. Depth of the water table for the baseline scenario of sections A–D, Assateague Island, Maryland and Virginia. (<, less than; note the different scales)

means that as the water table rises, it approaches the land surface and leaves by direct discharge, evapotranspiration, or extraction if wells are present. Barrier islands are dynamic systems, undergoing erosion and deposition in complex ways. In a topographically limited setting like Assateague Island, morphological processes may be an important factor in determining the fate of the fresh groundwater systems in the face of sea-level rise.

Limitations of Analysis

This study uses steady-state groundwater-flow models to evaluate the long-term effects of sea-level rise on the groundwater system of Assateague Island, Maryland and Virginia. This approach does not account for the potential transient effects that may be associated with long-term sea-level rise, such as increased high tidal events. Although this study does explore the effects of changes in long-term recharge to the system, individual precipitation events are not explored. Seasonal variations in hydrology are not accounted for in the sea-level-rise assessment. Groundwater observation data do show the transient response to these hydrologic processes, which may deserve further study.

The shape of the island is assumed constant for this study. Predicting geomorphological adaptation to sea-level rise is beyond the scope of this study, but the authors acknowledge changes in island morphology may be an important factor when evaluating long-term groundwater response to sea-level rise in a topographically limited system like Assateague Island. Because of the extensive area of the study that is less than 60 cm above current (2019) sea level, inundation of those areas affects the overall water budget of the island. In this study, a sharp interface approach was used to simulate variable density groundwater conditions. This approach allowed for a refined spatial discretization of the island, and finer resolution of the water table, at the expense of representing the freshwater/saltwater interface as a transition zone from freshwater to seawater. This approach is consistent with the modeling efforts on Fire Island, N.Y., (Misut and Dressler, 2021) and Sandy Hook, N.J., (Carleton and others, 2021) and is intended to provide comparable results between national seashores.

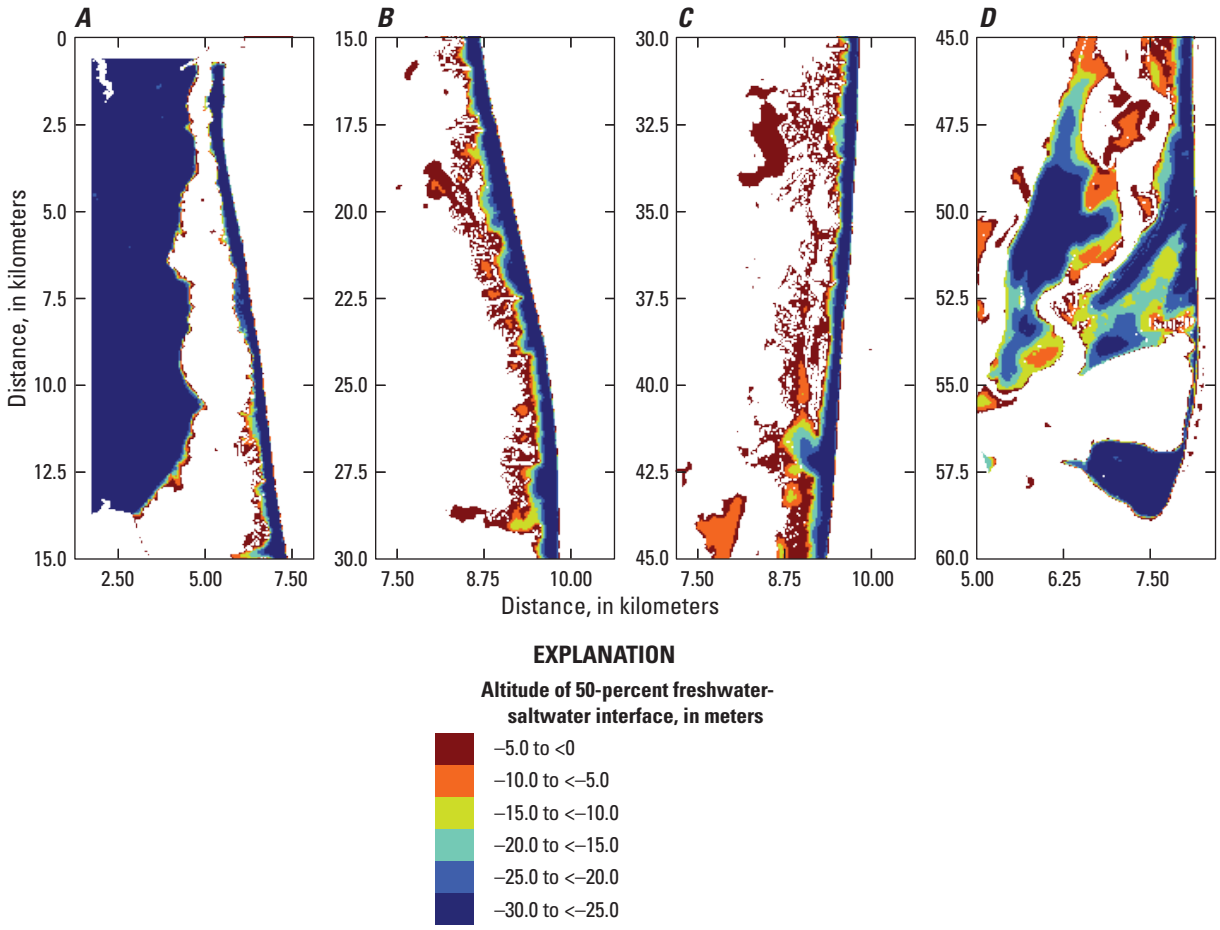

Figure 6. Altitude of the 50-percent freshwater/saltwater interface of sections A–D, Assateague Island, Maryland and Virginia. (<, less than; note the different scales)

Long-term Monitoring to Assess Water Resources

Continuous water levels in 32 wells were recorded at 6-minute intervals from October 1, 2014, to September 30, 2015. At four wells, specific conductance was recorded at 6-minute intervals for the same period. The purpose of collecting these high-frequency data was to observe groundwater response to hydrologic processes in different parts of the aquifer system, determine processes of interest for future monitoring, and identify wells that provide the most information regarding those hydrologic processes of interest. Seasonal and episodic variations in aquifer condition driven by precipitation, tides, and evapotranspiration vary spatially on Assateague Island. To evaluate similar transient water-table responses at various temporal scales, correlation analysis was applied to a groundwater-level time series at 14 shallow wells. Correlation coefficients for each combination of wells are used as input to a clustering algorithm to objectively group wells that respond in a similar fashion to hydrologic processes on the island.

Table 2. Simulated area of land inundated by sea-level rise, Assateague Island, Maryland and Virginia.

[SLR, sea-level rise; km^2, square kilometer; NA, not applicable; cm, centimeter]

SLR senario	Simulated area of inundated land (km^2)	Percent of island land area inundated
Baseline	NA	NA
20 cm	22.34	24.6
40 cm	35.18	38.7
60 cm	45.04	49.6

Groundwater Levels

Shallow wells with 12 months of high frequency water levels were used for an objective classification analysis. Time series were pre-processed for analysis by interpolating data missing as a result of equipment maintenance and resampling at the original data collection interval of 6 minutes. Pearson

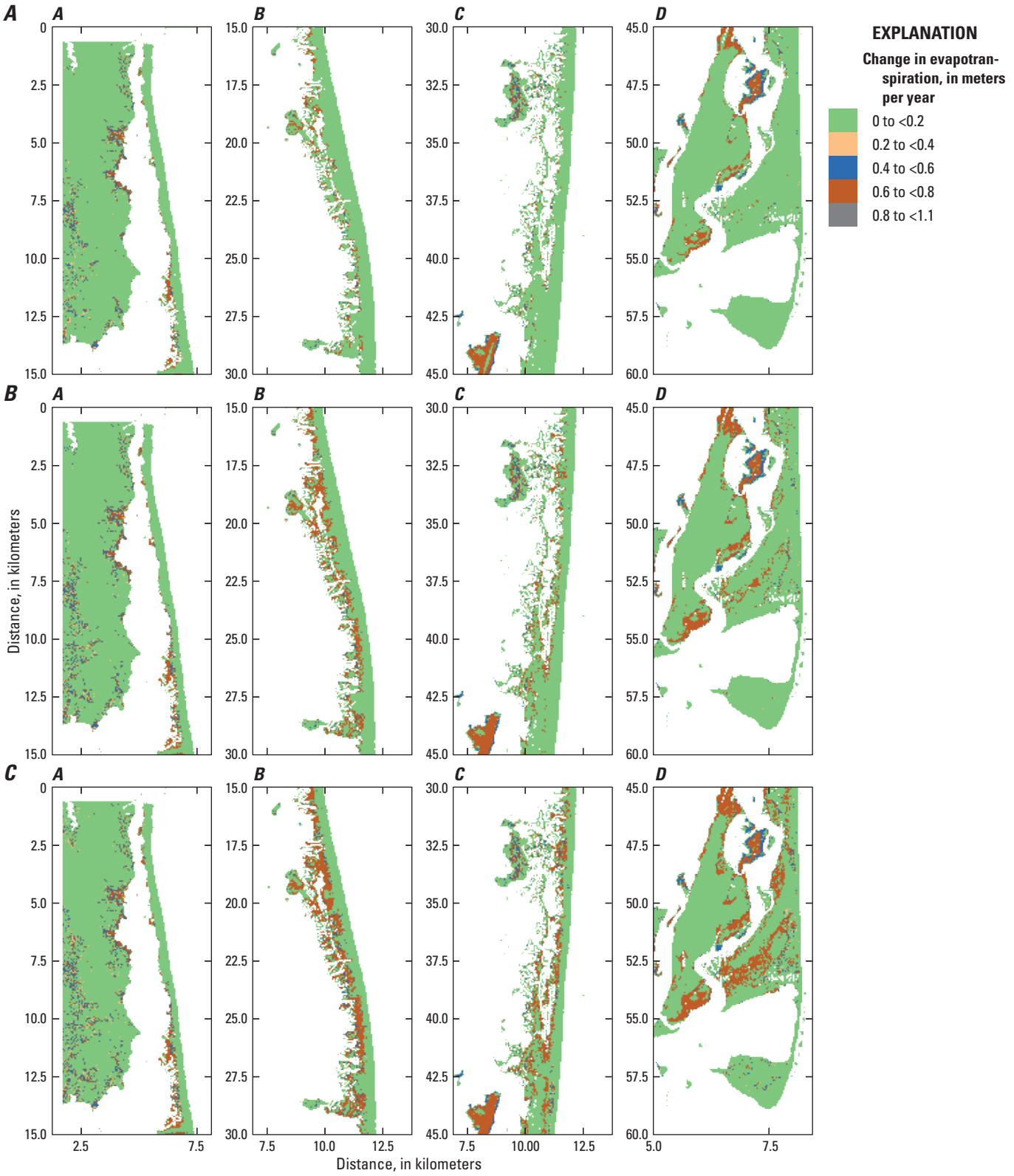

Figure 7. Changes in evapotranspiration for *A*, 20, *B*,40, and *C*, 60 centimeters of sea-level rise, sections A–D, Assateague Island, Maryland and Virginia. (<, less than; note the different scales)

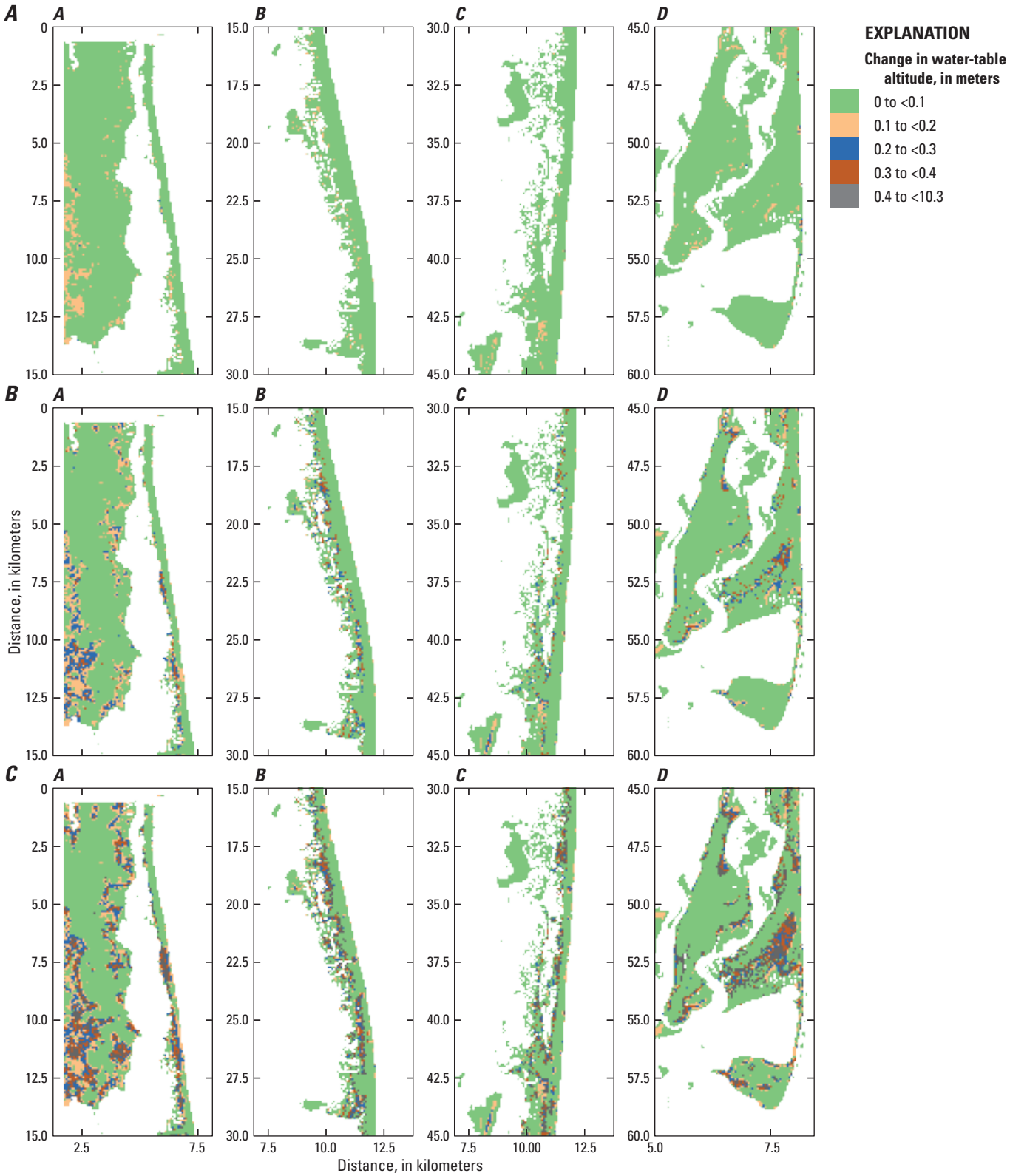

Figure 8. Change in water-table altitude for *A*, 20, *B*, 40, and *C*, 60 centimeters of sea-level rise, sections A–D, Assateague Island, Maryland and Virginia. (<, less than; note the different scales)

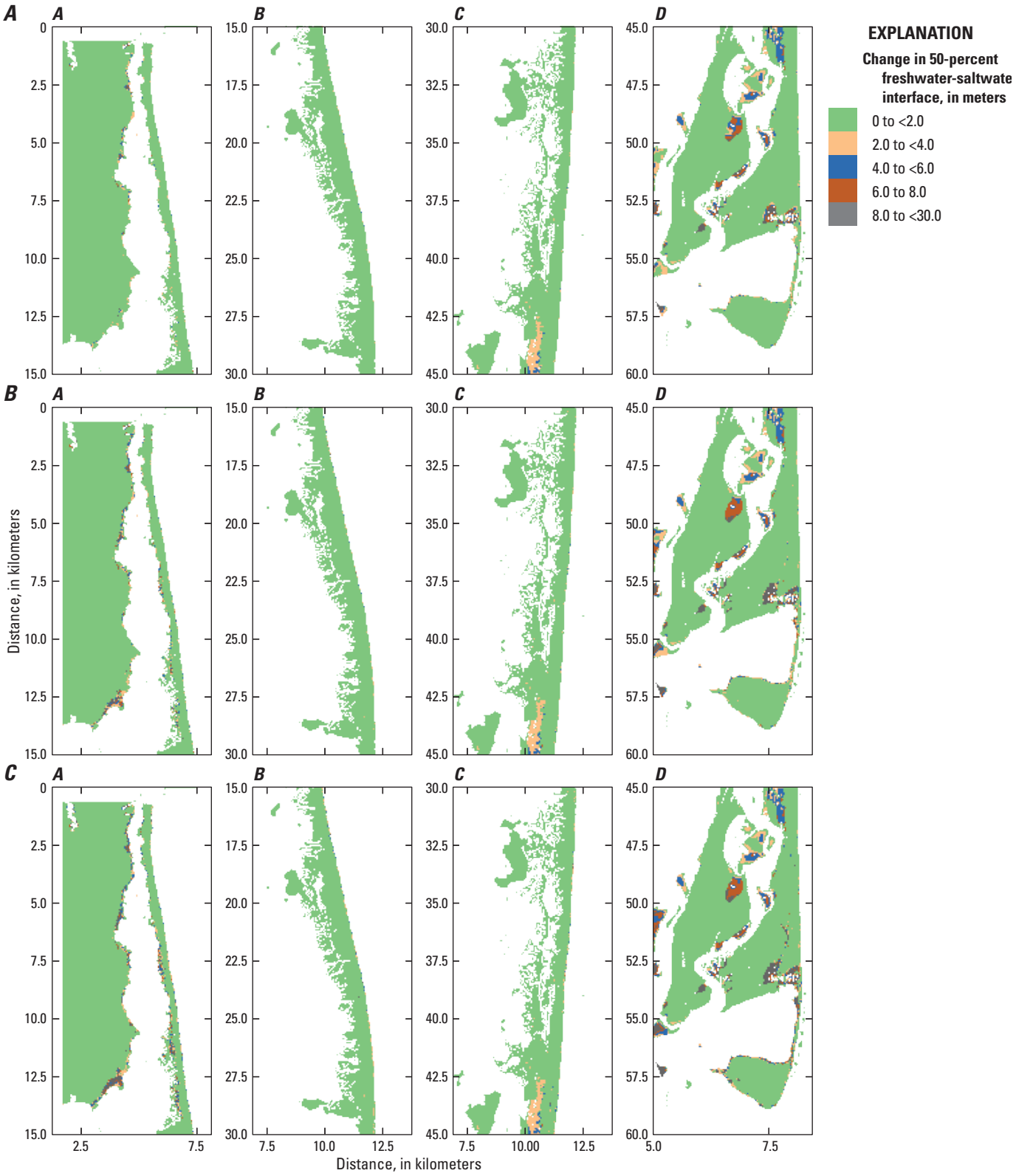

Figure 9. Changes in the 50-percent freshwater/saltwater interface altitude for *A*, 20, *B*, 40, and *C*, 60 centimeters of sea-level rise, sections A–D, Assateague Island, Maryland and Virginia. (<, less than; note the different scales)

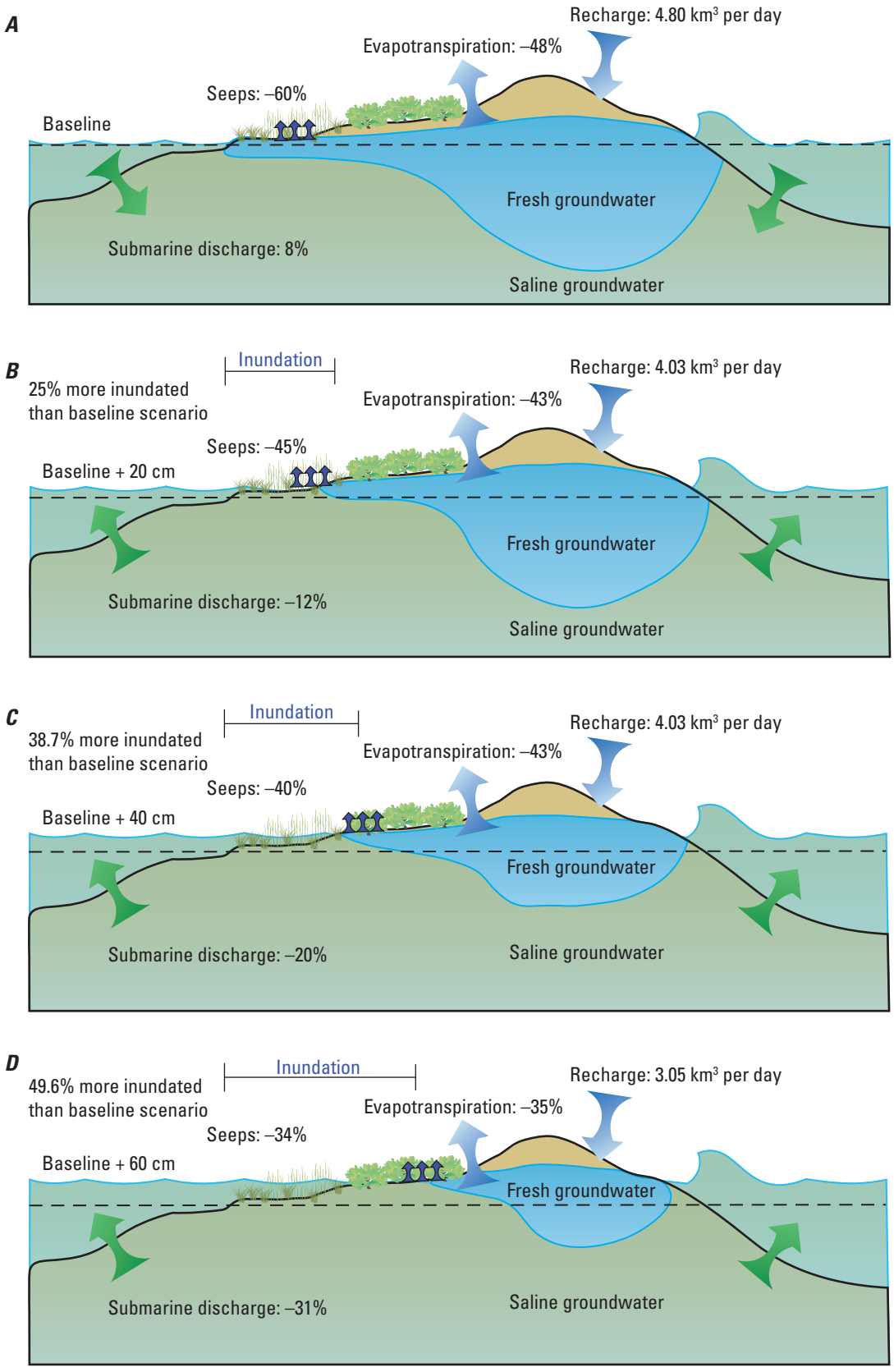

Figure 10. Schematic diagrams showing the change in simulated fluxes under *A*, baseline conditions, and *B*, 20, *C*, 40, and *D*, 60 centimeters of sea-level rise, Assateague Island, Maryland and Virginia. (%, percent; km³, cubic kilometer; cm, centimeter]

correlation coefficients were computed for each combination of wells, and a hierarchical agglomerative clustering algorithm was applied using Ward's minimum variance method (Ward, 1963). The results of the cluster analysis group wells with two distinct response patterns. The locations of the well groups are important to understanding the different aquifer response observed in each group. Figure 11 shows that wells in group 1 are located on the vegetated bay side of the primary dune, and wells in group 2 are on the unvegetated ocean side. Wells in group 1 (fig. 12*A*) appear to respond strongly to precipitation events, whereas wells in group 2 (fig. 12*B*) respond more strongly to tidal events.

Water Quality

Specific conductance time series data were collected at four wells between October 1, 2014, and September 30, 2015. Two wells are in group 1 (precipitation response), and two are in group 2 (tidal response). The group 1 specific conductance time series shows freshening conditions corresponding to precipitation events (fig. 13*A*). Wells in group 2 on the northern part of the island show distinct increases in specific conductance with high tide events (fig. 13*B*), possibly caused by overwash events. Overwash events are more evident from October through March.

Summary and Conclusions

Projected rates of sea-level rise near Assateague Island, Maryland and Virginia, are some of the highest on the east coast of the United States. Simulated results of sea-level rise show groundwater inundation, saltwater intrusion, and surface inundation of large parts of Assateague Island. The fresh groundwater system, on which many species of plants and animals are dependent, is susceptible to adverse effects of sea-level rise. Assateague Island is not unique in this regard; many barrier island complexes, which host important habitats and ecosystems along the east coast, are also susceptible to adverse effects of sea-level rise.

The U.S. Geological Survey is working with State and other Federal agencies to improve the understanding of climate change on coastal ecosystems, including the effects on groundwater flow; to develop capabilities for predicting potential climate-change effects; and to provide the tools for adaptation and mitigation of potentially adverse effects. As part of that effort, the U.S. Geological Survey, in cooperation with the National Parks Service, conducted a study of the Assateague Island groundwater system, in coordination with similar modeling efforts on Fire Island, New York, and the Sandy Hook section of Gateway National Recreation Area in New Jersey. Combined, these models aim to improve the regional capabilities for predicting climate-change effects on barrier islands and provide resource managers with a common set of tools for the adaptation and mitigation of potentially adverse effects of sea-level rise.

On Assateague Island, the calibrated three-dimensional groundwater-flow model was used to simulate a baseline scenario and sea-level-rise scenarios of 20 centimeters (cm), 40 cm, and 60 cm. Scenarios where recharge is modified ±10 percent also were evaluated. Results show that at greater stages of sea-level rise, low-lying areas of the island originally represented as receiving freshwater recharge in the baseline scenario are inundated by saltwater. This inundation of the island decreases the overall amount of freshwater recharging the system. As the water table rises in response to the higher sea levels, freshwater flow out of the system changes, with more freshwater leaving as submarine groundwater discharge and less freshwater leaving as seeps and evapotranspiration. At the current (2019) land-surface altitude, as much as 50 percent of the island may be inundated with a 60-cm rise in sea level, and the low-lying marshes may change from freshwater to saltwater.

Water levels and water quality were monitored in a network of wells installed in 2010 (Banks and others, 2012). Results from objective classification analysis of 14 shallow monitoring wells show two dominant processes affecting groundwater levels in two different settings on the island. On the western side of the island, between the primary dune and the inland bays, water levels respond strongly to precipitation events. This side of the island is more protected from ocean tides and typically is more vegetated than the eastern side. The western side of the island is most likely to be inundated as sea levels rise because of the extremely low topographic relief. On the eastern side of the island, between the Atlantic Ocean and the primary dune, water levels strongly respond to tidal events. Specific conductance was measured at four wells, two on the western side of the island and two on the eastern side of the island. Specific conductance values for the two wells west of the primary dune show episodic decreases, coinciding with precipitation events. Specific conductance values for the two wells on the eastern side of the primary dune show episodic increases, coinciding with high tide events. These high frequency monitoring data are intended to aid in designing a monitoring network that can document both short-term and long-term hydrologic processes on Assateague Island National Seashore.

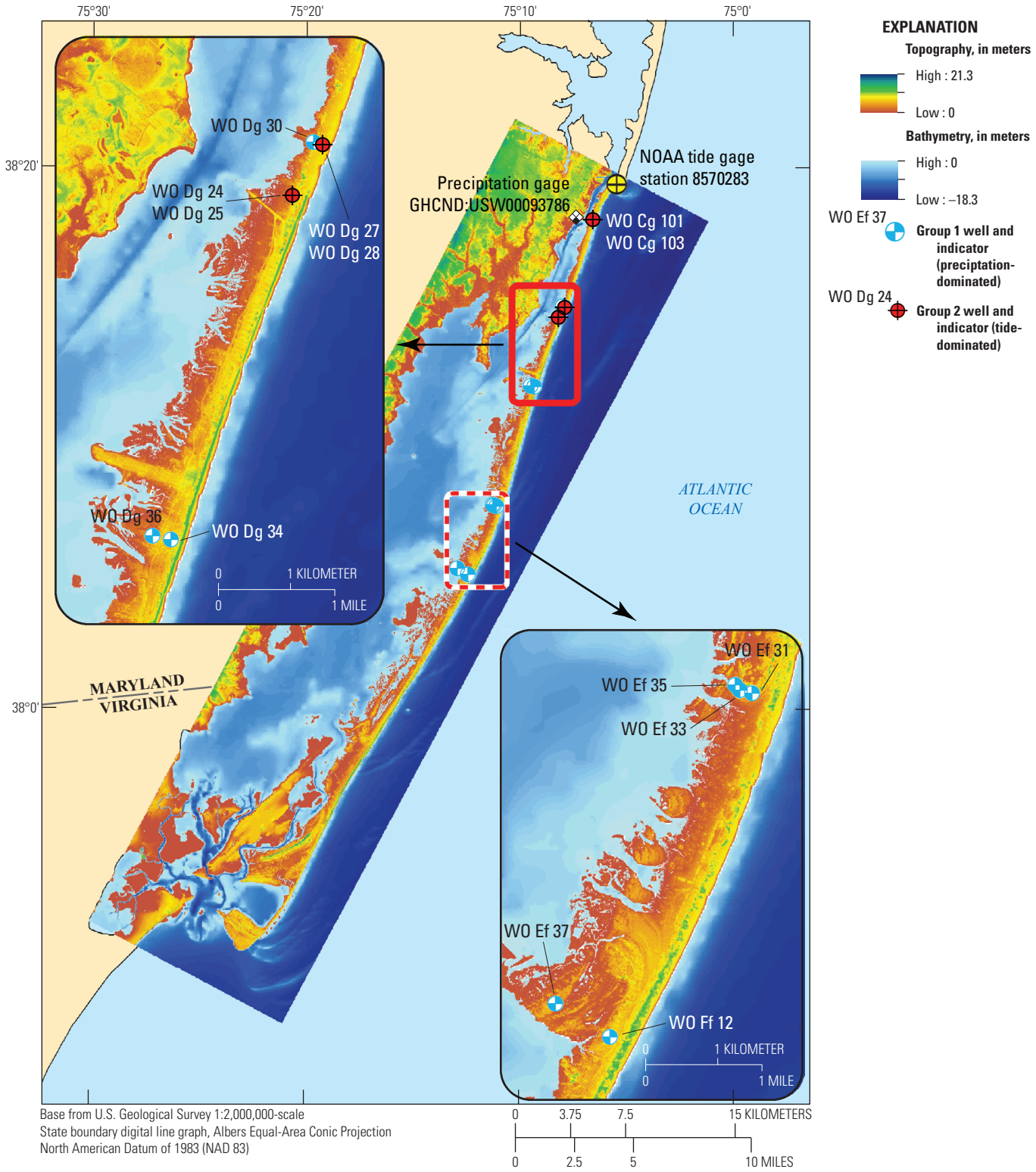

Figure 11. Location of wells grouped by correlation and cluster analysis into precipitation-dominated wells on the vegetated side and tide-dominated wells on the unvegetated side of Assateague Island, Maryland and Virginia. (NOAA, National Oceanic and Atmospheric Administration)

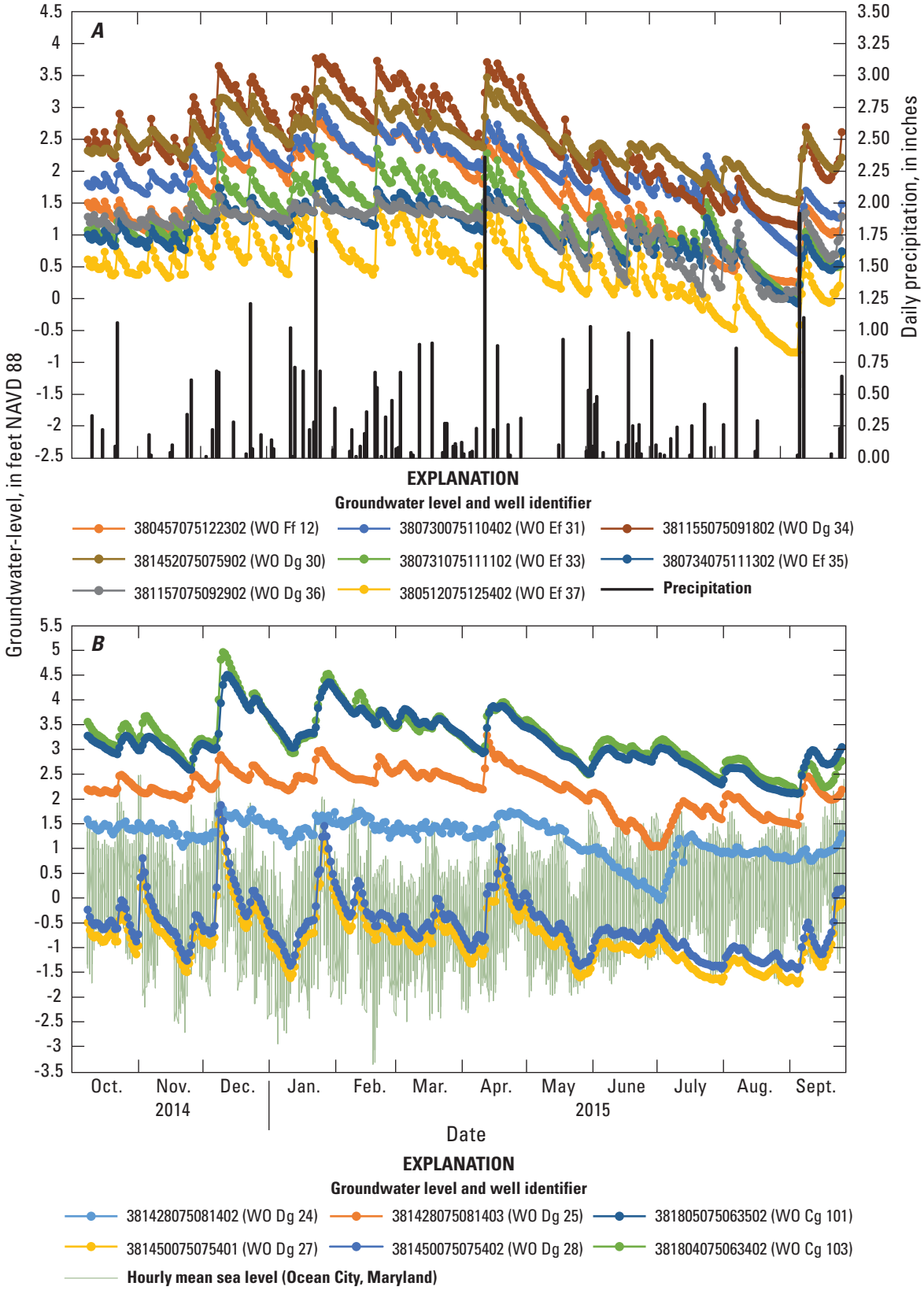

Figure 12. Groundwater levels clustered by *A*, precipitation for group 1 wells and *B*, tides for group 2 wells, Assateague Island, Maryland and Virginia, from October 1, 2014, to September 30, 2015. (Well locations are shown in figure 12.)

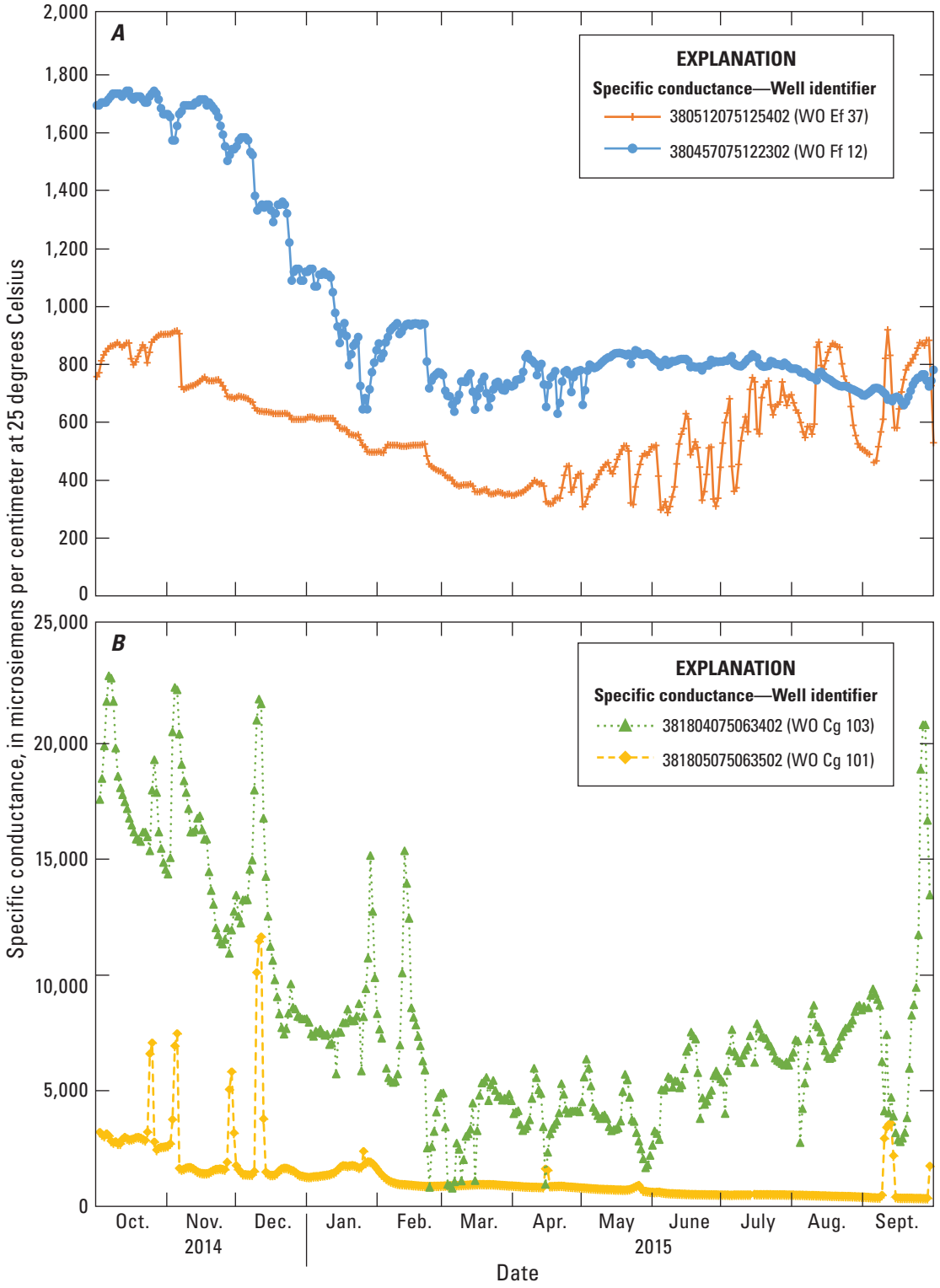

Figure 13. Specific conductance response in wells affected by *A*, precipitation (two wells) and *B*, tides (two wells), Assateague Island, Maryland and Virginia. (Note the different scales)

References Cited

Bakker, M., Schaars, F., Hughes, J.D., Langevin, C.D., and Dausman, A.M., 2013, Documentation of the seawater intrusion (SWI2) package for MODFLOW: U.S. Geological Survey Techniques and Methods, book 6, chap. A46, 47 p., accessed on December 15, 2014, at https://doi.org/10.3133/tm6A46.

Banks, W.S.L., Masterson, J.P., and Johnson, C.D., 2012, Well network installation and hydrogeologic data collection, Assateague Island National Seashore, Worcester County, Maryland, 2010: U.S. Geological Survey Scientific Investigations Report 2012–5079, 20 p., accessed on December 15, 2014, at https://doi.org/10.3133/sir20125079.

Carleton, G.B., Charles, E.G., Fiore, A.R., and Winston, R.B., 2021, Simulation of water-table response to sea-level rise and change in recharge, Sandy Hook unit, Gateway National Recreation Area, New Jersey: U.S. Geological Survey Scientific Investigations Report 2020–5080, 91 p., https://doi.org/10.3133/sir20205080.

Dillow, J.J.A., Banks, W.S.L., and Smigaj, M.J., 2002, Groundwater quality and discharge to Chincoteague and Sinepuxent Bays adjacent to Assateague Island National Seashore, Maryland: U.S. Geological Survey Water-Resources Investigations Report 02–4029, 42 p., accessed on December 15, 2014, at https://doi.org/10.3133/wri024029.

Dillow, J.J.A., and Greene, E.A., 1999, Ground-water discharge and nitrate loadings to the Coastal Bays of Maryland: U.S. Geological Survey Water-Resources Investigations Report 99–4167, 8 p., accessed on December 15, 2014, at https://doi.org/10.3133/wri994167.

Essaid, H., 1990, The computer model, SHARP, a quasi-three-dimensional finite-difference model to simulate freshwater and saltwater flow in layered coastal aquifer systems: U.S. Geological Survey Water-Resources Investigations Report 90–4130, 181 p., accessed on December 15, 2014, at https://doi.org/10.3133/wri904130.

Fienen, M.N., Masterson, J.P., Plant, N.G., Gutierrez, B.T., and Thieler, E.R., 2013, Bridging groundwater models and decision support with a Bayesian network: Water Resources Research, v. 49, no. 10, p. 6459–6473, accessed on December 15, 2014, at https://doi.org/10.1002/wrcr.20496.

Fleming, B.J., and Raffensperger, J.P., 2021, MODFLOW-NWT model with SWI2 used to evaluate the water-table response to sea-level rise and change in recharge, Assateague Island, Maryland and Virginia: U.S. Geological Survey data release, https://doi.org/10.5066/P9AJOLRK.

Gingerich, S.B., Voss, C.I., and Johnson, A.G., 2017, Seawater-flooding events and the impact on freshwater lenses of low-lying islands—Controlling factors, basic management and mitigation: Journal of Hydrology (Amsterdam), v. 551, p. 676–688, accessed on March 15, 2018, at https://doi.org/10.1016/j.jhydrol.2017.03.001.

Krantz, D.E., 2009, A hydrogeomorphic map of Assateague Island National Seashore, Maryland and Virginia: Toledo, Ohio, University of Toledo, accessed on February 29, 2016, at http://www.eeescience.utoledo.edu/Faculty/Krantz/download_files/NPS_Report.Assateague_Hydrogeomorphology.pdf.

Langevin, C.D., Shoemaker, W.B., and Guo, W., 2003, MODFLOW-2000, the U.S. Geological Survey Modular Ground-Water Model—Documentation of the SEAWAT-2000 version with variable-density flow process (VDF) and the integrated MT3DMS transport process (IMT): U.S. Geological Survey Open-File Report 03–426, 43 p., accessed on December 15, 2015, at https://doi.org/10.3133/ofr03426.

Langevin, C.D., and Zygnerski, M., 2013, Effect of sea-level rise on salt water intrusion near a coastal well field in southeastern Florida: Ground Water, v. 51, no. 5, p. 781–803, accessed on December 15, 2016, at https://doi.org/10.1111/j.1745-6584.2012.01008.x.

Masterson, J.P., Fienen, M.N., Gesch, D.B., and Carlson, C.S., 2013, Development of a numerical model to simulate groundwater flow in the shallow aquifer system of Assateague Island, Maryland and Virginia: U.S. Geological Survey Open-File Report 2013–1111, 34 p., accessed on December 15, 2014, at https://doi.org/10.3133/ofr20131111.

Masterson, J.P., Fienen, M.N., Thieler, E.R., Gesch, D.B., Gutierrez, B.T., and Plant, N.G., 2014, Effects of sea-level rise on barrier island groundwater system dynamics—Ecohydrological implications: Ecohydrology, v. 7, no. 3, p. 1064–1071, accessed on December 15, 2014, at https://doi.org/10.1002/eco.1442.

Masterson, J.P., and Garabedian, S.P., 2007, Effects of sea-level rise on groundwater flow in a coastal aquifer system: Ground Water, v. 45, no. 2, p. 209–217, accessed on January 15, 2016, at https://doi.org/10.1111/j.1745-6584.2006.00279.x.

Michael, H.A., Russoniello, C.J., and Byron, L.A., 2013, Global assessment of vulnerability to sea-level rise in topography-limited and recharge-limited coastal groundwater systems: Water Resources Research, v. 49, no. 4, p. 2228–2240, accessed on January 15, 2016, at https://doi.org/10.1002/wrcr.20213.

Misut, P.E., and Dressler, S., 2021, Simulation of water-table and freshwater/saltwater interface response to climate-change-driven sea-level rise and changes in recharge at Fire Island National Seashore, New York: U.S. Geological Survey Scientific Investigations Report 2020–5117, 47 p., https://doi.org/10.3133/sir20205117.

National Oceanic and Atmospheric Administration, 2016, accessed on April 15, 2017, at https://tidesandcurrents.noaa.gov/datums.html?datum=MSL&units=1&epoch=0&id=8570283&name=Ocean+City+Inlet&state=MD.

Niswonger, R.G., Panday, S., and Ibaraki, M., 2011, MODFLOW-NWT, A Newton formulation for MODFLOW-2005: U.S. Geological Survey Techniques and Methods 6–A37, 44 p., accessed on January 15, 2017, at https://doi.org/10.3133/tm6A37.

Pendleton, E.A., Williams, S.J., and Thieler, E.R., 2004, Coastal vulnerability assessment of Assateague Island National Seashore (ASIS) to lea-level rise: U.S. Geological Survey Open-File Report 2004–1020, 20 p., accessed on January 15, 2016, at https://doi.org/10.3133/ofr20041020.

Richardson, D.L., 1994, Hydrogeology and analysis of the ground-water-flow system of the Eastern Shore, Virginia: U.S. Geological Survey Water-Supply Paper 2401, 108 p., accessed on January 15, 2016, at https://doi.org/10.3133/wsp2401.

Sanford, W.E., Pope, J.P., Selnick, D.L., and Stumvoll, R.F., 2012, Simulation of groundwater flow in the shallow aquifer system of the Delmarva Peninsula, Maryland and Delaware: U.S. Geological Survey Open-File Report 2012–1140, 58 p., accessed on January 15, 2016, at https://doi.org/10.3133/ofr20121140.

Sanford, W.E., Pope, J.P., and Nelms, D.L., 2009, Simulation of groundwater-level and salinity changes in the Eastern Shore, Virginia: U.S. Geological Survey Scientific Investigations Report 2009–5066, 125 p., accessed on January 15, 2016, at https://doi.org/10.3133/sir20095066.

Schubert, C.E., 2010, Analysis of the shallow groundwater flow system at Fire Island National Seashore, Suffolk County, New York: U.S. Geological Survey Scientific Investigations Report 2009–5259, 106 p., accessed on January 15, 2016, at https://doi.org/10.3133/sir20095259.

Schupp, C., 2013, Assateague Island National Seashore—geologic resources inventory report: Fort Collins, Colo., National Park Service Natural resource report NPS/NRSS/GRD/NRR—2013/708.

Trapp, J., Jr., and Horn, M.A., 1997, Ground water atlas of the United States—Delaware, Maryland, New Jersey, North Carolina, Pennsylvania, Virginia, West Virginia: U.S. Geological Survey Hydrologic Investigations Atlas HA–730–L, 30 p., accessed on January 15, 2016, at https://doi.org/10.3133/ha730L.

U.S. Geological Survey (USGS), 2017, USGS water data for the Nation: U.S Geological Survey National Water Information System database, accessed on August 10, 2017, at https://doi.org/10.5066/F7P55KJN.

Voss, C.I., and Provost, A.M., 2002 (Version of September 22, 2010), SUTRA, A model for saturated-unsaturated variable-density ground-water flow with solute or energy transport: U.S. Geological Survey Water-Resources Investigations Report 02–4231, 291 p., accessed on January 15, 2016, at https://doi.org/10.3133/wri024231.

Walter, D.A., McCobb, T.D., Masterson, J.P., and Fienen, M.N., 2016, Potential effects of sea-level rise on the depth to saturated sediments of the Sagamore and Monomoy flow lenses on Cape Cod, Massachusetts: U.S. Geological Survey Scientific Investigations Report 2016–5058, 55 p., accessed on January 15, 2016, at https://doi.org/10.3133/sir20165058.

Ward, J.H., Jr., 1963, Hierarchical grouping to optimize an objective function: Journal of the American Statistical Association, v. 58, no. 301, p. 236–244, accessed on January 15, 2017, at https://doi.org/10.1080/01621459.1963.10500845.

Appendix 1. Water Level and Specific Conductance Data

Continuous water levels combined with specific conductance monitoring can provide information on the responsiveness of the shallow aquifer to precipitation, tides, and other hydrologic processes. Water levels were measured in 32 wells at 6-minute intervals for up to 12 months, from October 1, 2014, to September 30, 2015 (fig. 1.1; table 1.1). In four wells, specific conductance was recorded continuously. Hydrographs of water levels from well pairs and individual wells, and chemographs of specific conductance for the four wells are presented in figures.

Table 1.1. Description of wells used in study, Assateague Island, Maryland and Virginia.

[Sensor data refers to the type of continuous data that were collected. USGS, U.S. Geological Survey; latitude and longitude are reported in degrees, minutes, and seconds; ft, foot; NAVD 88, North American Vertical Datum of 1988; --, no data; WL, water level; SC, specific conductance]

USGS site number	Station name	Latitude	Longitude	Land-surface elevation (ft NAVD 88)	Well pair depth identifier	Well depth (ft)	Sensor data
380457075122301	WO Ff 11	38°04'57.7"	75°12'23.8"	3.15	Deep	52.5	WL
380457075122302	WO Ff 12	38°04'57.7"	75°12'23.8"	3.18	Shallow	12.1	WL; SC
380512075125401	WO Ef 36	38°05'12.4"	75°12'54.4"	2.02	Deep	50.8	WL
380512075125402	WO Ef 37	38°05'12.4"	75°12'54.4"	1.97	Shallow	11.7	WL; SC
380730075110401	WO Ef 30	38°07'30.5"	75°11'04.3"	3.52	Deep	52.4	WL
380730075110402	WO Ef 31	38°07'30.5"	75°11'04.3"	3.62	Shallow	11.7	WL
380731075105601	WO Ef 28	38°07'31.4"	75°10'56.2"	4.42	Deep	52	WL
380731075105602	WO Ef 29	38°07'31.4"	75°10'56.2"	4.44	Shallow	12.8	WL
380731075111101	WO Ef 32	38°07'31.0"	75°11'11.5"	2.32	Deep	52.7	WL
380731075111102	WO Ef 33	38°07'31.56"	75°11'11.26"	2.06	Shallow	9.9	WL
380734075111301	WO Ef 34	38°07'34.1"	75°11'13.8"	3.33	Deep	51.7	WL
380734075111302	WO Ef 35	38°07'34.1"	75°11'13.8"	3.63	Shallow	11.8	WL
380837075112201	WO Ef 26	38°08'34"	75°11'17"	5.33	Deep	100	WL
380837075112202	WO Ef 27	38°08'34"	75°11'17"	5.44	Shallow	35	WL
381155075091801	WO Dg 33	38°11'55.67"	75°09'19.30"	4.66	Deep	51.9	WL
381155075091802	WO Dg 34	38°11'55.6"	75°09'18.8"	4.28	Shallow	11.4	WL
381157075092901	WO Dg 35	38°11'57.1"	75°09'29.1"	1.45	Deep	51.9	WL
381157075092902	WO Dg 36	38°11'57.1"	75°09'29.1"	1.68	Shallow	9.4	WL
381427075081102	WO Dg 21	38°14'28.3"	75°08'10.8"	4.94	--	310	WL
381428075081401	WO Dg 23	38°14'28.3"	75°08'10.9"	4.45	Deep	85	WL
381428075081402	WO Dg 24	38°14'28.3"	75°08'10.9"	4.26	Shallow	35	WL
381428075081403	WO Dg 25	38°14'28.3"	75°08'10.8"	4.28	--	15	WL
381450075075401	WO Dg 27	38°14'50.6"	75°07'54.0"	2.83	Deep	22	WL
381450075075402	WO Dg 28	38°14'50.6"	75°07'54.0"	3.00	Shallow	12.1	WL
381452075075901	WO Dg 29	38°14'52.23"	75°07'58.93"	5.71	Deep	52.2	WL
381452075075902	WO Dg 30	38°14'52.0"	75°07'59.0"	5.88	Shallow	16.8	WL
381452075080101	WO Dg 31	38°14'52.9"	75°08'01.7"	7.45	Deep	52.7	WL
381452075080102	WO Dg 32	38°14'52.9"	75°08'01.7"	6.73	Shallow	12.4	WL
381804075063401	WO Cg 104	38°18'04.8"	75°06'34.2"	4.87	Deep	51.3	WL
381804075063402	WO Cg 103	38°18'04.81"	75°06'34.24"	4.91	Shallow	12.4	WL; SC
381805075063501	WO Cg 102	38°18'05.4"	75°06'35.5"	10.39	Deep	57.4	WL
381805075063502	WO Cg 101	38°18'05.4"	75°06'35.5"	10.24	Shallow	17	WL; SC

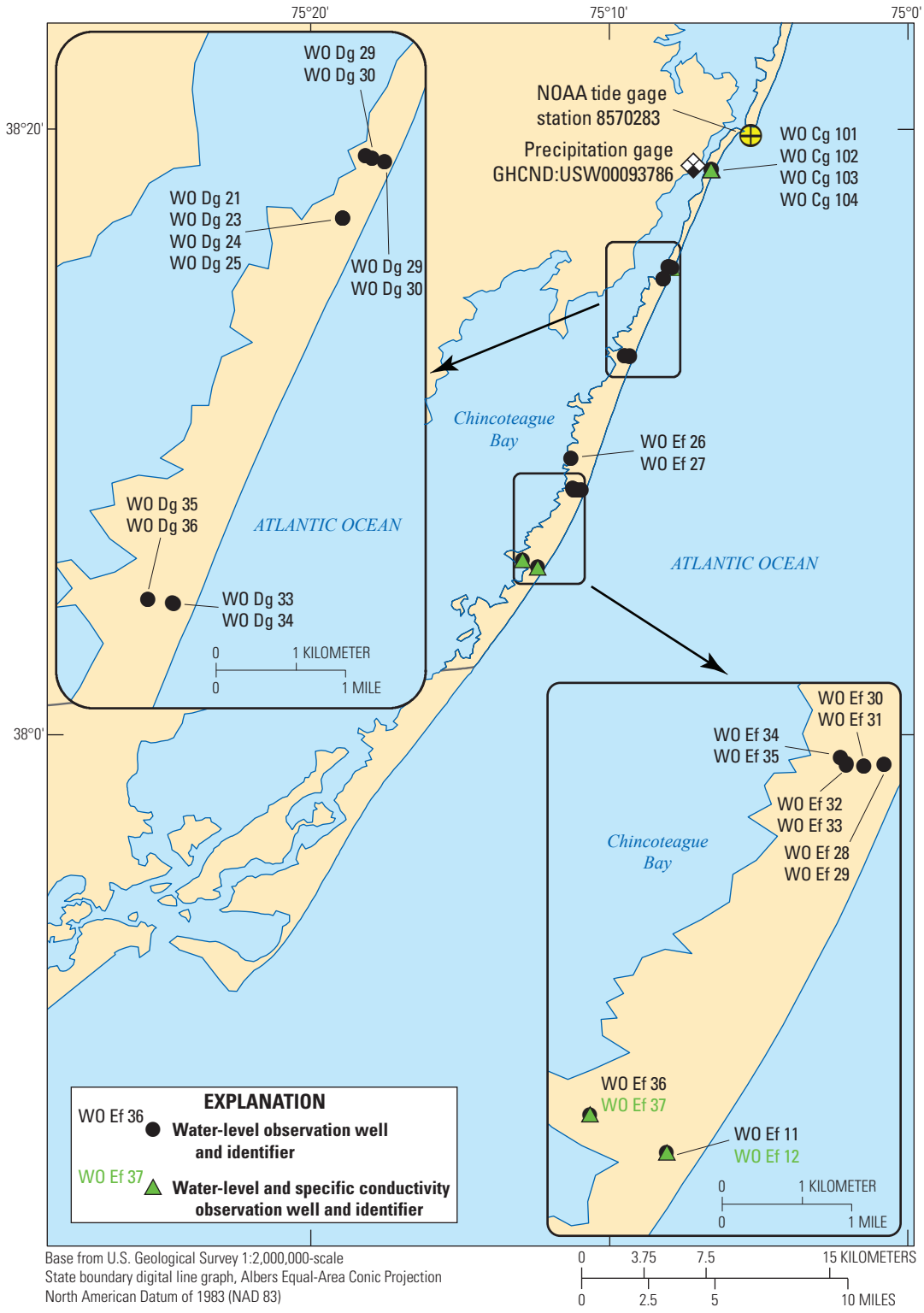

Figure 1.1. Locations of monitoring wells, tide gage, and precipitation gage at Ocean City Municipal Airport, Assateague Island and vicinity, Maryland and Virginia. (NOAA, National Oceanic and Atmospheric Administration)

Wells

The monitoring wells used in the study are listed in table 1.1. Wells that are part of a pair are designated as deep or shallow wells. Of the 32 monitoring wells used in this study, 26 were installed as 13 well pairs in five east-west trending transects (Banks and others, 2012). These well pairs have a shallow well screened approximately 10 feet (ft) below land surface and a deep well screened approximately 45–55 ft below land surface (Banks and others, 2012).

The other six wells in the study were installed as part of an effort to quantify the nutrient fluxes to the Chincoteague and Sinupuxent Bays (Dillow and others, 2002). Four (2 pairs) of these six wells are deeper than the well pairs installed by Banks and others (2012), with the shallow wells finished at 35 ft below land surface and the deep wells finished at 85 and 100 ft below land surface. One well from this study (381427075081102) accesses the deep Manokin aquifer, and one well (381428075081403) is finished in the shallow surficial aquifer.

Precipitation and Sea-level Observations

Hourly mean sea-level altitudes recorded at National Oceanic and Atmospheric Administration (NOAA) station 8570283 from October 1, 2014, to September 30, 2015, are displayed in figure 1.2, (NOAA, 2017). Although these data are the closest sea-level observations to Assateague Island, they do not necessarily represent the fluctuations in sea level observed within Sinepuxent and Chincoteague Bays, which are expected to experience a dampened and delayed tidal response. Daily precipitation data shown in figure 1.2 were collected at Ocean City Municipal Airport (Station identifier: GHCND:USW00093786) and accessed via the Global Historical Climatology Network (Menne and others, 2012). Recorded precipitation is evenly distributed seasonally, though the expected recharge from this precipitation will vary depending on the rainfall rate, antecedent soil moisture, evapotranspiration rate, topography, and other factors.

Continuous Water-Level Monitoring

Continuous water-level monitoring can provide information on the responsiveness of different parts of the shallow aquifer to precipitation, tidal cycles, and seasonal recharge variation. In the 32 wells listed in table 1.1, water levels were collected at 6-minute intervals using the CTD-DIVER Water Level Logger. Barometric measurements, made with the BARO-DIVER Water Level Logger, were made at five locations across Assateague Island, and these data were used to correct for atmospheric pressure variations. Manual water-level measurements were obtained monthly at all wells. Water levels were quality assured according to methods described in Cunningham and Schalk, (2011). In figure 1.3*A*–*Q*, the daily mean water-table altitudes for October 1, 2014, to September 30, 2015, are displayed for well pairs. The water-level data are available through the U.S. Geological Survey (USGS) National Water Information System (NWIS) database (USGS, 2017).

The manner in which groundwater levels respond to recharge events provides qualitative data on the sensitivity of the aquifer to changes in recharge. For most well pairs, shallow wells finished more than 20 ft deep are generally more responsive to precipitation than deeper wells. In these shallow wells, there is a quick rise in groundwater level coincident with observed precipitation and a gradual decrease over several days to weeks during periods without substantial recharge.

Deep wells and wells near the Atlantic shoreline are more responsive to changes in the tides, which is consistent with the 7 weeks of data collected by Banks and others (2012). For precipitation-affected wells, the greatest groundwater levels were observed from January to March, which can be attributed to decreased evapotranspiration during these months. The deepest well monitored in this study (381427075081102; 310 ft deep) displays a strong seasonal trend likely affected by seasonal withdrawals in nearby Ocean City, Md.

For most of the well pairs, the water level in the shallow well is consistently higher than that in the deep well, indicating downward groundwater movement for most of the observation period. One notable deviation from this pattern is for wells 381155075091801 and 381155075091802, where a substantial rise in water-level altitude from late February to early March 2015 caused an apparent head gradient reversal (fig. 1.3*H*).

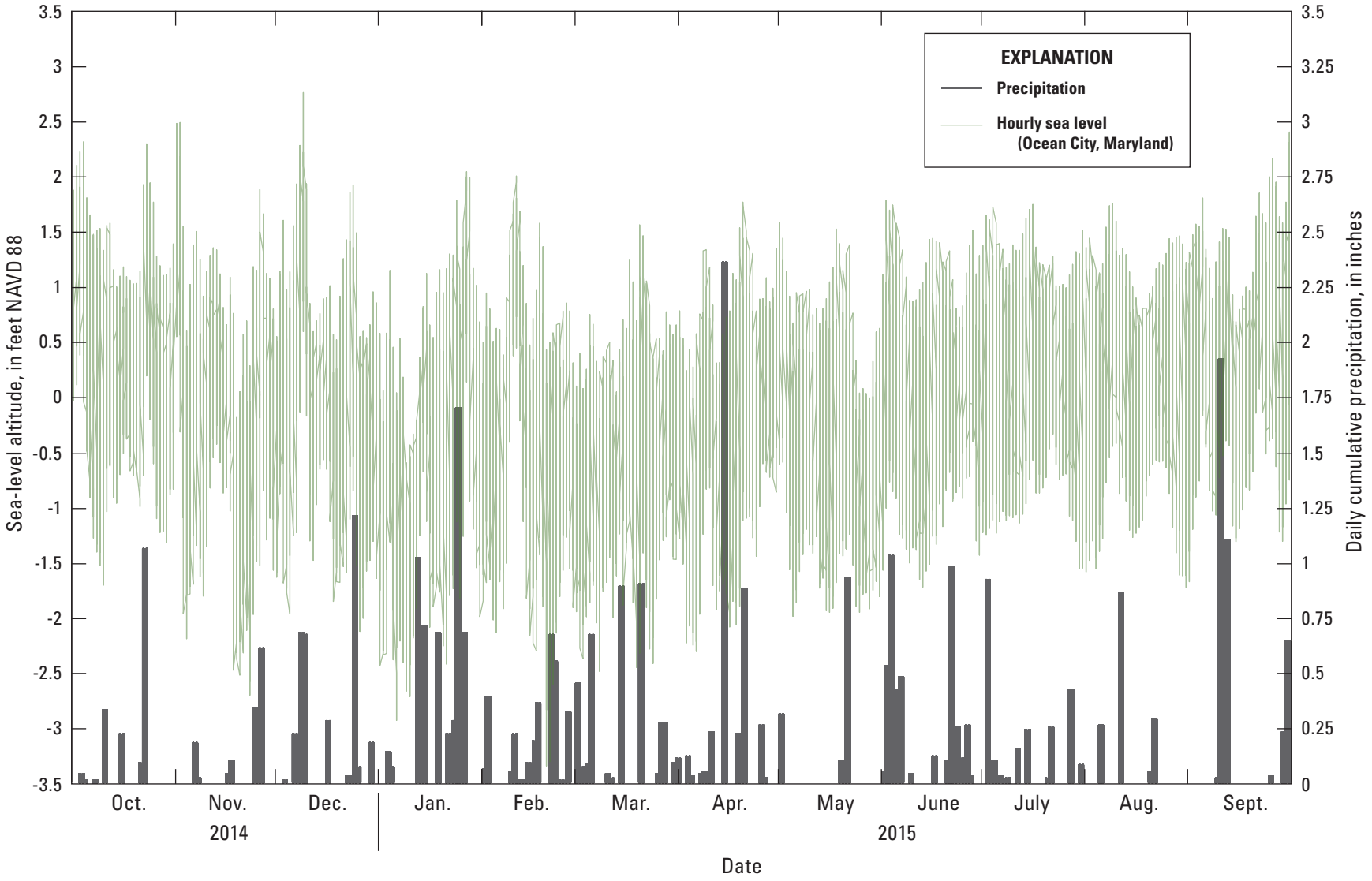

Figure 1.2. Hourly mean sea-level altitudes recorded by the National Oceanic and Atmospheric Administration tide gage at Ocean City Inlet and daily cumulative precipitation recorded by the precipitation gage at Ocean City Municipal Airport, Assateague Island and vicinity, Maryland and Virginia, from October 1, 2014, to September 30, 2015.

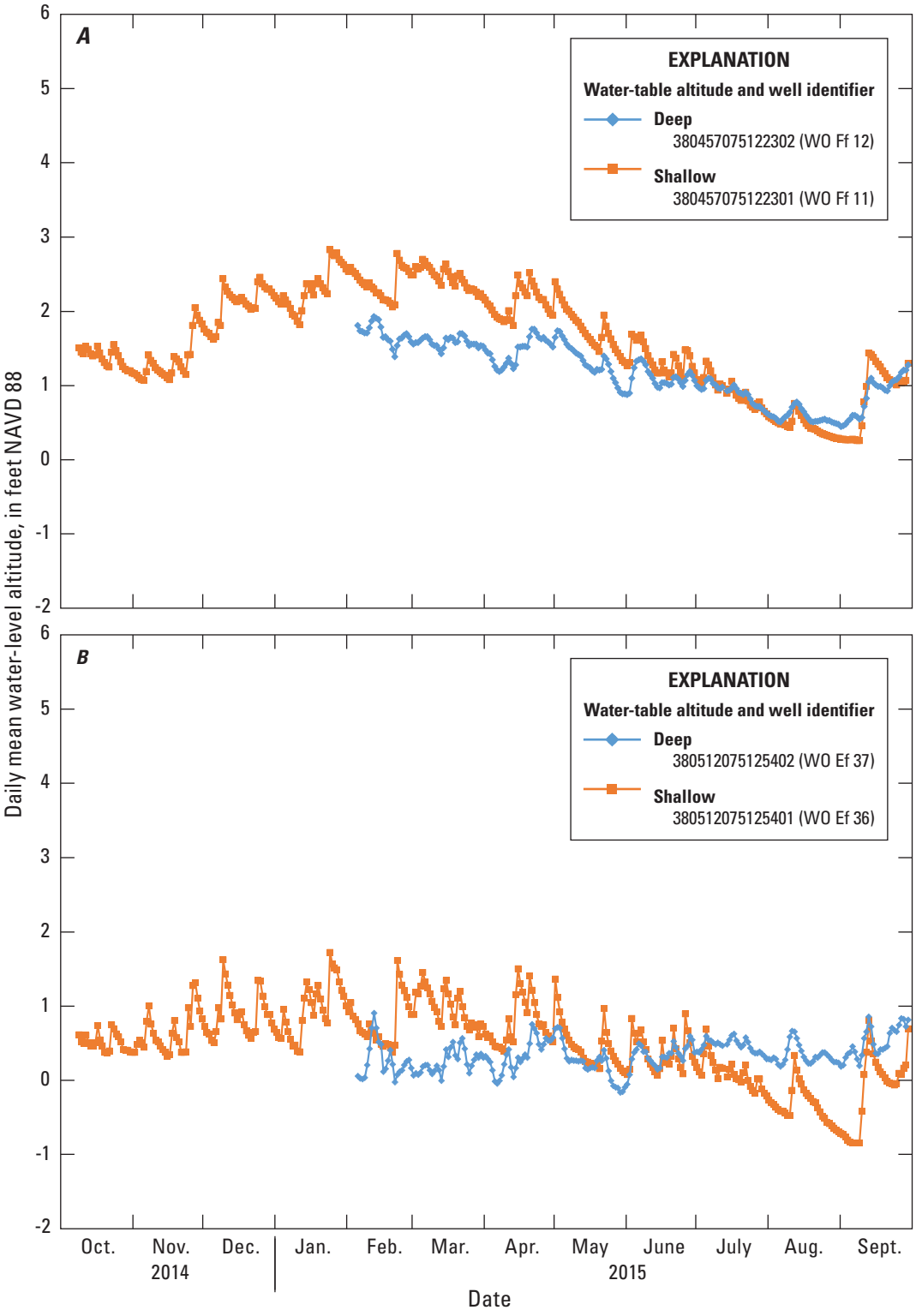

Figure 1.3. Daily mean water-table altitudes in, *A*–*Q*, 32 monitoring wells, Assateague Island, Maryland and Virginia. Deep and shallow wells are co-located to form a well pair and are plotted on the same axes in figure 1.3*A*–*O*. For a well pair, the last two digits of the 15-digit U.S. Geological Survey well identification number identifies a well as deep (01) or shallow (02). Figure 1.3*P* displays water-table altitudes for a shallow well, and figure 1.3*Q* displays water-table altitudes for a deep well accessing the regional aquifer.

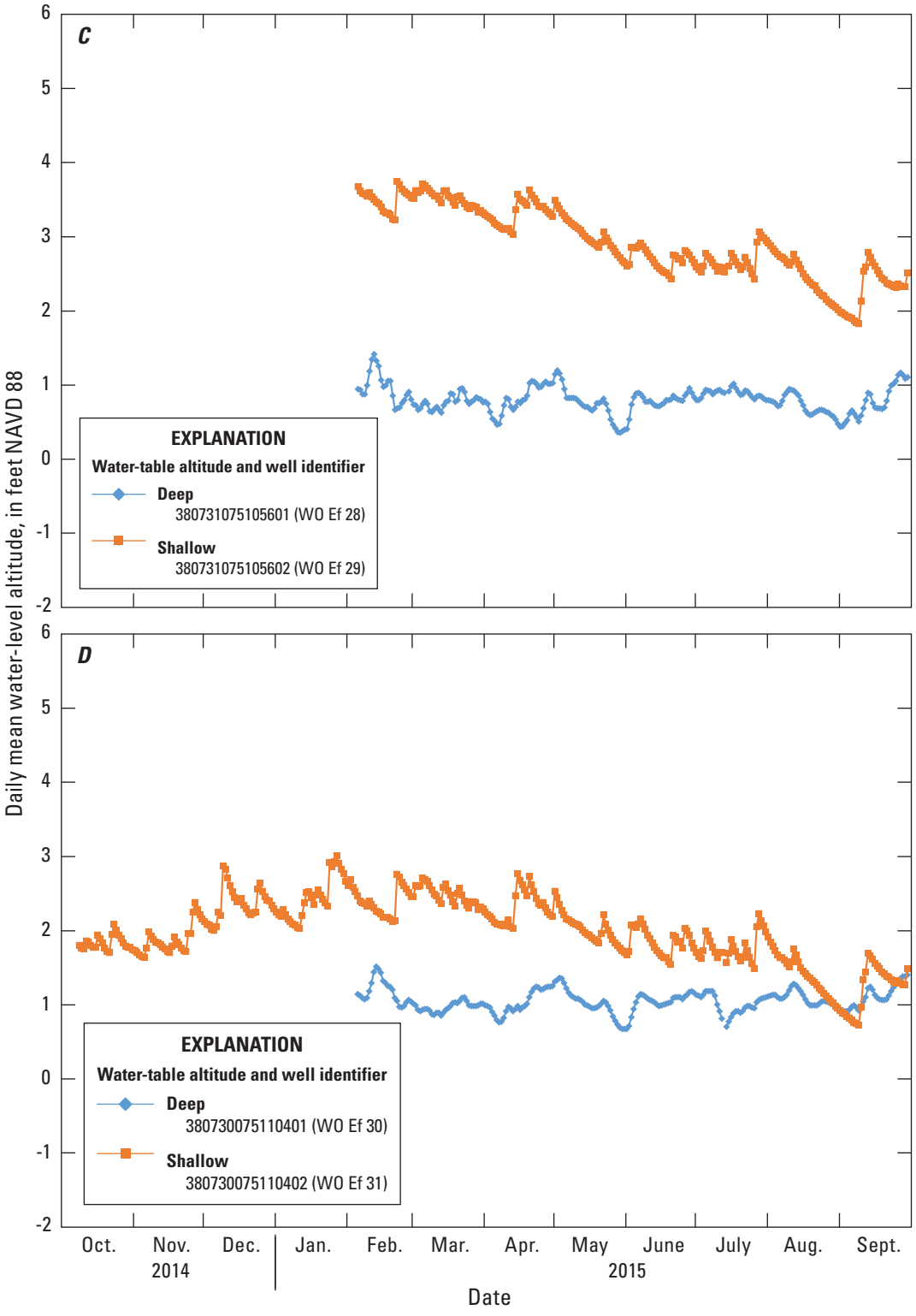

Figure 1.3.—Continued

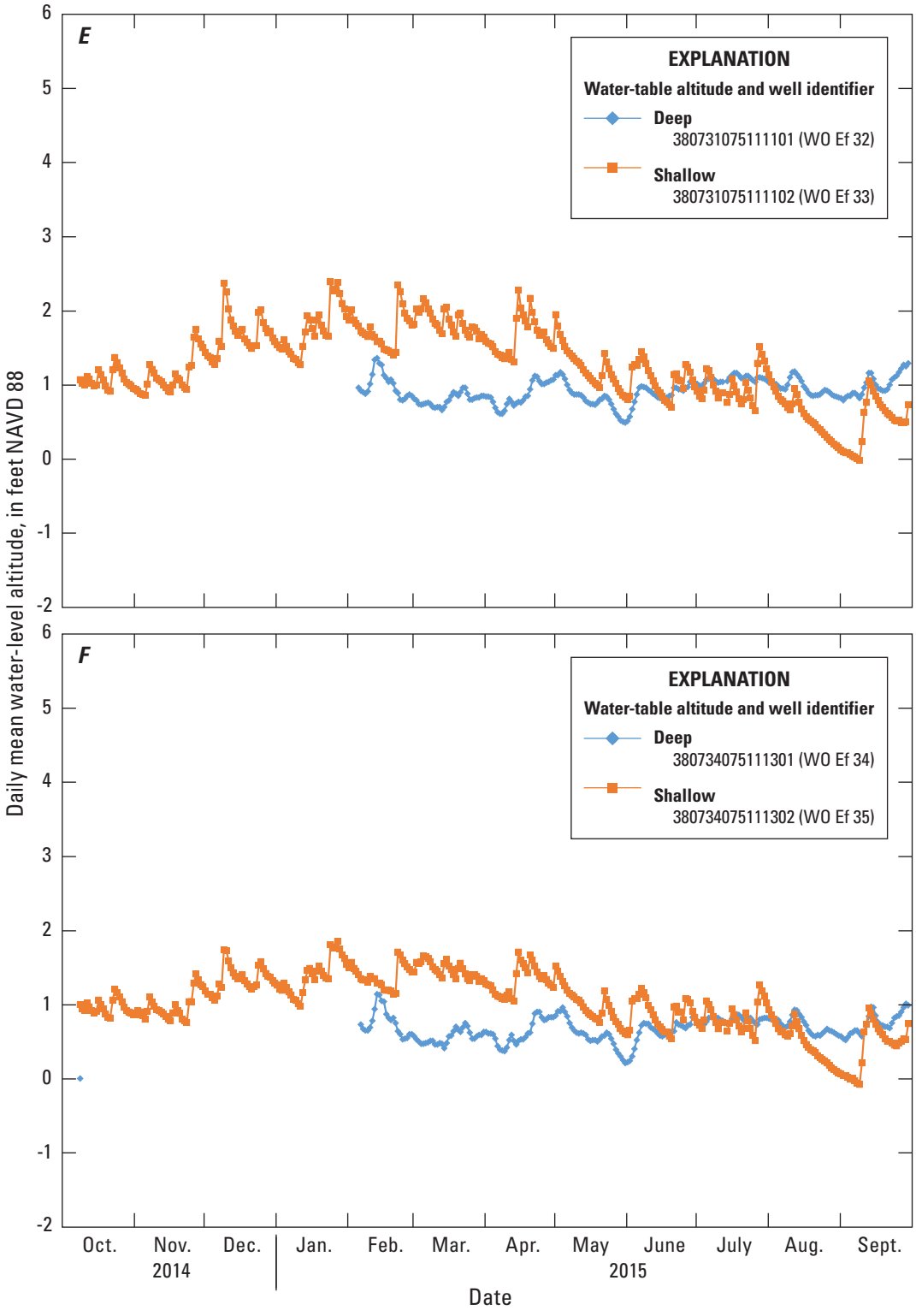

Figure 1.3.—Continued

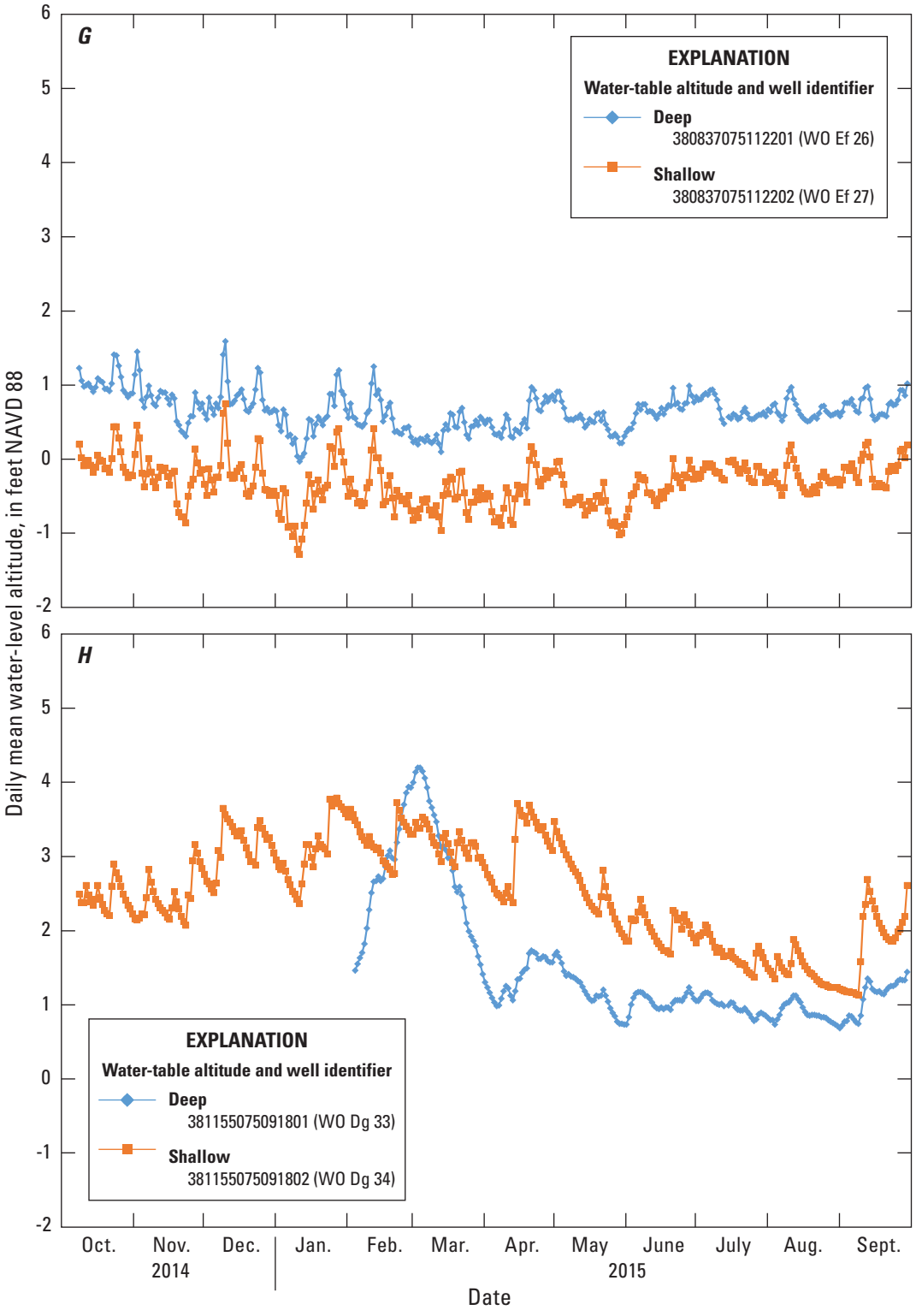

Figure 1.3.—Continued

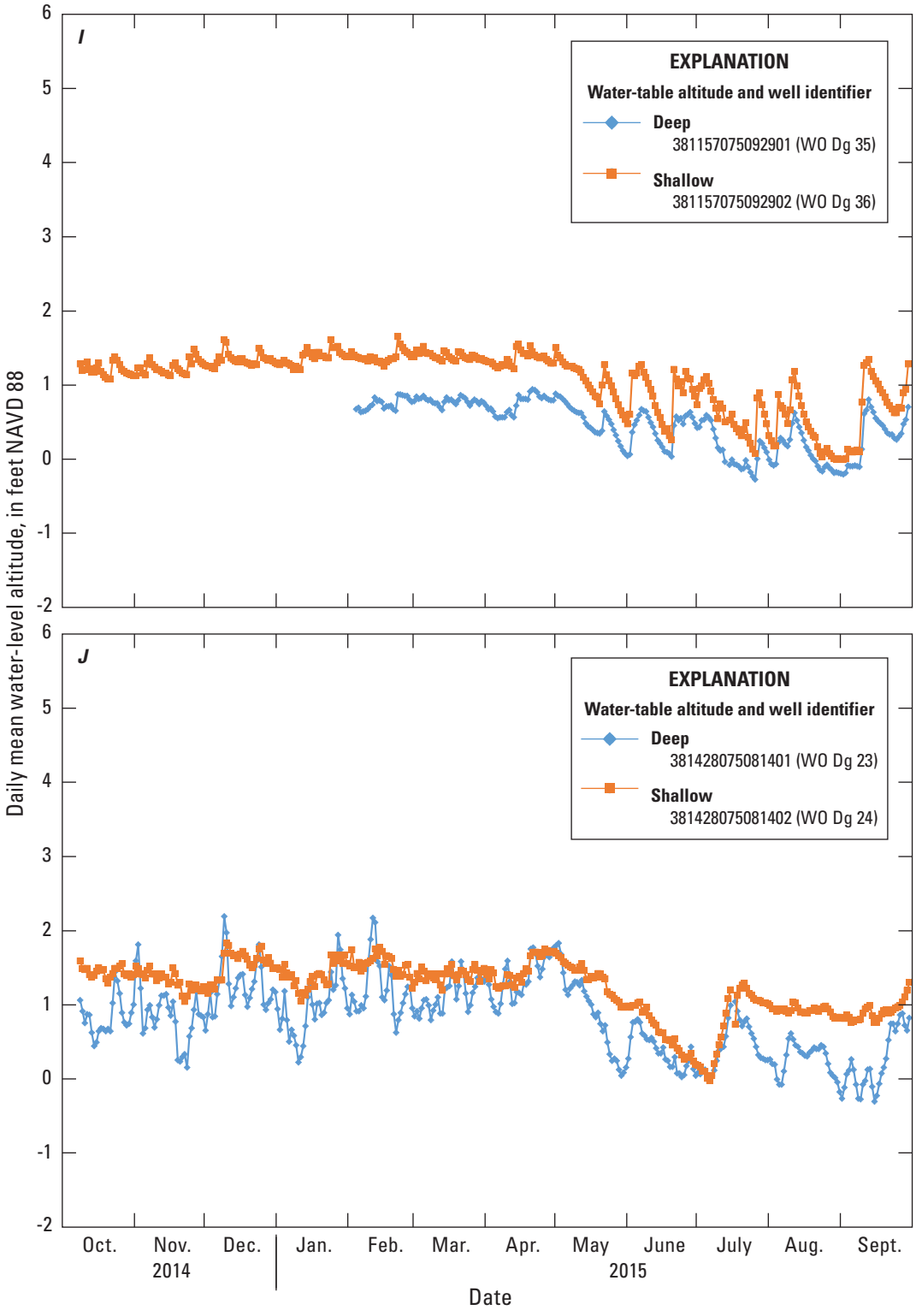

Figure 1.3.—Continued

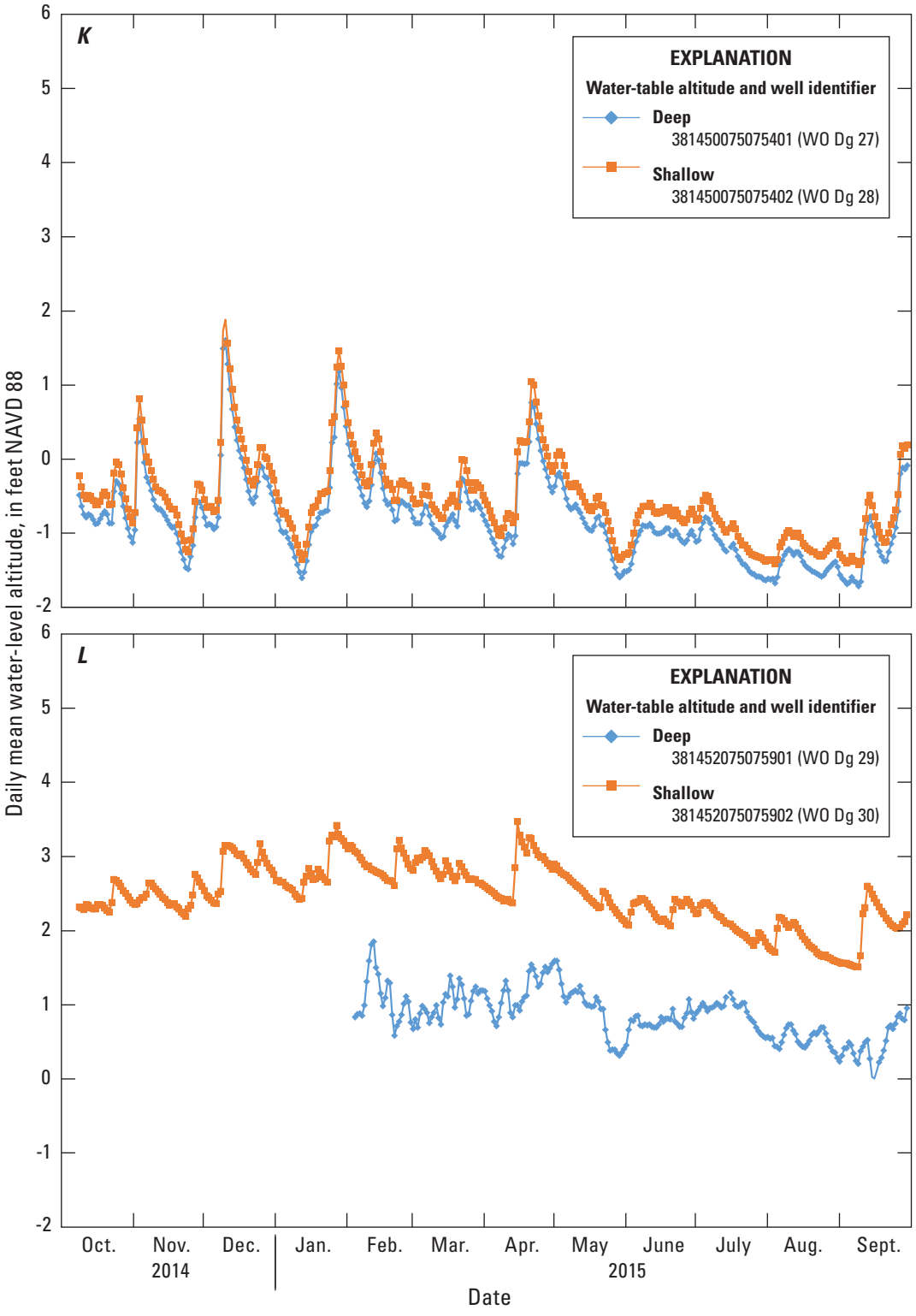

Figure 1.3.—Continued

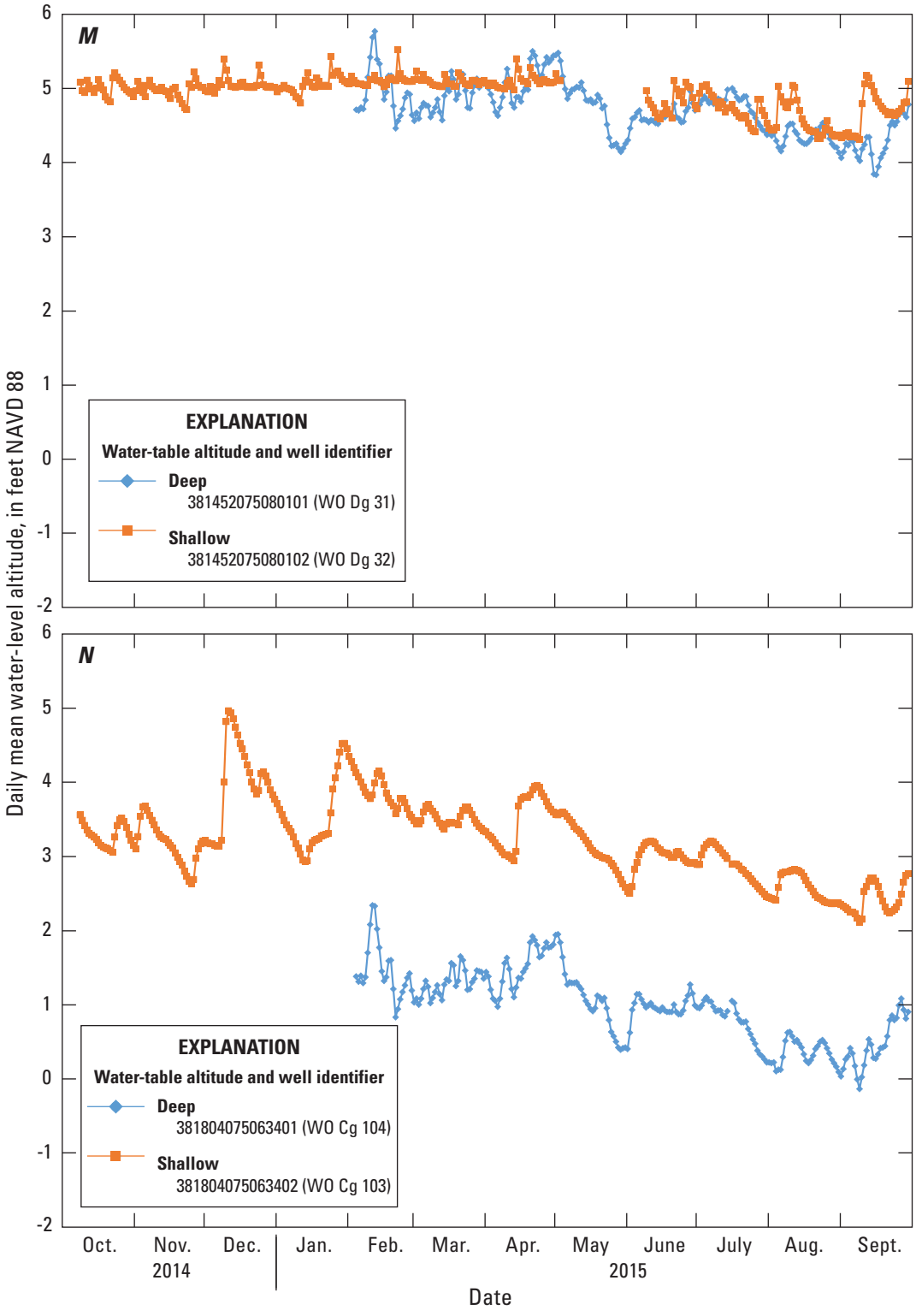

Figure 1.3.—Continued

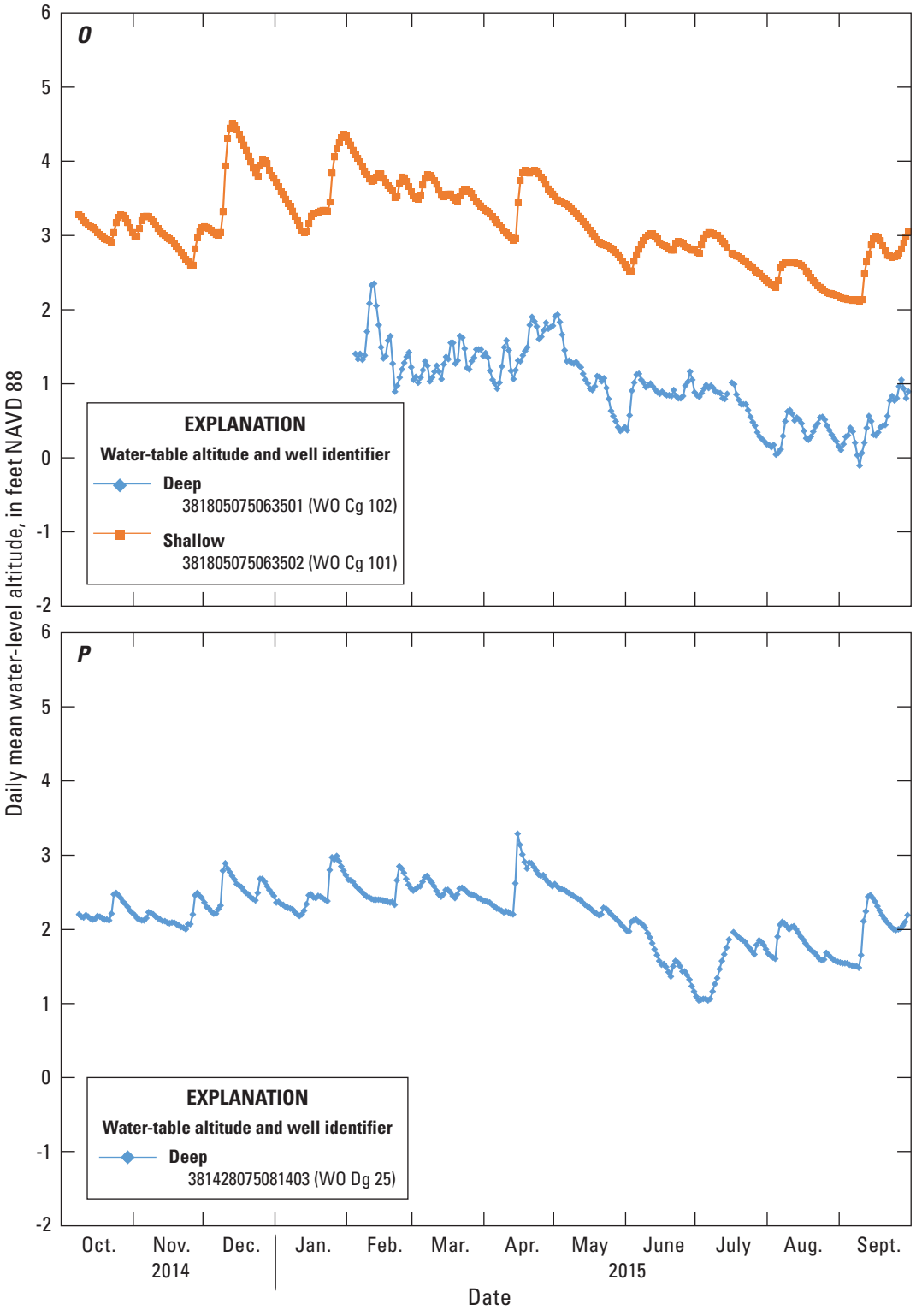

Figure 1.3.—Continued

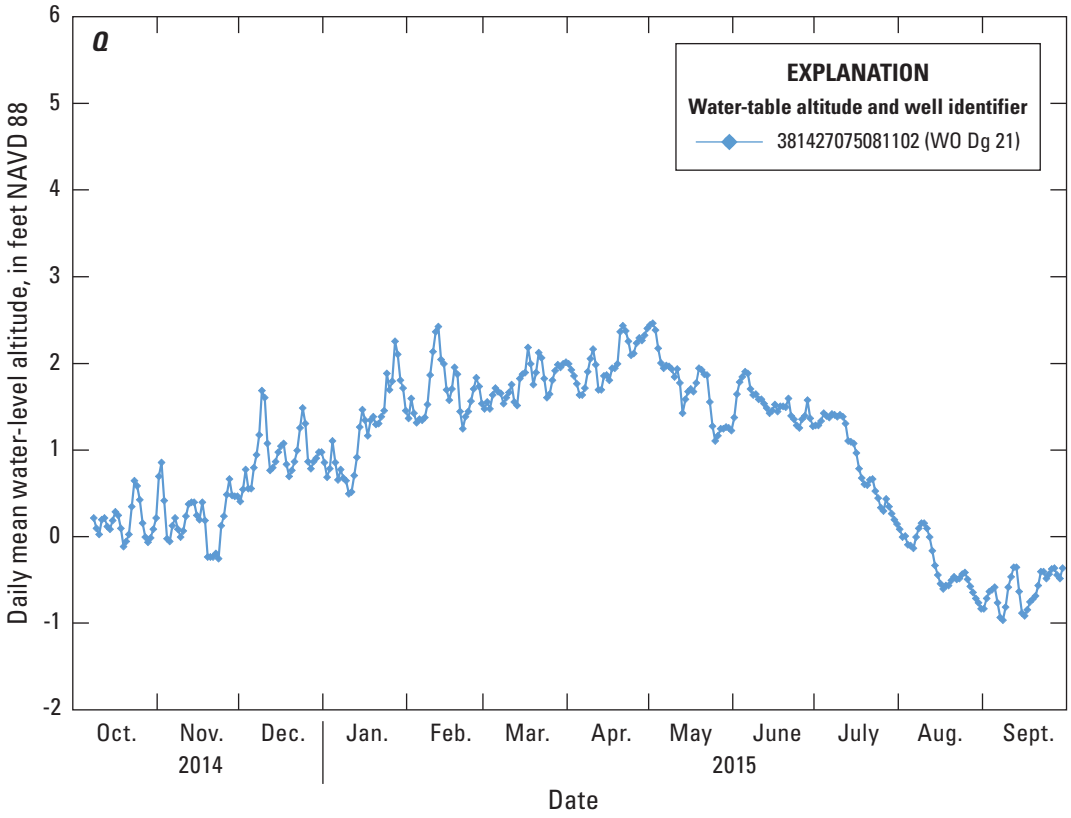

Figure 1.3.—Continued

Continuous Specific Conductance Monitoring

The continuous specific conductance monitoring in this study allows for the evaluation of transient and seasonal changes in dissolved ion content in the shallow aquifer. Specific conductance is an established proxy for dissolved salt content, with seawater approaching 50,000 microsiemens per centimeter at 25 degrees Celsius (µS/cm). For this study, four shallow monitoring wells (12–17 ft below land surface) along two sections across the island were monitored continuously. These wells are identified in table 1.1, and the data for these wells are available on the USGS NWIS database (USGS, 2017). Specific conductance was measured every 6 minutes by a Van Essen CTD Diver conductance probe. A water temperature correction was applied to report the data in µS/cm at 25 °C. Manual measurements of specific conductance were made July 13 and 15, 2015, following well evacuation and purging; these data were used to confirm that the specific conductance data observed by the well sensor was representative of aquifer conditions. In some deep wells, the continuous specific conductance observations changed following well purging, indicating well stratification or other factors are affecting the representativeness of the specific conductance observations. These data were excluded from the following analysis.

In figure 1.4, daily mean specific conductance values are shown for the 2014–15 period. The two wells in the southern part of the island have specific conductance concentrations of less than 1,800 µS/cm and do not respond to high sea-level events. Well 380457075122302 (fig. 1.4*A*) is closer to the Atlantic side of the island and has higher specific conductance, but groundwater is still relatively fresh and consistent throughout the year. From October 2014 to February 2015, the specific conductance shows stepwise decreases coincident with precipitation, indicating aquifer recharge and freshening. Both southern wells are on a narrow island section behind a high Atlantic Ocean facing dune, which may be preventing storm overwash or saline deposition.

The two northern monitoring wells (381804075063402 and 381805045063502) had greater specific conductance concentrations than the two southern monitoring wells. Several episodic increases in specific conductance lasting several days

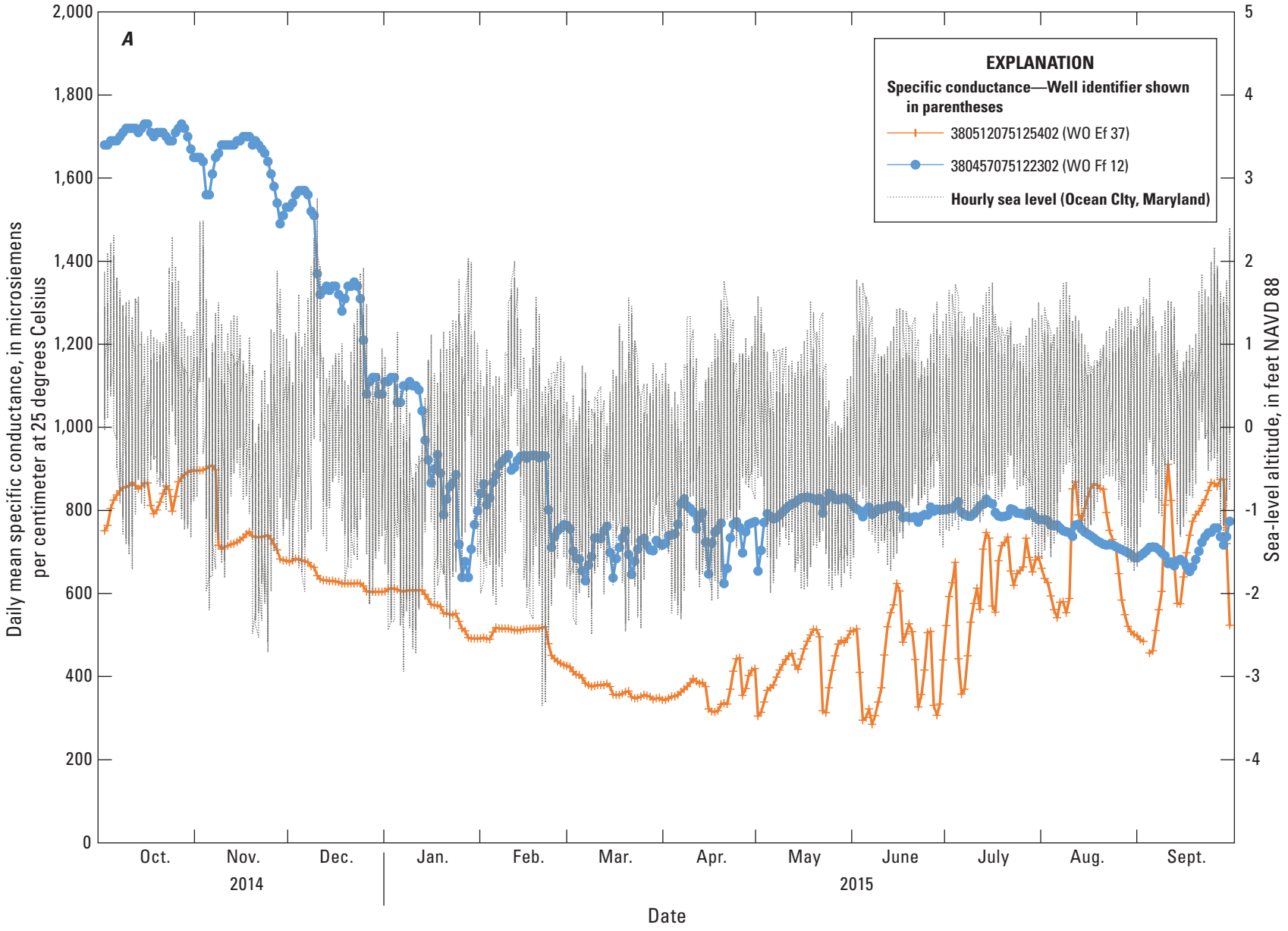

Figure 1.4. Daily mean specific conductance and sea-level altitude in four shallow monitoring wells on Assateague Island, Maryland and Virginia: *A*, two shallow wells in the southern part of Assateague Island and *B*, two shallow wells in the northern part of the island. (Note the y axis scale difference in *A* and *B*).

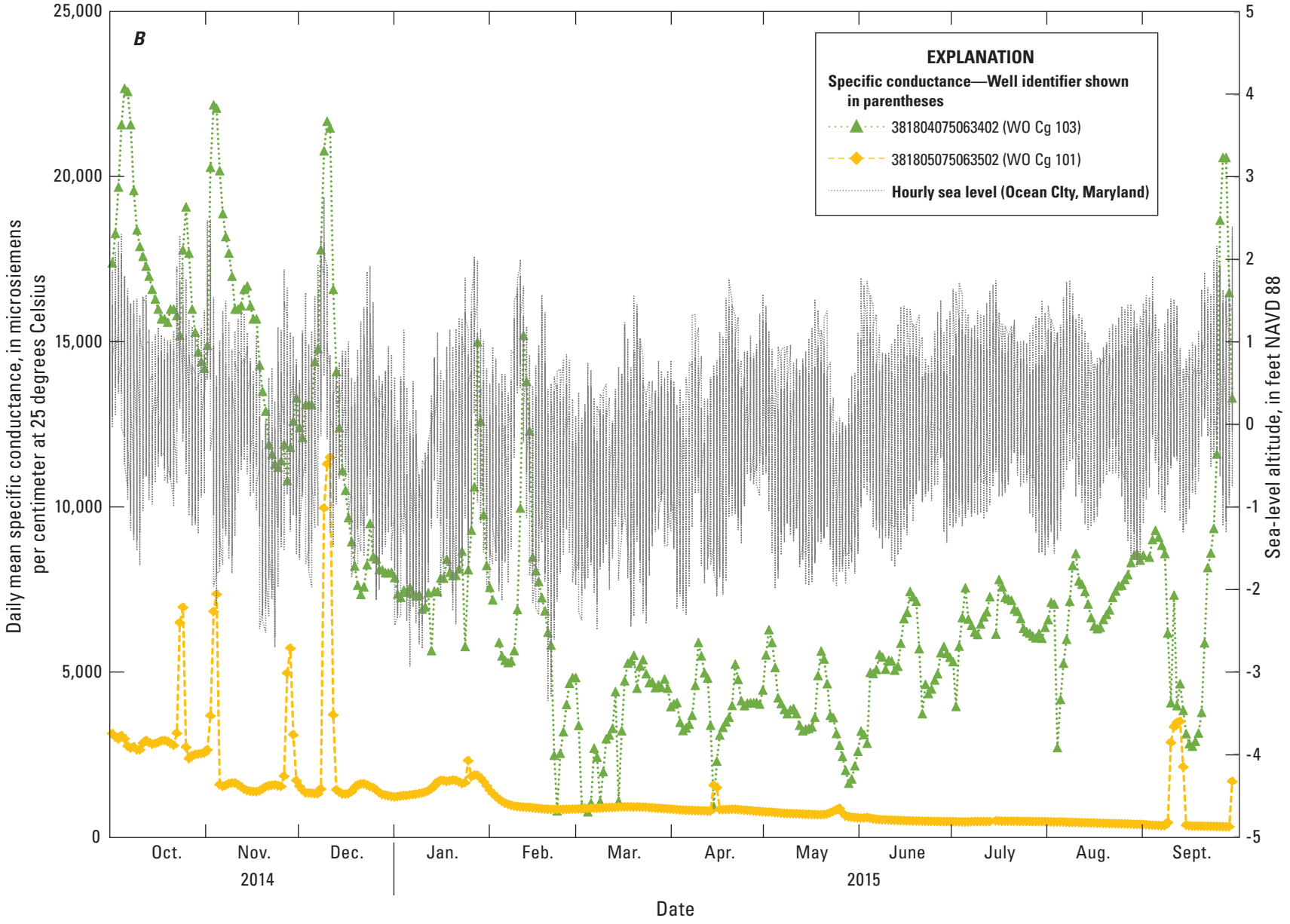

Figure 1.4.—Continued

during October 2014–February 2015 were observed to be coincident with peaks in sea level. Well 381804075063402, which experienced the highest specific conductance approaching one-half the concentration for that of seawater, is closest to the Atlantic shoreline and resides in a low-lying land-surface depression 4.91 ft above sea level (asl). The other northern well (381805045063502) is more inland and at a higher land-surface altitude (10.24 ft asl). The observed peaks in specific conductance may be the result of storm overwash events. A seasonal variation in specific conductance is observed only in well 381804075063402, which likely decreases in specific conductance in the winter and spring 2015 because of decreased evapotranspiration.

References Cited

Banks, W.S.L., Masterson, J.P., and Johnson, C.D., 2012, Well network installation and hydrogeologic data collection, Assateague Island National Seashore, Worcester County, Maryland, 2010: U.S. Geological Survey Scientific Investigations Report 2012–5079, 20 p., accessed on December 15, 2014, at https://doi.org/10.3133/sir20125079.

Cunningham, W.L., and Schalk, C.W., comps., 2011, Groundwater technical procedures of the U.S. Geological Survey: U.S. Geological Survey Techniques and Methods 1–A1, 151 p., accessed on December 15, 2015, at https://pubs.usgs.gov/tm/1a1/

Dillow, J.J.A., Banks, W.S.L., and Smigaj, M.J., 2002, Groundwater quality and discharge to Chincoteague and Sinepuxent Bays adjacent to Assateague Island National Seashore, Maryland: U.S. Geological Survey Water-Resources Investigations Report 02–4029, 42 p., accessed on December 15, 2014, at https://doi.org/10.3133/wri024029.

Menne, M.J., Durre, I., Korzeniewski, B., McNeal, S., Thomas, K., Yin, X., Anthony, S., Ray, R., Vose, S.R., Gleason, B.E., and Houston, T.G., 2012, Global Historical Climatology Network—Daily (GHCN-Daily), version 3, Station USW00093786: NOAA National Climatic Data Center, accessed on May 26, 2016, at https://doi.org/10.7289/V5D21VHZ.

National Oceanic and Atmospheric Administration (NOAA), 2017, Mean sea level trend at tide gauge 8570283 Ocean City Inlet, MD: NOAA, accessed on August 10, 2017, at https://tidesandcurrents.noaa.gov/sltrends/sltrends_station.shtml?stnid=8570283.

U.S. Geological Survey (USGS), 2017, USGS water data for the Nation: U.S. Geological Survey National Water Information System database, accessed on August 10, 2017, at https://doi.org/10.5066/F7P55KJN.

Appendix 2. Model Development

Development of the Groundwater-Flow Model

A steady-state three-dimensional groundwater-flow model was developed to simulate the groundwater system of Assateague Island National Seashore. The coastal model used in this analysis was developed using the Seawater Intrusion SWI2 Package (Bakker and others, 2013), a MODFLOW package capable of simulating a dynamic saltwater interface position. SWI2 allows three-dimensional vertically integrated variable-density groundwater flow with MODFLOW-NWT (Niswonger and others, 2011) through the addition of pseudo-source terms to the groundwater flow equation. Vertical and horizontal movement of a defined isodensity surface is calculated separately using a combination of flows calculated through the solution of the groundwater flow equation and a simple algorithm to track the front end of the freshwater/saltwater interface (Bakker and others, 2013; Walter and others, 2016).

This model is based on a previous groundwater-flow model developed for Assateague Island (Masterson and others, 2013) that used the U.S. Geological Survey (USGS) computer program SEAWAT (Langevin and others, 2008) to simulate the groundwater-flow system. The previous model simulates variable-density groundwater flow by coupling the groundwater-flow code MODFLOW-2000 (Harbaugh and others, 2000) and the solute transport code MT3D (Zheng and Wang, 1999). Dispersive solute transport simulations require relatively fine discretization, resulting in a large number of grid cells, which can reach computational limitations of some desktop computers. Numerical simulations using the SWI2 package require far fewer cells than solute transport simulations (Bakker and others, 2013) because they can represent three-dimensional vertically integrated variable-density flow without the need to discretize the aquifer vertically. In the case of Assateague Island National Seashore, reducing the number of layers in the model allows for a finer horizontal grid spacing, thus improving the spatial discretization of the groundwater-flow model while staying within computational limits of a desktop computer.

The USGS computer program UCODE_2014 (Poeter and others, 2005; Poeter and others, 2014) was used to estimate model parameters, perform sensitivity analysis, and calibrate the model to measured water levels from wells and estimated water levels from detailed vegetation community surveys (Sneddon and others, 2017).

Model Discretization

The finite-difference model grid consists of uniformly spaced model cells that are 25 meters (m) on a side. The grid consists of 2,480 rows and 600 columns that extend from the Ocean City inlet in Maryland to Toms Cove, Virginia. The upper left corner of the model domain is at x = 485,048 m and y = 4,246,162 m (UTM zone 18) and is rotated −28 degrees. This model shares the same extent as the earlier model (Masterson and others, 2013), and the model grid includes parts of the mainland west of Chincoteague and Sinepuxent Bays, but the active model domain includes only an area around the barrier island approximately 3,000 m to the west into Chincoteague and Sinepuxent Bays and 2,000 m to the east into the Atlantic Ocean. Included in the active model domain is Sinepuxent Neck in the northern extent of the model.

The model has 1 layer that extends from land surface to a maximum depth of 30 m below the North American Vertical Datum of 1988 (NAVD 88), coincident with the top of the Upper Chesapeake confining unit, which separates the surficial aquifer from the underlying confined aquifers of the North Atlantic Coastal Plain. The top of the model grid was defined by using the central node of each 25 m by 25 m model cell to extract an altitude from a merged topographic-bathymetric digital surface constructed for the study area by Masterson and others (2013). Extracting altitudes with the refined model grid produces four times the spatial resolution of the island topography than the previous groundwater-flow model.

Boundary Conditions

Boundary conditions control the movement of water in a groundwater-flow model and can be thought of as a series of water sources and sinks. In the case of Assateague Island, there are sources and sinks of freshwater (recharge, evapotranspiration, surface seepage) and saltwater (saline water bodies) that in combination with the model hydraulic properties determine the position of the water table and the freshwater/saltwater interface. Initial values of these boundary conditions were taken from Masterson and others (2013) and modified in this study through the model calibration process.

Recharge

Recharge occurs as direct percolation of infiltrating precipitation. Recharge to the groundwater system was simulated using the recharge package (RCH) of MODFLOW-NWT. Recharge values were assigned to five zones across the

island on the basis of vegetation and groundcover (fig. 2.1). The range of recharge values is similar to the values used in Masterson and others (2013).

Evapotranspiration

Evapotranspiration from groundwater is simulated explicitly as a head-dependent flux boundary condition using the EVT package. The required inputs for the EVT package are evapotranspiration rate, extinction depth, and surface altitude. A maximum evapotranspiration rate was assigned uniformly to each land-surface cell across the model. The extinction depth was assigned to five zones on the basis of vegetation and ground cover coincident with the five recharge zones (fig. 2.1). The evapotranspiration flux decreased linearly with depth and with a decrease in water-table altitude, whereas the water level was above the extinction depth in a cell.

Freshwater/Saltwater Interface

The ultimate position of the freshwater/saltwater interface was determined by the model; however, the model required an initial position of the freshwater/saltwater interface, just as it required an initial head distribution. This initial freshwater/saltwater interface position was calculated using the Ghyben-Herzberg relation (Ghyben, 1889; Herzberg, 1901) and the final head solution extrapolated from Masterson and others (2013).

General-Head Boundaries

Head-dependent flux boundaries were used to represent the saltwater bodies surrounding Assateague Island, including the Atlantic Ocean, Chincoteague Bay, and Sinepuxent Bay. The following equation was used to calculate the freshwater equivalent head altitudes for the coastal and inland bay general-head boundaries on the basis of the depth of open saltwater and the estimated density of back bay or ocean water:

$$h_{fw} = -0.109m + (\rho_{sw} - \rho_{fw}) * Depth_{sw}, \quad (1)$$

where

h_{fw} is the equivalent freshwater altitude (NAVD 88);

−0.109 m is the 1981–2000 mean sea level at Ocean City, Md., inlet (NAVD 88);

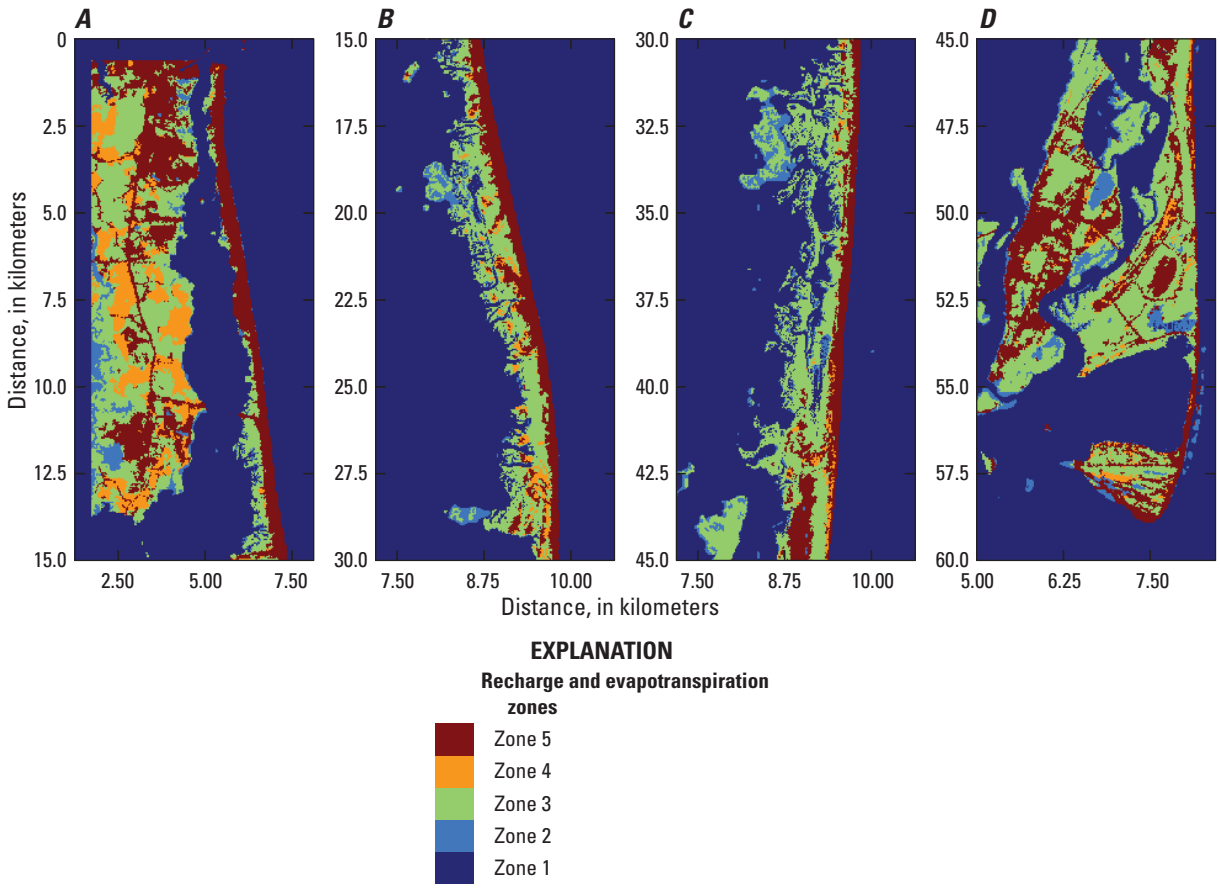

Figure 2.1. Recharge and evapotranspiration zones within model sections A–D, Assateague Island, Maryland and Virginia.

ρ_{sw} is the estimated density of saltwater at a given location;
ρ_{fw} is the density of freshwater; and
$Depth_{sw}$ is the depth of open saltwater at a given location.

Surface Seepage

A seepage face boundary was assigned to each land-surface cell of the model using the DRN (drain) package in MODFLOW-NWT (Niswonger and others, 2011). In this approach, all cells are represented as drains, which remove water from the aquifer at a rate proportional to the difference between the head in the aquifer and some fixed head or altitude, called the drain altitude (the altitude assigned to each DRN cell is the same as land surface), as long as the head in the aquifer is above that altitude (Harbaugh, 2005). If, however, the aquifer head falls below the drain altitude, the drain has no effect on head in the aquifer. The constant of proportionality is called the drain conductance. When using the drain approach, it is assumed that there are no losing cells in the model domain.

Hydraulic Properties

The hydraulic properties of an aquifer system at steady state govern the transmission of groundwater. Hydraulic properties input into the model include horizontal hydraulic conductivity. The determination of hydraulic properties was based on previous investigations of Assateague Island (Banks and others, 2012; Dillow and others, 2002; Krantz, 2009) and synthesized in Masterson and others (2013). Initial hydraulic properties for the 1-layer model developed in this study were derived by calculating the mean conductivity used in Masterson and others (2013), as determined by parameter estimation. The harmonic mean was used to calculate the new initial horizontal conductivity. Hydraulic conductivity was subdivided into zones (fig. 2.2) along the north-south axis to separate coarser, more permeable beach sediments on the ocean side from finer, less permeable sediments on the bay side and was based on the zonation of layer 1 of the previous model (Masterson and others, 2013). The final hydraulic conductivity properties as determined by parameter estimation are discussed in more detail in the section "Model Calibration and Sensitivity Analysis Approach."

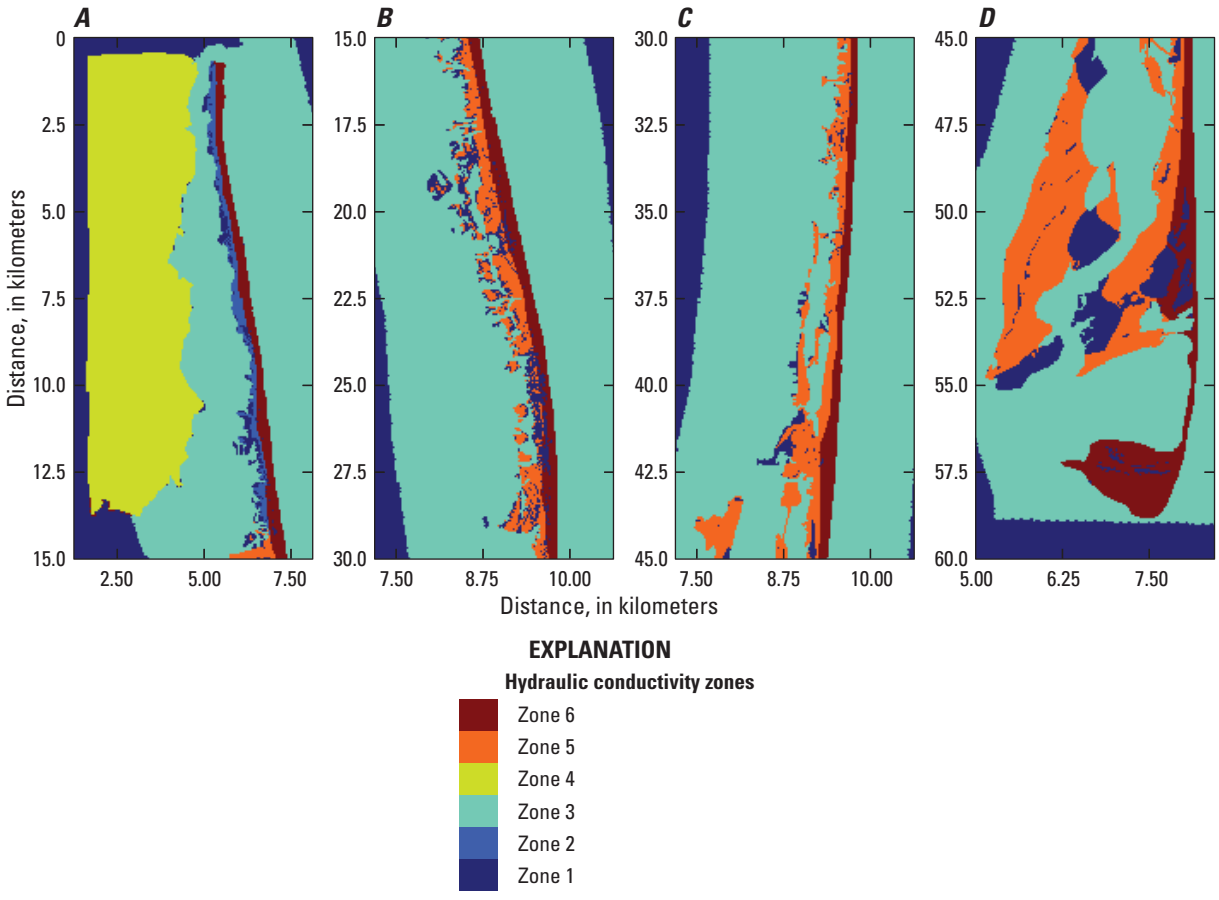

Figure 2.2. Hydraulic conductivity zones within model sections A–D, Assateague Island, Maryland and Virginia.

Model Calibration and Sensitivity Analysis Approach

Model calibration involves the adjustment of model inputs so that the differences between simulated and measured quantities (errors) are minimized with respect to an objective function. During calibration, model input such as system geometry and hydraulic properties, initial and boundary conditions, and stresses are changed so that model output matches related measured values. Many of the model inputs that are changed can be characterized using what are referred to as "parameters" (Hill and Tiedeman, 2007). The measured values are referred to as "observations" or "observed values." Effective use of system information and observations to constrain a model is likely to produce a model that more accurately represents the simulated system and produces more accurate model predictions, compared to a modeling procedure that uses these types of data less effectively. This section of the report describes the calibration method, the treatment of observations, and sensitivity analysis methods.

Prior to the development of objective parameter estimation (Cooley and others, 1986; Hill and others, 2000; Hill and Tiedeman, 2007; Poeter and Hill, 1997; Poeter and others, 2005), sensitivity analysis was an exercise conducted after trial-and-error model calibration by examining the effect of variations in model inputs on the simulation output or errors. With these recent developments, parameters often are estimated only after using starting values to evaluate model fit and perform a sensitivity analysis to identify insensitive and correlated parameters. Fit-independent statistics are calculated using sensitivities and do not use the residual in the calculation of the statistic. These statistics were calculated during calibration of the Assateague model and provided important guidance for model development and calibration. Finally, the nonlinear least-squares regression method used by UCODE_2014 involves calculation of perturbation sensitivities in estimating objective and optimal parameter values. The methods used to calculate sensitivities and fit-independent statistics are presented at the end of this section.

Nonlinear Least-Squares Regression Method

The match of observed to simulated values is one of the most important indicators of how well a model represents an actual system. Objective functions measure this fit by quantitatively comparing simulated and observed values. The simulated and observed values include easily measurable system-dependent variables such as hydraulic head and stream base-flow contributions. Model calibration efforts mainly involve attempting to construct a model that produces the "best fit" to observed heads and flows. When the objective function is defined as the sum of squared differences between simulated and observed heads and flows, the goal of the calibration is to find the set of model parameters that makes this sum as small as possible without overfitting. Methods such as regression provide a rigorous mathematical framework within which optimal parameter values that produce the best fit given the constructed model can be identified. The resulting parameter values are said to be optimal, optimized, or estimated by the regression (Hill and Tiedeman, 2007).

Using hydraulic heads and flows as the observations, the weighted least-squares objective function (see Hill and Tiedeman, 2007), $S(\mathbf{b})$, can be expressed as

$$S(\mathbf{b}) = \sum_{i=1}^{NH} \omega_{h_i} \left[y_{h_i} - y'_{h_i}(\mathbf{b}) \right]^2 + \sum_{j=1}^{NQ} \omega_{q_j} \left[y_{q_j} - y'_{q_j}(\mathbf{b}) \right]^2 , \quad (2)$$

where

b	is a vector containing values of each of the *NP* parameters being estimated;
NP	is the number of estimated parameters;
NH	is the number of hydraulic-head observations;
NQ	is the number of flow observations;
y_{h_i}	is the *i*th observed hydraulic head being matched by the regression;
$y'_{h_i}(\mathbf{b})$	is the simulated hydraulic head that corresponds to the *i*th observed hydraulic head (a function of **b**);
y_{q_j}	is the *j*th observed flow being matched by the regression;
$y'_{q_j}(\mathbf{b})$	is the simulated flow that corresponds to the *j*th observed flow (a function of **b**);
ω_{h_i}	is the weight for the *i*th head observation; and
ω_{q_j}	is the weight for the *j*th flow observation.

In theory, the objective function can be used to produce a model that accurately represents a system and provides reliable measures of model uncertainty only if three conditions are met. Two of these conditions relate to true errors, which equal the unknown amounts by which an observation differs from the value in the actual system. The conditions are (1) relevant processes, system geometry, and so forth are adequately represented and simulated; (2) true errors of the observations are random and have a mean of zero; and (3) weighted true errors are independent, which means that the weighting needs to be proportional to the inverse of the variance-covariance matrix on the true observation errors (Hill and Tiedeman, 2007). The true errors are unknown and therefore cannot be analyzed. Instead, weighted residuals are investigated, and the characteristics of the true errors are inferred. Mathematically, conditions 2 and 3 can be represented as

$$E(\varepsilon) = 0, \quad (3)$$

$$\omega_i \propto 1/\sigma_i^2, \quad (4)$$

(for a diagonal weight matrix; see Hill and Tiedeman, 2007, p. 28–31)where

E is the expected value or mean;
E is a vector of true errors;
Ω is the weight matrix; and
σ_i^2 is the variance of the true error of observation i.

Weighting performs two related functions. First, weighting is needed to produce weighted residuals that have the same units so that they can be squared and summed using equation 4. Second, weighting is needed to reduce the effect of observations that are less accurate relative to those that are more accurate. Hence the weights are proportional to the variance, which is a measure of the accuracy of the observation. This is referred to as error-based weighting. The inverse variance error-based weighting scheme provided by equation 4 allows the incorporation of variables originating from different types of groundwater-flow processes into the model so that their different measurement accuracies are accounted for.

For this modeling study, weighting was important because measured water-level observations and estimates of depth to water based on vegetation type were used, which have different errors, or variances, associated with them.

For many observations, errors are typically thought to be proportional to the true value so that

$$\mathbf{y} = \mathbf{y}^{\text{true}}(1+\varepsilon) = \mathbf{y}^{\text{true}} + \mathbf{y}^{\text{true}}\varepsilon, \quad (5)$$

where

y is the vector of observations; and
$\mathbf{y}^{\text{true}}$ is the vector of true, unknown values.

Therefore, one appropriate weighting strategy can be achieved by specifying the coefficient of variation as the statistic from which the weight is calculated and using observed or simulated values to estimate $\mathbf{y}^{\text{true}}$. The variance is then calculated as $[(c.v.) \times a]^2$, where $c.v.$ is the coefficient of variation and a is the observed or simulated value. The standard deviation equals $[(c.v.) \times a]$. UCODE_2014 supports using either observations or simulated values to calculate weights (Poeter and others, 2005).

Error-based weighting provides a way for data-error analysis to be formally included in model development. An approach that is consistent with is to define the weighting in an attempt to achieve the stricter requirement that

$$\omega_{ii} = 1/\sigma_i^2. \quad (6)$$

Setting the weights to be equal to, rather than proportional to, the observation error variance results in some very useful properties and is one approach used by UCODE_2014.

UCODE_2014 was used to estimate the optimal parameter values. Parameters are estimated using nonlinear regression: the weighted least-squares objective function (eq. 2) is minimized with respect to the parameter values using a modified Gauss-Newton method or a double-dogleg technique (Poeter and others, 2005; Poeter and others, 2014). Sensitivities needed for the method are calculated by UCODE_2014 using a forward- or central-difference perturbation technique.

Residuals and Weighted Residuals

Residuals were calculated as

$$[y_i - y'_i(\mathbf{b})]. \quad (7)$$

They represent the deviation between observed and simulated values. For a diagonal weight matrix, weighted residuals are calculated as

$$\omega_i^{1/2}[y_i - y'_i(\mathbf{b})] \quad (8)$$

and are dimensionless. Weighted residuals represent the fit of the regression in the context of the expected accuracy of the observations. Observations expected to be less accurate are de-emphasized when weighted residuals are considered; observations expected to be more accurate are emphasized. The approach used to weight the observations is described in the next section.

Observations Used in Model Calibration

Observations provide information about model construction and parameter definition (parameterization) as well as the value of model parameters (Hill and Tiedeman, 2007). Successful model calibration is often dependent on multiple observation types; water levels (hydraulic head), base flow to streams, apparent groundwater ages, and solute concentrations have all been used to calibrate models (Hill and Tiedeman, 2007; Sanford and others, 2004). Two types of observations are used to calibrate the groundwater-flow model of Assateague Island National Seashore—water levels from selected wells and estimates of depth to water based on vegetation data (fig. 2.3).

Monthly water levels were measured in 14 shallow wells from October 2014 to September 2015 to account for seasonal variability, and an average annual water level was calculated. The altitude of the freshwater was inferred from a vegetation survey that mapped individual vegetation communities for the entire island. Each vegetation community's preferences for the salinity and depth of water below the root zone was used to identify freshwater communities with varying depth to water settings. These observation altitudes are less precise than manually measured water levels from wells but provide 70 additional observation points to calibrate the model.

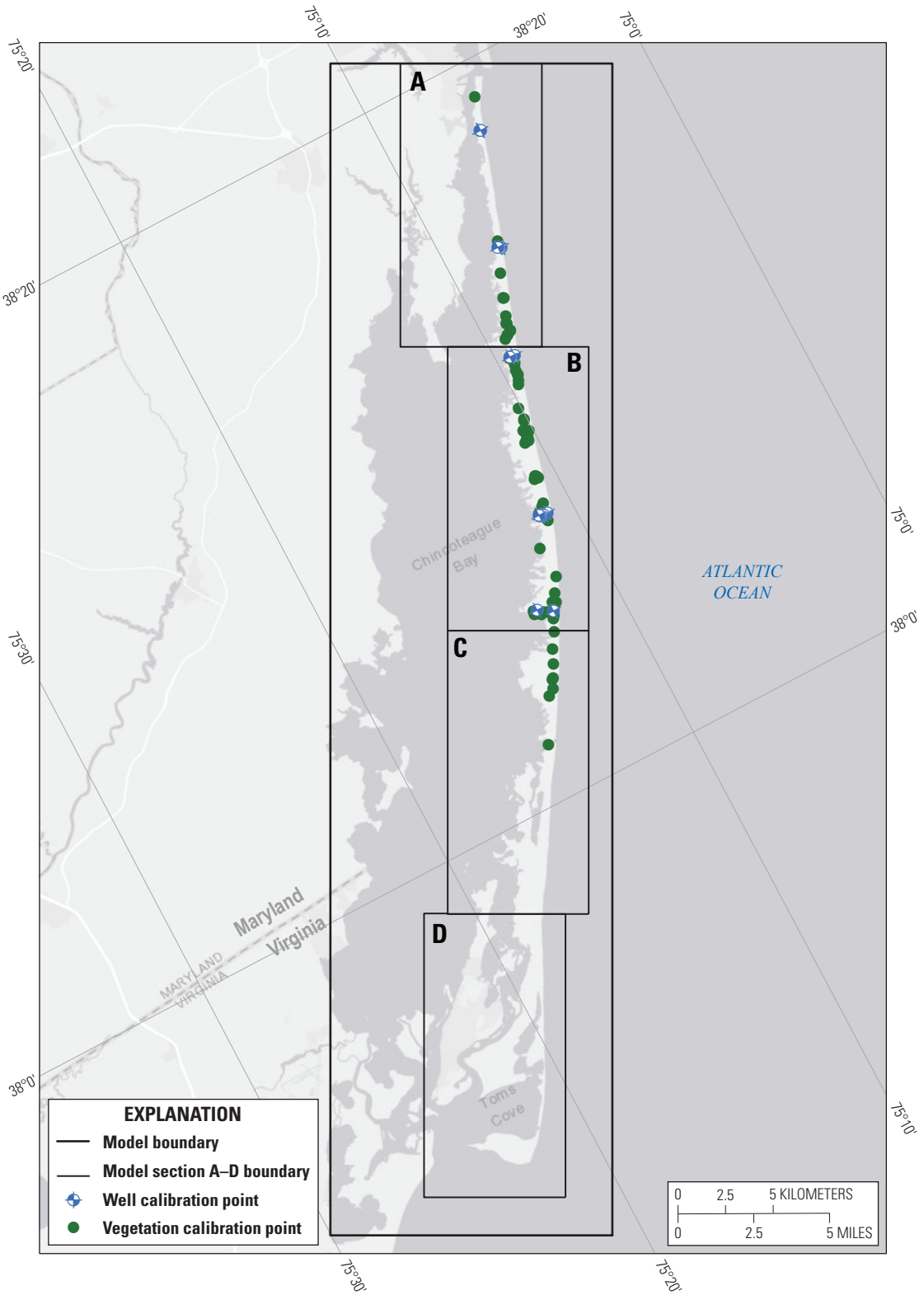

Base from U.S. Geological Survey 1:2,000,000-scale
State boundary digital line graph, Albers Equal-Area Conic Projection
North American Datum of 1983 (NAD 83)

Figure 2.3. Locations of vegetation and well calibration points, Assateague Island, Maryland and Virginia.

Water Levels and Associated Errors

The water levels used in calibrating the model were retrieved from the U.S. Geological Survey National Water Information System database. Groundwater levels for 14 wells were used for model calibration. No effort was made to reduce spatial clustering of the observations. For each well, the mean monthly water level for water year 2015 (October 2014 to September 2015) was used as the head observation, and the variance was calculated for use in error-based weighting.

Errors that contribute the most uncertainty in water-level observations are associated with potential inaccuracies in the altitude and location given for a well, fluctuations introduced by variations in climate or any other nonsimulated transient stress, and measurement of a water level (Faunt and others, 2004; San Juan and others, 2004). These errors were estimated from available information and were used to quantify the uncertainty of a water-level observation. Because of the lack of accurate measurements of the location (which may be an area rather than a point) and altitude of the vegetation-based estimates, a constant variance of 12.5 m was assumed.

Well-altitude error directly affects the calculation of the water level as referenced to a common datum. The error associated with the potential inaccuracy in well altitude was computed from the altitude accuracy code given in the USGS Ground-Water Site-Inventory (GWSI) System, expressed as a plus/minus (±) range related directly to the method by which the altitude was determined. The range defined by the altitude accuracy code is assumed to represent, with 95-percent confidence (two standard deviations)[1], the true well-altitude uncertainty. Assuming that the head observation represents the mean value and that the error is normally distributed, the uncertainty of the head observation, with respect to the well-altitude error, can be expressed as a standard deviation by the following equation

$$\sigma_{alt} = AAC/1.96, \quad (9)$$

where

σ_{alt} is the standard deviation; and
AAC is the value of the GWSI altitude accuracy code; in m.

The standard deviation for well-altitude error ranges from 0.0016 to 0.0156 m.

Well-location errors can cause a discrepancy between observed and simulated water levels. The magnitude of this discrepancy depends directly on the hydraulic gradient at the well—the steeper the gradient, the greater the discrepancy. Well-location error was calculated as the product of the distance determined from the coordinate accuracy code values given in GWSI and the hydraulic gradient estimated for a given well location. The hydraulic gradient at an individual well could not be estimated from available information and so was set to 0.001 for all wells. The range defined by the value of the coordinate accuracy code is assumed to represent, with 95-percent confidence (or two standard deviations), the true error in the head observation as related to well-location uncertainty. Assuming that the head observation represents the mean value and that the error is normally distributed, the uncertainty of the head observation, with respect to the well-location error, can be expressed as a standard deviation calculated by the following equation:

$$\sigma_{loc} = (CAC/1.96) \times HG, \quad (10)$$

where

σ_{loc} is the standard deviation;
CAC is the value of the GWSI coordinate accuracy code, in m; and
HG is the hydraulic gradient (assumed to be 0.001).

Using this equation, the standard deviation associated with well-location error ranges from 0.0002 to 0.158 m.

Nonsimulated transient errors result from uncertainty in the magnitude of water-level response caused by stresses not simulated in the flow model and are typically associated with seasonal and long-term climate changes. Seasonal water-level fluctuations of nearly several feet have been measured in shallow wells in the model region. The variation caused by seasonal variations over water year 2015 was used to represent the nonsimulated transient error. The long-term climatic response in the water-level record is much more difficult to discern and commonly is masked by pumping effects. Long-term climatic response is unknown but is believed to be relatively small throughout the region (less than 0.3 m). The potential error associated with long-term climate response at a well was not calculated independently but was instead accounted for by adding 0.3 m to the seasonal fluctuation assigned to each well (San Juan and others, 2004). The range defined by this value is assumed to represent, with 95-percent confidence (or two standard deviations), the true error in the head observation as related to nonsimulated transient uncertainty. Assuming that the head observation represents the mean value and that the error is normally distributed, the uncertainty of the head observation attributed to nonsimulated transient error can be expressed as a standard deviation calculated by the following equation:

$$\sigma_{tran} = (SF + LTC/4), \quad (11)$$

where

σ_{tran} is the standard deviation;
SF is the seasonal fluctuation as defined by water-level measurements, in m; and
LTC is the long-term climate trend defined

[1]Throughout this section, 1.96 is used as the approximate value of the 97.5 percentile point of the normal distribution; 95 percent of the area under a normal curve lies within roughly 1.96 standard deviations of the mean, and this number is therefore used in the construction of approximate 95-percent confidence intervals.

as 0.3 m.

The standard deviation in head error observed at the 14 wells owing to non-simulated, transient effects ranges from 0.36 to 1.04 m.

In addition to errors associated with well altitude and location, and non-simulated transient fluctuations, measurement errors also can result from inaccuracies in the instruments used to measure depth to water. In this case, measurement accuracy depends primarily on the device being used to make the measurement. Most water-level measurements were made by USGS Maryland-Delaware-D.C. Water Science Center personnel using either a steel tape or an electric tape, both with an accuracy of ±0.01 foot (ft; 0.003048 m). Assuming that the head observation represents the mean value and that the error is normally distributed, the uncertainty of the head observation, with respect to the measurement-accuracy error, can be expressed as a standard deviation calculated by the following equation:

$$\sigma_{meas} = 0.003048/1.96 = 0.0016, \quad (12)$$

where

σ_{meas} is the standard deviation; and

0.003048 is the assumed accuracy of steel and electric tapes, in m.

The standard deviation for measurement error at all 14 wells is 0.0016 m.

Finally, the head variances owing to all errors can be summed and the standard deviation of head observation error () calculated as

$$\sigma_h = \left(\sigma_{alt}^2 + \sigma_{loc}^2 + \sigma_{tran}^2 + \sigma_{meas}^2\right)^{1/2}, \quad (13)$$

UCODE_2005 allows for the errors to be input as a scaled standard deviation, scaled variance, or a scaled coefficient of variation, or by directly entering the weight or the square root of the weight. For the Assateague model, the head variances were included in the observation file for heads. Weights were calculated as the square root of the inverse variance and used to weight observations, simulated values, and residuals (table 2.1).

Table 2.1. Vegetation-based water-level observation estimates and water levels from observation wells used to calibrate the groundwater-flow model, with associated errors (variance), weights, and weighted observations, Assateague Island, Maryland and Virginia.

[USGS, U.S. Geological Survey; observation name, text title given to observations in the UCODE_2005 and MODFLOW-NWT input files (names must begin with a letter); m asl, meters above sea level; m^2, square meters; m, meters; n/a, not applicable; observation types: BIB, Barrier Island Bog; CLPWF, Coastal Loblolly Pine Wetland Forest; FRDS, Forked Rush Dune Swale; SPSP, *Schoenoplectus pungens* (= *Scirpus pungens*); SRMBSF, Southern Red Maple - Blackgum Swamp Forest; WRM, Western Reed Marsh; WSS, Wax-myrtle Shrub Swamp]

USGS site number	Station name	Observation name	Observation type	Observed/estimated water level (m asl)	Statistic	Standard deviation (m)	Variance (m^2)	Weight ($1/m^2$)	SQRT(Weight) (1/m)	Weighted observation (m)
n/a	n/a	veg_101	BIB	0.80	VAR	n/a	12.50	0.08	0.28	0.23
n/a	n/a	veg_103	FRDS	1.12	VAR	n/a	12.50	0.08	0.28	0.32
n/a	n/a	veg_118	WSS	0.70	VAR	n/a	12.50	0.08	0.28	0.20
n/a	n/a	veg_12	WSS	0.89	VAR	n/a	12.50	0.08	0.28	0.25
n/a	n/a	veg_124	WSS	0.94	VAR	n/a	12.50	0.08	0.28	0.27
n/a	n/a	veg_125	WSS	1.14	VAR	n/a	12.50	0.08	0.28	0.32
n/a	n/a	veg_128	WRM	0.53	VAR	n/a	12.50	0.08	0.28	0.15
n/a	n/a	veg_129	WSS	0.86	VAR	n/a	12.50	0.08	0.28	0.24
n/a	n/a	veg_132	SPSP	0.92	VAR	n/a	12.50	0.08	0.28	0.26
n/a	n/a	veg_134	WRM	0.66	VAR	n/a	12.50	0.08	0.28	0.19
n/a	n/a	veg_138	WSS	0.93	VAR	n/a	12.50	0.08	0.28	0.26
n/a	n/a	veg_139	WSS	1.27	VAR	n/a	12.50	0.08	0.28	0.36
n/a	n/a	veg_143	BIB	0.87	VAR	n/a	12.50	0.08	0.28	0.24
n/a	n/a	veg_146	WSS	0.39	VAR	n/a	12.50	0.08	0.28	0.11
n/a	n/a	veg_165	BIB	1.00	VAR	n/a	12.50	0.08	0.28	0.28
n/a	n/a	veg_166	BIB	0.64	VAR	n/a	12.50	0.08	0.28	0.18
n/a	n/a	veg_167	BIB	0.70	VAR	n/a	12.50	0.08	0.28	0.20
n/a	n/a	veg_169	BIB	1.13	VAR	n/a	12.50	0.08	0.28	0.32
n/a	n/a	veg_170	SRMBSF	0.49	VAR	n/a	12.50	0.08	0.28	0.14
n/a	n/a	veg_178	SRMBSF	0.71	VAR	n/a	12.50	0.08	0.28	0.20
n/a	n/a	veg_181	WRM	0.64	VAR	n/a	12.50	0.08	0.28	0.18
n/a	n/a	veg_183	WSS	1.47	VAR	n/a	12.50	0.08	0.28	0.42
n/a	n/a	veg_189	WRM	0.45	VAR	n/a	12.50	0.08	0.28	0.13
n/a	n/a	veg_190	BIB	0.87	VAR	n/a	12.50	0.08	0.28	0.25
n/a	n/a	veg_191	SPSP	1.06	VAR	n/a	12.50	0.08	0.28	0.30
n/a	n/a	veg_193	CLPWF	0.53	VAR	n/a	12.50	0.08	0.28	0.15
n/a	n/a	veg_203	WSS	0.58	VAR	n/a	12.50	0.08	0.28	0.16
n/a	n/a	veg_211	BIB	0.38	VAR	n/a	12.50	0.08	0.28	0.11

Table 2.1. Vegetation-based water-level observation estimates and water levels from observation wells used to calibrate the groundwater-flow model, with associated errors (variance), weights, and weighted observations, Assateague Island, Maryland and Virginia.—Continued

[USGS, U.S. Geological Survey; observation name, text title given to observations in the UCODE_2005 and MODFLOW-NWT input files (names must begin with a letter); m asl, meters above sea level; m^2, square meters; m, meters; n/a, not applicable; observation types: BIB, Barrier Island Bog; CLPWF, Coastal Loblolly Pine Wetland Forest; FRDS, Forked Rush Dune Swale; SPSP, *Schoenoplectus pungens* (= *Scirpus pungens*); SRMBSF, Southern Red Maple - Blackgum Swamp Forest; WRM, Western Reed Marsh; WSS, Wax-myrtle Shrub Swamp]

USGS site number	Station name	Observation name	Observation type	Observed/estimated water level (m asl)	Statistic	Standard deviation (m)	Variance (m^2)	Weight ($1/m^2$)	SQRT(Weight) (1/m)	Weighted observation (m)
n/a	n/a	veg_224	SPSP	0.90	VAR	n/a	12.50	0.08	0.28	0.25
n/a	n/a	veg_244	SPSP	0.95	VAR	n/a	12.50	0.08	0.28	0.27
n/a	n/a	veg_251	WSS	0.77	VAR	n/a	12.50	0.08	0.28	0.22
n/a	n/a	veg_252	FRDS	1.23	VAR	n/a	12.50	0.08	0.28	0.35
n/a	n/a	veg_261	SPSP	1.18	VAR	n/a	12.50	0.08	0.28	0.33
n/a	n/a	veg_268	CLPWF	0.41	VAR	n/a	12.50	0.08	0.28	0.12
n/a	n/a	veg_269	CLPWF	0.44	VAR	n/a	12.50	0.08	0.28	0.12
n/a	n/a	veg_270	WSS	0.63	VAR	n/a	12.50	0.08	0.28	0.18
n/a	n/a	veg_273	SRMBSF	1.12	VAR	n/a	12.50	0.08	0.28	0.32
n/a	n/a	veg_278	CLPWF	0.53	VAR	n/a	12.50	0.08	0.28	0.15
n/a	n/a	veg_280	CLPWF	0.77	VAR	n/a	12.50	0.08	0.28	0.22
n/a	n/a	veg_282	SRMBSF	0.61	VAR	n/a	12.50	0.08	0.28	0.17
n/a	n/a	veg_285	CLPWF	1.11	VAR	n/a	12.50	0.08	0.28	0.31
n/a	n/a	veg_288	WSS	0.65	VAR	n/a	12.50	0.08	0.28	0.18
n/a	n/a	veg_292	WSS	0.63	VAR	n/a	12.50	0.08	0.28	0.18
n/a	n/a	veg_303	BIB	0.58	VAR	n/a	12.50	0.08	0.28	0.16
n/a	n/a	veg_310	BIB	1.12	VAR	n/a	12.50	0.08	0.28	0.32
n/a	n/a	veg_313	WSS	1.30	VAR	n/a	12.50	0.08	0.28	0.37
n/a	n/a	veg_314	WRM	0.37	VAR	n/a	12.50	0.08	0.28	0.10
n/a	n/a	veg_316	WSS	0.59	VAR	n/a	12.50	0.08	0.28	0.17
n/a	n/a	veg_319	WSS	0.92	VAR	n/a	12.50	0.08	0.28	0.26
n/a	n/a	veg_335	WSS	0.64	VAR	n/a	12.50	0.08	0.28	0.18
n/a	n/a	veg_39	SPSP	0.83	VAR	n/a	12.50	0.08	0.28	0.23
n/a	n/a	veg_50	WSS	0.41	VAR	n/a	12.50	0.08	0.28	0.12
n/a	n/a	veg_53	CLPWF	0.47	VAR	n/a	12.50	0.08	0.28	0.13
n/a	n/a	veg_54	WRM	0.48	VAR	n/a	12.50	0.08	0.28	0.14
n/a	n/a	veg_57	WSS	0.45	VAR	n/a	12.50	0.08	0.28	0.13
n/a	n/a	veg_61	WSS	1.13	VAR	n/a	12.50	0.08	0.28	0.32

Table 2.1. Vegetation-based water-level observation estimates and water levels from observation wells used to calibrate the groundwater-flow model, with associated errors (variance), weights, and weighted observations, Assateague Island, Maryland and Virginia.—Continued

[USGS, U.S. Geological Survey; observation name, text title given to observations in the UCODE_2005 and MODFLOW-NWT input files (names must begin with a letter); m asl, meters above sea level; m^2, square meters; m, meters; n/a, not applicable; observation types: BIB, Barrier Island Bog; CLPWF, Coastal Loblolly Pine Wetland Forest; FRDS, Forked Rush Dune Swale; SPSP, *Schoenoplectus pungens* (= *Scirpus pungens*); SRMBSF, Southern Red Maple - Blackgum Swamp Forest; WRM, Western Reed Marsh; WSS, Wax-myrtle Shrub Swamp]

USGS site number	Station name	Observation name	Observation type	Observed/estimated water level (m asl)	Statistic	Standard deviation (m)	Variance (m^2)	Weight ($1/m^2$)	SQRT(Weight) (1/m)	Weighted observation (m)
n/a	n/a	veg_62	WSS	0.30	VAR	n/a	12.50	0.08	0.28	0.09
n/a	n/a	veg_64	SPSP	1.22	VAR	n/a	12.50	0.08	0.28	0.34
n/a	n/a	veg_66	WSS	0.75	VAR	n/a	12.50	0.08	0.28	0.21
n/a	n/a	veg_68	WSS	0.57	VAR	n/a	12.50	0.08	0.28	0.16
n/a	n/a	veg_69	WSS	0.79	VAR	n/a	12.50	0.08	0.28	0.22
n/a	n/a	veg_73	WRM	0.61	VAR	n/a	12.50	0.08	0.28	0.17
n/a	n/a	veg_79	WRM	0.80	VAR	n/a	12.50	0.08	0.28	0.23
n/a	n/a	veg_83	WRM	0.43	VAR	n/a	12.50	0.08	0.28	0.12
n/a	n/a	veg_84	CLPWF	0.64	VAR	n/a	12.50	0.08	0.28	0.18
n/a	n/a	veg_87	WSS	0.96	VAR	n/a	12.50	0.08	0.28	0.27
n/a	n/a	veg_88	WSS	0.54	VAR	n/a	12.50	0.08	0.28	0.15
n/a	n/a	veg_92	BIB	1.04	VAR	n/a	12.50	0.08	0.28	0.29
n/a	n/a	veg_96	SPSP	1.42	VAR	n/a	12.50	0.08	0.28	0.40
n/a	n/a	veg_97	FRDS	0.77	VAR	n/a	12.50	0.08	0.28	0.22
381805075063502	WO Cg 101	WOCg101	Head	0.94	VAR	1.04	1.08	0.92	0.96	0.91
381804075063402	WO Cg 103	WOCg103	Head	0.98	VAR	0.78	0.61	1.65	1.28	1.26
381452075080102	WO Dg 32	WODg27	Head	−0.26	VAR	1.04	1.08	0.93	0.96	−0.25
381452075075902	WO Dg 30	WODg28	Head	−0.17	VAR	1.05	1.10	0.91	0.95	−0.16
381450075075402	WO Dg 28	WODg30	Head	0.74	VAR	0.66	0.44	2.27	1.51	1.11
381450075075401	WO Dg 27	WODg32	Head	1.52	VAR	0.36	0.13	7.62	2.76	4.19
381157075092902	WO Dg 36	WODg34	Head	0.73	VAR	0.81	0.65	1.54	1.24	0.90
381155075091802	WO Dg 34	WODg36	Head	0.32	VAR	0.47	0.23	4.44	2.11	0.67
380734075111302	WO Ef 35	WOEf29	Head	0.90	VAR	0.69	0.47	2.11	1.45	1.31
380731075111102	WO Ef 33	WOEf31	Head	0.59	VAR	0.67	0.45	2.21	1.49	0.87
380731075105602	WO Ef 29	WOEf33	Head	0.36	VAR	0.68	0.46	2.15	1.47	0.53
380730075110402	WO Ef 31	WOEf35	Head	0.30	VAR	0.54	0.29	3.41	1.85	0.55
380512075125402	WO Ef 37	WOEf37	Head	0.12	VAR	0.79	0.63	1.58	1.26	0.15
380457075122302	WO Ff 12	WOFf12	Head	0.45	VAR	0.77	0.59	1.69	1.30	0.59

Model Parameters

In current usage, a parameter is a single value assigned to a variable used in the finite-difference groundwater-flow equation at one or more model cells. The definition of a parameter specifies which variable is being defined and the cells to which the parameter applies. For example, a parameter might define the aquifer hydraulic conductivity for a group of cells in a model layer, or a parameter might define the riverbed conductance for one or more reaches of a river.

When parameters are used, the data value for a cell is calculated as the product of the dimensionless scalar parameter value, which might apply to many cells, and a starting value for the hydraulic property or other model input that is defined for that cell. In the Assateague model, parameters are defined for both list and layer data. List data refer to any type of data for which values are specified in some subset of the grid cells. The only packages that are parameterized in the model using list data are the drain package, for which the drain hydraulic conductance is parameterized as parameter type DRN, and the general-head boundary package, which is parameterized as parameter type GHB. A single parameter was established for each (DRN_1 and GHB_1).

Each MODFLOW package that incorporates layer data may have any number of types of data to be defined. The input instructions for a package indicate which data types can be defined using parameters. Each data type is given a specific name that must be included as part of the input data that defines a parameter of that type. Packages that use parameter values for layer data in the Assateague model include the Upwind-Weighting (UPW) package of MODFLOW-NWT, the recharge package (parameter type RCH), and the evapotranspiration package (parameter type EVT). The parameters are defined in the respective package files. For layer data, parameter multipliers are defined using multiplier arrays. In this case, each multiplier array contains values for every cell in a layer, and the values can be individually referenced using a row and column index. There can be a different multiplier array for every layer to which the parameter applies, and these are identified when the parameter is defined.

To allow only some of the cells of a layer to be associated with a layer parameter, a capability called zonation is used. Like multiplier arrays, each zone array is named and contains values for every cell in a layer. Values in a zone array are integers. There can be a different zone array for every layer to which the parameter applies. When a parameter is defined, the zone array and one or more integer zone values are specified to denote which zone each cell in the array is located in. The parameter applies to cells at which the value of the zone array matches any one of the specified zone values; that is, the data value at a cell is the product of the multiplier array at the cell and the parameter value only if the value of the zone array matches one of the zone values specified for the parameter. Zonation for recharge, evapotranspiration, and hydraulic conductivity are shown in figures 2.1 and 2.2.

A complete list of parameters defined for the model is given in table 2.2. Not all model parameters were adjusted during model calibration. Initial sensitivity analyses of all model parameters were conducted to determine which were unlikely to be optimally estimated. Sensitivity analysis is described in the next section.

Table 2.2. Description of defined model parameters.

[Parameter identifier, text title given to parameters in the UCODE_2005 and MODFLOW-NWT input files]

Parameter identifier	Description
HK_1	Horizontal hydraulic conductivity of zone 1
HK_2	Horizontal hydraulic conductivity of zone 2
HK_3	Horizontal hydraulic conductivity of zone 3
HK_4	Horizontal hydraulic conductivity of zone 4
HK_5	Horizontal hydraulic conductivity of zone 5
HK_6	Horizontal hydraulic conductivity of zone 6
VK_1	Vertical hydraulic conductivity of zone 1
VK_2	Vertical hydraulic conductivity of zone 2
VK_3	Vertical hydraulic conductivity of zone 3
VK_4	Vertical hydraulic conductivity of zone 4
VK_5	Vertical hydraulic conductivity of zone 5
VK_6	Vertical hydraulic conductivity of zone 6
GHB_1	General-head boundary conductance
DRN_1	Drain conductance for drain cells
RCH_1	Maximum recharge specified in layer 1
RCH_2	Maximum recharge specified in layer 2
RCH_3	Maximum recharge specified in layer 3
RCH_4	Maximum recharge specified in layer 4
RCH_5	Maximum recharge specified in layer 5
EVT_1	Maximum rate of evapotranspiration for layer 1
EVT_2	Maximum rate of evapotranspiration for layer 2
EVT_3	Maximum rate of evapotranspiration for layer 3
EVT_4	Maximum rate of evapotranspiration for layer 4
EVT_5	Maximum rate of evapotranspiration for layer 5

Sensitivity Analysis

Sensitivities are calculated as the derivatives of simulated water-level values with respect to the model parameters

$$\left(\frac{\partial y'_i}{\partial b_j}\right)\Bigg|_{\mathbf{b}}, \tag{14}$$

where the terms have been defined previously. Sensitivities can be used to determine the importance of observations to the estimation of parameter values. Observations are likely to be valuable in estimating a parameter if the simulated values change substantially given a small change in model parameter value. Observations contribute little to the estimation of a parameter if the simulated values change very little, even with a large change in parameter value (Hill and Tiedeman, 2007).

Fit-independent statistics are calculated using sensitivities and do not use the residual in the calculation of the statistic. The sensitivity analysis focused on identifying parameter values that could be estimated by regression and identifying key observations that supported each parameter. As part of this analysis, two statistics were evaluated: dimensionless scaled sensitivity and composite scaled sensitivity.

Dimensionless Scaled Sensitivity

When a diagonal weight matrix is used, dimensionless scaled sensitivities (*dss*) are calculated as

$$dss_{ij} = \left(\frac{\partial y'_i}{\partial b_j}\right)\Bigg|_{\mathbf{b}} |b_j| \omega_{ii}^{1/2}, \tag{15}$$

where

y'_i is a simulated value associated with the *i*th observation;

b_j is the *j*th estimated parameter;

b is a vector containing the parameter values at which the sensitivities are evaluated; and

ω_{ii} is the weight on the *i*th observation.

Dimensionless scaled sensitivities can be used to (1) compare the importance of different observations to the estimation of a single parameter b_j and (2) compare the importance of different parameters to the calculation of a single simulated value .

Composite Scaled Sensitivity

The analysis of overall model parameter sensitivity may be evaluated using composite scaled sensitivities (*css*). They are calculated for each parameter using *dss* and may be calculated for some or all observations. The *css* (dimensionless) for the *j*th parameter calculated for *ND* observations is

$$css_j = \sum_{i=1}^{ND}\left[\left(dss_{ij}\right)^2\Big|_{\mathbf{b}} / ND\right]^{1/2}. \tag{16}$$

The *css* indicates the magnitude to which a change in the value of the parameter causes a change in the simulated water-level observations. Highly sensitive parameters, therefore, exert greater control over the simulated water levels, whereas relatively insensitive parameters have less control over the simulated water levels. Composite scaled sensitivities reflect the total amount of information provided by the observations in the estimation of one parameter and therefore indicate the importance of observations as a whole to a single parameter.

Model Evaluation

The calibrated Assateague model was evaluated to assess the likely accuracy of simulated results. An advantage of using nonlinear regression to calibrate the model is that a substantial methodology exists for model evaluation that facilitates a better understanding of model strengths and weaknesses, and provides opportunity for future investigation of model parameter and model prediction uncertainty (D'Agnese and others, 1999; Faunt and others, 2004; Fienen and others, 2010; Hill and Tiedeman, 2007).

Parameter Values and Model Fit

In objective parameter estimation using nonlinear regression, the classical problem of model calibration is inverted, so that the observations are used to guide determination of the values of the variables in the governing equations. This entails an iterative process, not unlike traditional trial-and-error calibration, in which fit-independent statistics are used to guide the choice of parameters to be estimated; parameter estimates and model fit are then evaluated, alternate models are possibly considered, and the process is repeated until reasonable parameter estimates result.

The procedure for arriving at the final parameter values involved multiple sensitivity analysis and parameter estimation simulations. Model fit was evaluated after each set of

Table 2.3. Final parameter values and fit-independent statistics.

[Parameter identifiers, text titles given to parameters in the UCODE_2005 and MODFLOW-NWT input files, are defined in table 2.2. Observation names are provided in table 2.1. css, composite scaled sensitivity; dss, dimensionless scaled sensitivity]

Parameter identifier	Value	css	Largest dss for the parameter	Observation with largest dss
HK_2	0.499	4.03E−02	−0.316	veg_39
HK_5	0.001	7.42E−02	−0.526	veg_125
RCH_2	1.644	6.82E−02	0.323	veg_39
RCH_3	1.326	1.31E−02	0.113	veg_285
RCH_4	0.990	9.52E−01	3.613	veg_273
RCH_5	0.403	0.10	0.494	WODg28

simulations by examining residuals (the differences between observed values and simulated values) and weighted residuals. An initial set of model runs was conducted to calculate sensitivities and fit-independent statistics (*css* and *dss*) for all 24 model parameters (table 2.2). For many reasons, relatively few parameters could be reliably estimated. Composite scaled sensitivities were very low for most parameters.

The final parameter values for the Assateague model are provided in table 2.3, along with associated fit-independent statistics. For all zones and parameters not shown in table 2.3, parameters were held fixed at their initial values and not adjusted during the regression, effectively excluding them from the calibration procedure. Parameters were omitted from the calibration because they had either low *css* values, indicating little effect on simulated heads at observation sites, or one or more high *pcc* values that would indicate a strong correlation to parameters included in the regression and the potential for producing biased regression coefficients.

The final calibrated model produced a set of unweighted (fig. 2.4*A*) and weighted simulated water levels that were then compared to the weighted mean observed and estimated water levels (fig. 2.4*B*, table 2.4). Plots of weighted simulated and weighted observed water levels indicate that the values match reasonably closely, indicating that the dominant physical processes governing groundwater flow are largely accounted for and that little structural model error remains in the flow model. The root mean square error for water levels for the unweighted and weighted residuals was 0.27 m and 0.28 m, respectively.

Examination of the weighted residuals is of greater interest because one goal of parameter estimation using nonlinear regression is to produce weighted residuals that are well behaved, with a mean near zero, a minimal standard deviation, a distribution that can reasonably be considered normal, homoscedastic behavior characterized by a constant variance that does not depend on the magnitude of the observation, and negligible spatial bias. The weighted residuals for water-level observations are given in table 2.4. The distribution of the error in the simulated water-level observations does not show any bias with respect to the unweighted simulated values (fig. 2.5) or position in space (fig. 2.6).

Sensitivity Analysis Results

The calibration procedure calculates a *css* (Hill, 1998; Hill and Tiedeman, 2007) (eq. 16) for each parameter that is estimated. These sensitivities can be used in a comparative manner, in which larger values indicate parameters for which the observations provide more information. The calculated *css* for the six parameters estimated by the calibrated model are shown in figure 2.7. Parameters not shown in figure 2.7 were not estimated and either had substantially smaller *css* values or were excluded owing to high correlation with another parameter. The highest *css* value is for the recharge rate to layer 4 (RCH_4).

Another way of evaluating the relative importance of different model parameters is by examining the degree of confidence in an estimated parameter value based on its 95-percent linear confidence interval. These intervals are calculated partly on the basis of the sensitivity of the parameter (Hill and Tiedeman, 2007) and indicate a range of values within which the parameter value could be set and still give similar simulated values. The confidence intervals and coefficients of variation for the six estimated parameters are given in table 2.5. The parameters that were reliably estimated have relatively small confidence intervals and coefficients of variation.

Dimensionless scaled sensitivity values can be used to compare the importance of different observations to the estimation of a single parameter. One important outcome of an analysis of *dss* values is that it provides useful information on the value of continued monitoring. A large *dss* value indicates an observation that provides substantial information in estimating one or more parameters (eq. 15). Many of the monitoring wells used in calibration of the Assateague model are part of an ongoing monitoring network. Although there may be

other benefits to the monitoring, an assessment of *dss* values enables evaluation of wells that might not be providing valuable information for regional flow analysis. It may be beneficial in some instances to modify or discontinue monitoring at those sites in favor of monitoring other existing or new sites. Dimensionless scaled sensitivity values for the 84 observations and 6 estimated parameters are provided in table 2.6. The conclusion from this analysis is that vegetation observation locations could be locations where it would be useful to have an actual observation. Observations with the largest absolute *dss* values provide important information about parameters.

There may be some benefit to continued monitoring at the wells with low *dss* values that is not readily apparent from this analysis of model sensitivity. Moreover, recent evaluations of data worth have focused on specific predictions rather than a more general calibration (Dausman and others, 2010; Fienen and others, 2010). All these wells have been logged for specific conductance and other parameters, providing additional beneficial data. Finally, low *dss* values might be associated with the weight assigned to the observation at the well, and an alternative interpretation is that additional effort could be placed on improving the accuracy of the information on the well and measurements at the well in order to increase its weight.

Model Limitations and Suggestions for Additional Work

The goal of this modeling study was to develop a groundwater-flow model capable of being accurate at scales relevant to current and future studies regarding the effects of sea-level rise at Assateague Island National Seashore, focusing on changes to the depth to the water table with implications for ecosystem health. A groundwater-flow model is a tool for simulating and testing a conceptual understanding of a real system. Because groundwater-flow systems are inherently complex, simplifying assumptions were made in developing this model (Anderson and Woessner, 1992). Models solve for average conditions within each cell during a time step, the parameters for which are interpolated or extrapolated from measurements or ancillary estimates and (or) estimated during calibration. In light of this, the intent in developing the groundwater-flow model for Assateague Island was not to reproduce every detail of the natural system, but rather to capture its general characteristics.

All models are based on a limited amount of data and are therefore simplifications of the actual system. Model limitations result from uncertainty in four aspects of the model, including inadequacies or inaccuracies in (1) conceptualization of the flow system; (2) model discretization and heterogeneity; (3) the method or methods used to estimate model parameters, sensitivity, and uncertainty; and (4) observations used to calibrate the model. It is important to understand how these uncertainties limit the use of the model.

The accuracy of a groundwater-flow model depends on the accuracy of the conceptual model. Three simplifications were invoked to make the problem tractable, given available data.

1. The system was modeled as being at steady state or as representing a long-term average condition, neglecting transient effects such as daily tides, seasonality of recharge and other stresses, and short-term effects from storms.

2. Net recharge is modeled as the difference between recharge (spatially variable based on land cover) and evapotranspiration (similarly spatially variable but with an extinction depth). Future improvements to the model might include application of the Unsaturated-Zone Flow (UZF) package (Niswonger and others, 2006) in place of the recharge and evapotranspiration packages to improve simulation of the water table.

3. The conceptual model simplifies the hydrogeologic system vertically (one layer) and employs a sharp interface method (SWI2) to represent the effects of variations in fluid density on groundwater flow and movement of the freshwater/saltwater interface.

Limitations result from the method used to estimate model parameters, sensitivity, and uncertainty (Fienen and others, 2010; Hill, 1998; Hill and Tiedeman, 2007; Poeter and others, 2005). Parameter estimation and sensitivity analysis rely heavily on observations. Prior information was used only indirectly, as a guide in establishing initial parameter values, especially for parameters that were not estimated by regression. In this case, the calibrated model provided by Masterson and others (2013) could be considered prior information and was important in calibrating the final model.

Another limitation of a regression-based calibration approach includes potential nonlinearities in the error surface defined by the sum of squared weighted residuals that can cause the regression to converge to a sub-optimal parameter set. Extreme nonlinearity can produce a model that simulates inaccurate water levels and base flows.

Observations of hydraulic head (water level) constrain model calibration through parameter estimation, and their level of accuracy creates additional uncertainty affecting model limitations. The quality of the water-level observations was used directly in error-based weighting of the regression, but the errors were composed of multiple components, some of which were estimates. Spatial clustering of observations and the need to select a single water level at a location that may have nested wells (owing to the lack of explicit layering in the model) may have adversely affected parameter estimation and provided an additional source of uncertainty that limits model applicability.

Table 2.4. Observed and simulated water levels, with calculated residuals, and weighted observed, weighted simulated, and calculated weighted residuals.

[Observation name, text title given to observations in the UCODE_2005 and MODFLOW-NWT input files (names must begin with a letter); m, meters; m asl, meters above sea level; m^2, square meters; observation types: BIB, Barrier Island Bog; CLPWF, Coastal Loblolly Pine Wetland Forest; FRDS, Forked Rush Dune Swale; SPSP, *Schoenoplectus pungens* (= *Scirpus pungens*); SRMBSF Southern Red Maple - Blackgum Swamp Forest; WRM, Western Reed Marsh; WSS, Wax-myrtle Shrub Swamp]

Observation name	Observation type	Observed/estimated water level (m asl)	Simulated water level (m asl)	Residual (m)	Weighted observed water level (m)	Weighted simulated water level (m)	Weighted residual
veg_101	BIB	0.80	0.80	-4.83E-03	1.51	1.52	-9.13E-03
veg_103	FRDS	1.12	1.02	9.57E-02	2.12	1.94	1.81E-01
veg_118	WSS	0.70	0.70	-2.84E-03	1.32	1.33	-5.37E-03
veg_12	WSS	0.89	0.82	6.58E-02	1.68	1.56	1.24E-01
veg_124	WSS	0.94	0.95	-5.22E-03	1.78	1.79	-9.87E-03
veg_125	WSS	1.14	1.10	4.37E-02	2.15	2.07	8.26E-02
veg_128	WRM	0.53	0.49	3.85E-02	1.00	0.93	7.27E-02
veg_129	WSS	0.86	0.80	5.94E-02	1.63	1.51	1.12E-01
veg_132	SPSP	0.92	0.92	-1.72E-03	1.74	1.74	-3.25E-03
veg_134	WRM	0.66	0.62	3.54E-02	1.25	1.18	6.68E-02
veg_138	WSS	0.93	0.93	-2.36E-03	1.76	1.76	-4.45E-03
veg_139	WSS	1.27	1.23	4.37E-02	2.40	2.32	8.26E-02
veg_143	BIB	0.87	0.87	-1.31E-03	1.64	1.65	-2.47E-03
veg_146	WSS	0.39	0.35	3.51E-02	0.74	0.67	6.64E-02
veg_165	BIB	1.00	1.00	-1.90E-03	1.89	1.89	-3.59E-03
veg_166	BIB	0.64	0.64	-7.13E-04	1.21	1.21	-1.35E-03
veg_167	BIB	0.70	0.70	-3.11E-03	1.32	1.33	-5.87E-03
veg_169	BIB	1.13	1.14	-5.39E-03	2.14	2.15	-1.02E-02
veg_170	SRMBSF	0.49	0.45	3.98E-02	0.93	0.85	7.53E-02
veg_178	SRMBSF	0.71	0.67	3.85E-02	1.34	1.27	7.28E-02
veg_181	WRM	0.64	0.61	2.91E-02	1.21	1.15	5.49E-02
veg_183	WSS	1.47	1.43	4.29E-02	2.78	2.70	8.10E-02
veg_189	WRM	0.45	0.41	4.02E-02	0.85	0.77	7.60E-02
veg_190	BIB	0.87	0.88	-7.51E-03	1.64	1.66	-1.42E-02
veg_191	SPSP	1.06	1.02	3.77E-02	2.00	1.93	7.13E-02
veg_193	CLPWF	0.53	0.54	-5.51E-03	1.00	1.01	-1.04E-02
veg_203	WSS	0.58	0.58	-1.95E-03	1.10	1.10	-3.68E-03
veg_211	BIB	0.38	0.38	-2.51E-03	0.72	0.72	-4.75E-03
veg_224	SPSP	0.90	0.90	-4.84E-03	1.70	1.71	-9.15E-03

Table 2.4. Observed and simulated water levels, with calculated residuals, and weighted observed, weighted simulated, and calculated weighted residuals.—Continued

[Observation name, text title given to observations in the UCODE_2005 and MODFLOW-NWT input files (names must begin with a letter); m, meters; m asl, meters above sea level; m^2, square meters; observation types: BIB, Barrier Island Bog; CLPWF, Coastal Loblolly Pine Wetland Forest; FRDS, Forked Rush Dune Swale; SPSP, *Schoenoplectus pungens* (= *Scirpus pungens*); SRMBSF Southern Red Maple - Blackgum Swamp Forest; WRM, Western Reed Marsh; WSS, Wax-myrtle Shrub Swamp]

Observation name	Observation type	Observed/estimated water level (m asl)	Simulated water level (m asl)	Residual (m)	Weighted observed water level (m)	Weighted simulated water level (m)	Weighted residual
veg_244	SPSP	0.95	0.95	-3.93E-03	1.80	1.80	-7.43E-03
veg_251	WSS	0.77	0.77	1.82E-03	1.46	1.45	3.45E-03
veg_252	FRDS	1.23	1.09	1.37E-01	2.32	2.07	2.58E-01
veg_261	SPSP	1.18	1.18	-8.49E-04	2.23	2.23	-1.60E-03
veg_268	CLPWF	0.41	0.39	2.11E-02	0.77	0.73	3.99E-02
veg_269	CLPWF	0.44	0.40	4.27E-02	0.83	0.75	8.07E-02
veg_270	WSS	0.63	0.59	3.75E-02	1.19	1.12	7.08E-02
veg_273	SRMBSF	1.12	1.08	3.96E-02	2.12	2.04	7.49E-02
veg_278	CLPWF	0.53	0.49	3.85E-02	1.00	0.93	7.27E-02
veg_280	CLPWF	0.77	0.78	-5.01E-03	1.46	1.46	-9.47E-03
veg_282	SRMBSF	0.61	0.57	4.27E-02	1.15	1.07	8.07E-02
veg_285	CLPWF	1.11	0.82	2.91E-01	2.10	1.55	5.50E-01
veg_288	WSS	0.65	0.65	-4.67E-03	1.23	1.24	-8.82E-03
veg_292	WSS	0.63	0.64	-6.70E-03	1.19	1.20	-1.27E-02
veg_303	BIB	0.58	0.54	3.72E-02	1.10	1.03	7.02E-02
veg_310	BIB	1.12	1.09	3.47E-02	2.12	2.05	6.55E-02
veg_313	WSS	1.30	1.30	-4.34E-03	2.46	2.46	-8.20E-03
veg_314	WRM	0.37	0.33	3.92E-02	0.70	0.63	7.41E-02
veg_316	WSS	0.59	0.58	1.40E-02	1.11	1.09	2.65E-02
veg_319	WSS	0.92	0.88	3.77E-02	1.74	1.67	7.12E-02
veg_335	WSS	0.64	0.60	3.50E-02	1.21	1.14	6.62E-02
veg_39	SPSP	0.83	0.63	2.05E-01	1.57	1.18	3.87E-01
veg_50	WSS	0.41	0.40	1.02E-02	0.77	0.76	1.93E-02
veg_53	CLPWF	0.47	0.42	5.47E-02	0.89	0.78	1.03E-01
veg_54	WRM	0.48	0.48	-1.91E-03	0.91	0.91	-3.61E-03
veg_57	WSS	0.45	0.45	-3.67E-03	0.85	0.86	-6.93E-03
veg_61	WSS	1.13	0.78	3.48E-01	2.14	1.48	6.59E-01
veg_62	WSS	0.30	0.26	3.63E-02	0.57	0.50	6.85E-02
veg_64	SPSP	1.22	1.22	-1.58E-03	2.31	2.31	-2.99E-03

Table 2.4. Observed and simulated water levels, with calculated residuals, and weighted observed, weighted simulated, and calculated weighted residuals.—Continued

[Observation name, text title given to observations in the UCODE_2005 and MODFLOW-NWT input files (names must begin with a letter); m, meters; m asl, meters above sea level; m^2, square meters; observation types: BIB, Barrier Island Bog; CLPWF, Coastal Loblolly Pine Wetland Forest; FRDS, Forked Rush Dune Swale; SPSP, *Schoenoplectus pungens* (= *Scirpus pungens*); SRMBSF Southern Red Maple - Blackgum Swamp Forest; WRM, Western Reed Marsh; WSS, Wax-myrtle Shrub Swamp]

Observation name	Observation type	Observed/estimated water level (m asl)	Simulated water level (m asl)	Residual (m)	Weighted observed water level (m)	Weighted simulated water level (m)	Weighted residual
veg_66	WSS	0.75	0.75	-3.80E-03	1.42	1.42	-7.18E-03
veg_68	WSS	0.57	0.53	3.55E-02	1.08	1.01	6.71E-02
veg_69	WSS	0.79	0.75	4.02E-02	1.49	1.42	7.59E-02
veg_73	WRM	0.61	0.57	4.40E-02	1.15	1.07	8.32E-02
veg_79	WRM	0.80	0.76	4.18E-02	1.51	1.43	7.90E-02
veg_83	WRM	0.43	0.43	-3.10E-04	0.81	0.81	-5.85E-04
veg_84	CLPWF	0.64	0.63	6.77E-03	1.21	1.20	1.28E-02
veg_87	WSS	0.96	0.70	2.61E-01	1.81	1.32	4.93E-01
veg_88	WSS	0.54	0.54	-4.40E-03	1.02	1.03	-8.32E-03
veg_92	BIB	1.04	1.05	-5.70E-03	1.97	1.98	-1.08E-02
veg_96	SPSP	1.42	0.98	4.42E-01	2.68	1.85	8.34E-01
veg_97	FRDS	0.77	0.78	-1.07E-02	1.46	1.48	-2.02E-02
WOCg101	Head	0.94	1.20	-2.65E-01	0.96	1.23	-2.70E-01
WOCg103	Head	0.98	1.17	-1.86E-01	0.87	1.03	-1.65E-01
WODg27	Head	-0.26	0.92	-1.18E+00	-0.27	0.94	-1.21E+00
WODg28	Head	-0.17	0.92	-1.09E+00	-0.17	0.95	-1.12E+00
WODg30	Head	0.74	0.96	-2.15E-01	0.60	0.78	-1.75E-01
WODg32	Head	1.52	0.54	9.84E-01	0.91	0.32	5.92E-01
WODg34	Head	0.73	1.00	-2.71E-01	0.66	0.90	-2.43E-01
WODg36	Head	0.32	0.66	-3.37E-01	0.22	0.45	-2.32E-01
WOEf29	Head	0.90	0.83	7.06E-02	0.75	0.69	5.86E-02
WOEf31	Head	0.59	0.98	-3.90E-01	0.48	0.80	-3.20E-01
WOEf33	Head	0.36	0.92	-5.63E-01	0.30	0.76	-4.64E-01
WOEf35	Head	0.30	0.86	-5.56E-01	0.22	0.63	-4.09E-01
WOEf37	Head	0.12	0.78	-6.64E-01	0.11	0.70	-5.92E-01
WOFf12	Head	0.45	1.19	-7.36E-01	0.39	1.04	-6.45E-01

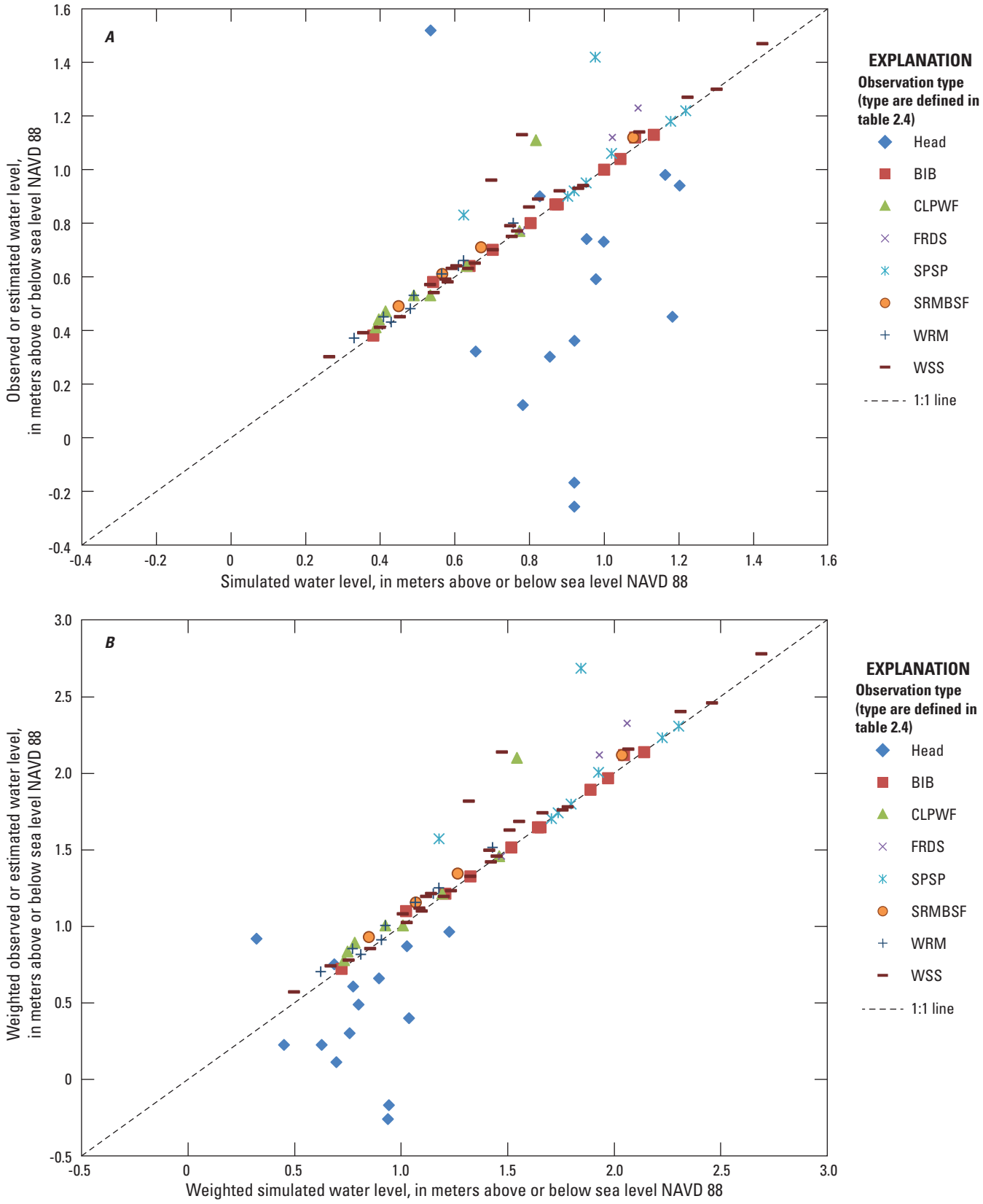

Figure 2.4. *A,* Simulated versus observed parameter values and *B,* weighted simulated versus weighted observed parameter values for the calibrated model, by observation type. (Observation types are defined in table 2.4.)

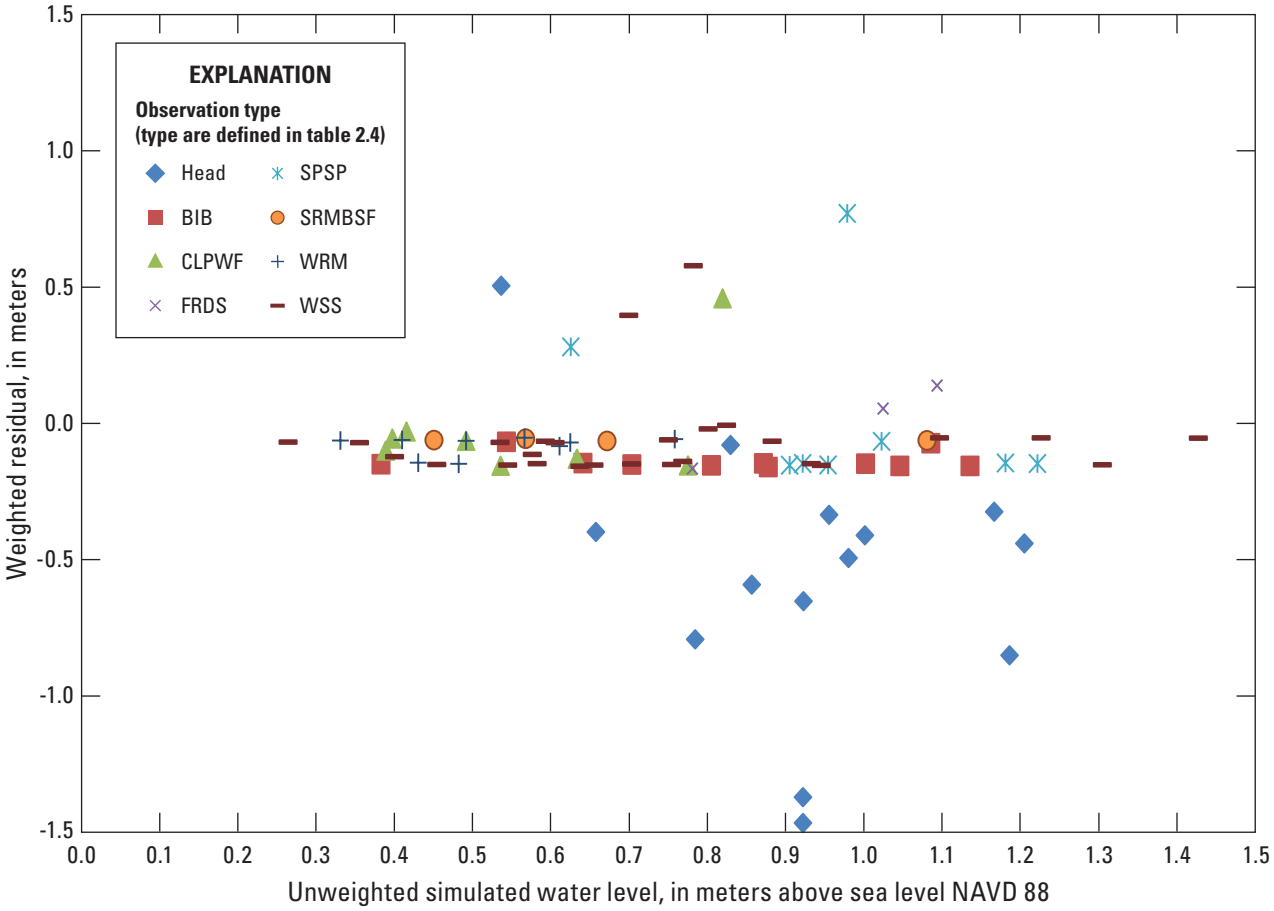

Figure 2.5. Weighted residuals versus unweighted simulated residuals. The lack of trend is an indicator of lack of bias in the simulation, by observation type. (Observation types are defined in table 2.4)

In addition to the 14 observed water levels, 70 depth to water estimates, based on vegetation type, were used to calibrate the model. These represent a subset of estimates and were selected as being representative of wetland areas. It was deemed that these estimates were more accurate than those not selected as they represent a water table in close proximity to the land surface.

A critical limitation of any model is resolution. For the Assateague Island model, resolution was refined in comparison with the model published by Masterson and others (2013), from 50-m cells to 25-m cells. However, in any discretized model, values must be assigned to discrete areas or volumes that represent an average over that area or volume. For example, the land-surface altitude assigned to the node (the centroid of the cell) represents an average over the 625-square-meter cell area. Three-dimensional properties (horizontal hydraulic conductivity) represent averages over the entire cell volume, keeping in mind that the model consists of a single layer. Finally, observed water levels and vegetation-based water-level estimates were assigned to the centroid of the cell. The observed water levels may have been measured at a different vertical point. The vegetation-based estimates were provided as surface point data. Points contained within a cell were assigned to the centroid, regardless of actual extent or location of the vegetation type.

The performance, utility, detail, and accuracy of the Assateague Island groundwater-flow model could be improved in several ways. These improvements can be classified in one of two ways: as limitations to address or as potential enhancements. In terms of limitations, the model could benefit from additional hydrogeologic and observational data. The *dss* values (table 2.6) can provide some guidance on the relative value of the existing observations to model calibration. There are other statistical methods available as well that can provide guidance by indicating additional monitoring locations, such as those described by Tonkin and others, (2007).

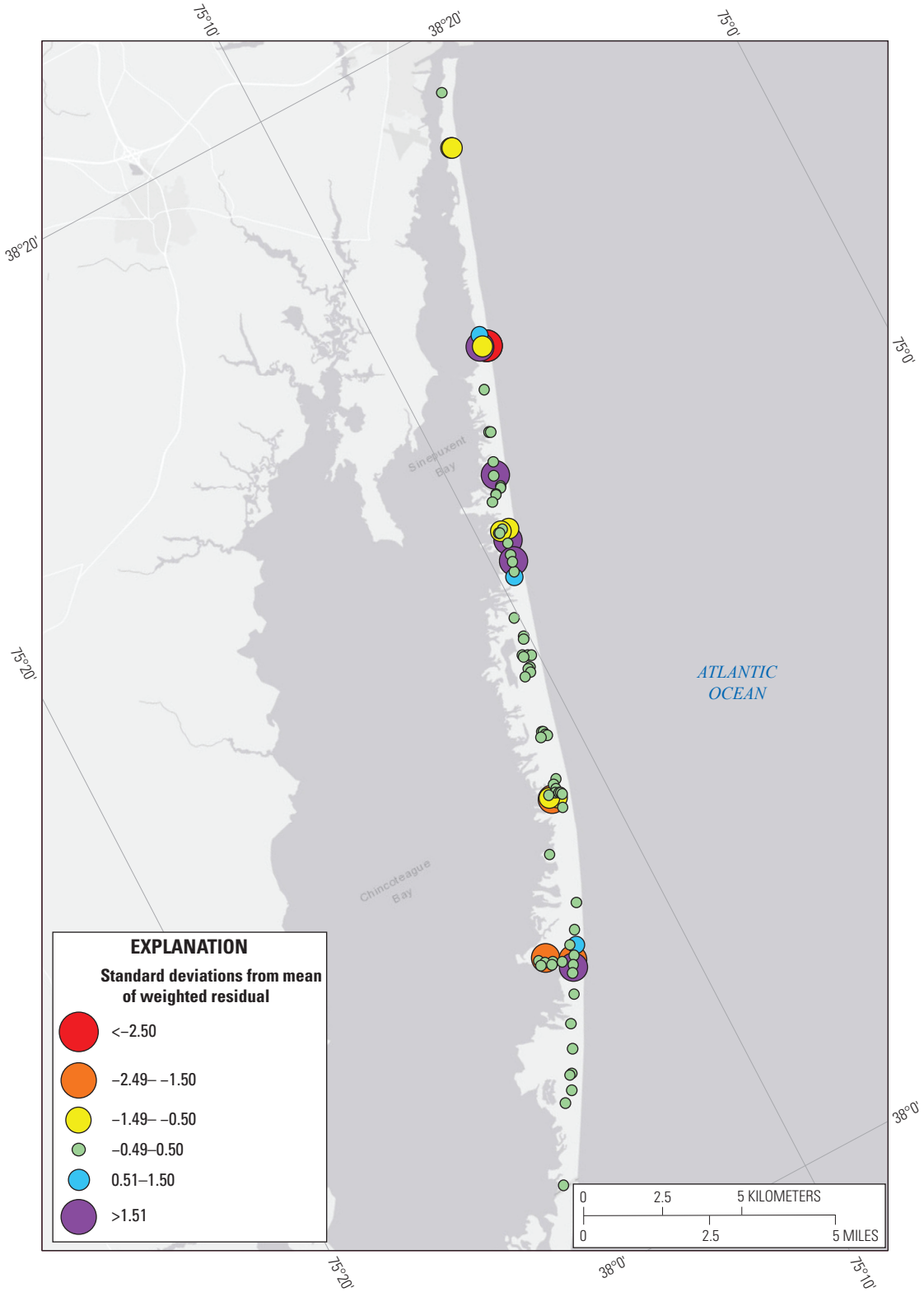

Base from U.S. Geological Survey 1:2,000,000-scale
State boundary digital line graph, Albers Equal-Area Conic Projection
North American Datum of 1983 (NAD 83)

Figure 2.6. Magnitude and distribution of model residuals from observations of water levels in wells and water levels estimated using vegetation type. Residuals are presented in standard deviations from the mean weighted residual. Symbol color indicates residual sign and size indicates relative magnitude. (<, less than; >, greater than)

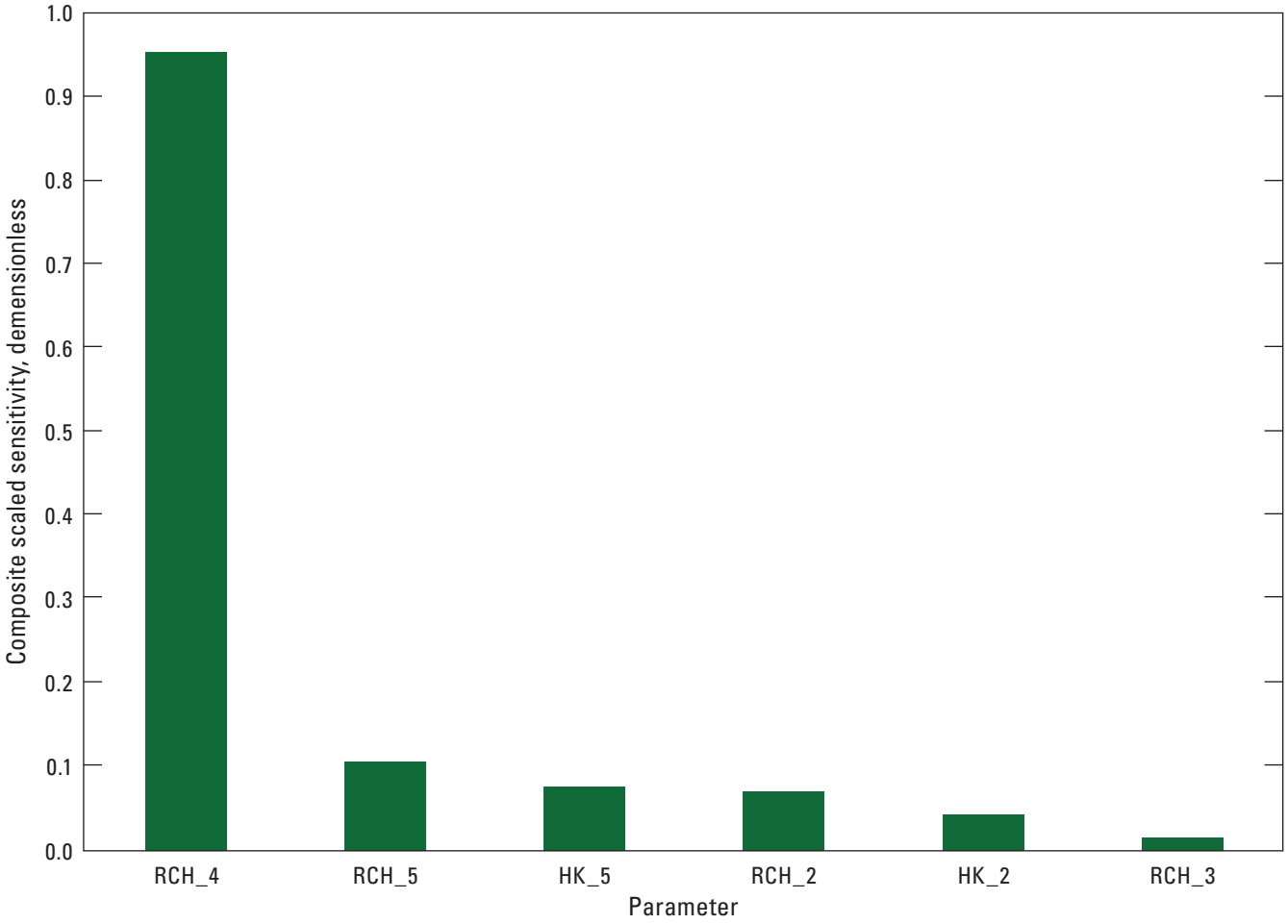

Figure 2.7. Composite scaled sensitivities for the six estimated model parameters. (Parameter identifiers are defined in table 2.2)

Table 2.5. Optimal values, confidence intervals, and coefficients of variation for the estimated model parameters.

[Parameter identifiers are defined in table 2.2. m/d, meters per day; m/y, meters per year]

Parameter identifier	Optimal value	Lower confidence interval limit	Upper confidence interval limit	Coefficient of variation
Horizontal hydraulic conductivity (m/d)				
HK_2	0.499	−0.48	1.47	0.98
HK_5	0.001	−0.01	0.01	4.77
Recharge (m/y)				
RCH_2	1.644	−0.15	3.43	0.55
RCH_3	1.326	−5.16	7.81	2.45
RCH_4	0.990	0.92	1.06	0.04
RCH_5	0.403	0.14	0.67	0.33

Table 2.6. Dimensionless scaled sensitivity (*dss*) values for all water-level observations or estimates for the six model parameters, with maximum absolute values, by parameter and observation type. Water-level observations or estimates in shaded rows have maximum *dss* absolute values of less than 10 percent of the greatest maximum (3.6135) and therefore provide relatively little information in support of model parameter estimates.

[Observation name, text title given to observations in the UCODE_2005 and MODFLOW-NWT input files (names must begin with a letter); observation type, indicator of whether observations are vegetation-based estimates (Veg), or measured (WL); |Max|, maximum absolute value]

Observation name	Observation type	dss values by parameter						|Max|
		HK_2	HK_5	RCH_2	RCH_3	RCH_4	RCH_5	
Veg_101	Veg	0	0.0005	0	0	0	0.0062	**0.0062**
Veg_103	Veg	0	0.0066	0	0	0	0.0885	**0.0885**
Veg_118	Veg	0	−0.0002	0	0.0011	0.0001	0	**0.0011**
Veg_12	Veg	−0.0583	0	0.1067	0.0001	0	0.0029	**0.1067**
Veg_124	Veg	0	0	0.0003	0	0	0.0020	**0.0020**
Veg_125	Veg	0	−0.5263	0.0028	0	3.4593	0.0001	**3.4593**
Veg_128	Veg	0	−0.0008	0.1097	0	0	0	**0.1097**
Veg_129	Veg	0	0.0025	0.0386	0.0375	0	0.0160	**0.0386**
Veg_132	Veg	0	0	0	0	0	0.0051	**0.0051**
Veg_134	Veg	0	−0.0015	0.1097	0	0	0	**0.1097**
Veg_138	Veg	0	−0.0001	0.0002	0	0	0.0018	**0.0018**
Veg_139	Veg	0	−0.0398	0.1096	0	0	0	**0.1096**
Veg_143	Veg	0	0.0002	0.0001	0	0	0.0025	**0.0025**
Veg_146	Veg	0	0.0048	0.1097	0	0	0	**0.1097**
Veg_165	Veg	0	0	0	0	0	0.0006	**0.0006**
Veg_166	Veg	0	0.0002	0	0	0	0.0006	**0.0006**
Veg_167	Veg	0	0.0001	0	0	0	0.0006	**0.0006**
Veg_169	Veg	0	−0.0001	0	0	0	0.0006	**0.0006**
Veg_170	Veg	0	0.0345	0.1095	0	0	0	**0.1095**
Veg_178	Veg	0	0.0104	0.1095	0	0	0.0002	**0.1095**
Veg_181	Veg	0	−0.0404	0	0.0001	3.4783	0	**3.4783**
Veg_183	Veg	0	−0.0577	0.1093	0	0.0038	0	**0.1093**
Veg_189	Veg	0	0.0235	0.1097	0	0	0	**0.1097**
Veg_190	Veg	0	0.0002	0	0	0	0.0006	**0.0006**
Veg_191	Veg	0	0.0055	0.0001	0	0	0.1583	**0.1583**
Veg_193	Veg	0	0.0002	0	0	0	0.0006	**0.0006**
Veg_203	Veg	0	−0.0001	0	0.0011	0	0	**0.0011**
Veg_211	Veg	0	0.0002	0	0	0	0.0006	**0.0006**
Veg_224	Veg	0	0	0	0	0	0.0112	**0.0112**
Veg_244	Veg	0	0	0.0033	0.0001	0	0.0018	**0.0033**
Veg_251	Veg	0	0.0240	0	0	2.6576	0	**2.6576**
Veg_252	Veg	0	0	0.0073	0.0038	0.0001	0.3417	**0.3417**
Veg_261	Veg	0	0	0	0.0011	0	0	**0.0011**
Veg_268	Veg	0	−0.0248	0.0054	0	3.4943	0	**3.4943**
Veg_269	Veg	0	0.0027	0.1097	0	0	0	**0.1097**
Veg_270	Veg	0	−0.0047	0.1093	0	0	0	**0.1093**
Veg_273	Veg	0	−0.3768	0.0001	0	3.6135	0	**3.6135**
Veg_278	Veg	0	−0.0079	0.1095	0	0	0	**0.1095**
Veg_280	Veg	0	0.0002	0.0001	0.0060	0	0.0007	**0.0060**
Veg_282	Veg	0	0.0161	0.1091	0	0.0164	0	**0.1091**
Veg_285	Veg	0	0.0016	0.0011	0.1134	0	0.0589	**0.1134**
Veg_288	Veg	0	0	0.0012	0	0	0	**0.0012**
Veg_292	Veg	0	0	0	0	0	0.0006	**0.0006**

Table 2.6. Dimensionless scaled sensitivity (*dss*) values for all water-level observations or estimates for the six model parameters, with maximum absolute values, by parameter and observation type. Water-level observations or estimates in shaded rows have maximum *dss* absolute values of less than 10 percent of the greatest maximum (3.6135) and therefore provide relatively little information in support of model parameter estimates.—Continued

[Observation name, text title given to observations in the UCODE_2005 and MODFLOW-NWT input files (names must begin with a letter); observation type, indicator of whether observations are vegetation-based estimates (Veg), or measured (WL); |Max|, maximum absolute value]

Observation name	Observation type	dss values by parameter						|Max|
		HK_2	HK_5	RCH_2	RCH_3	RCH_4	RCH_5	
Veg_303	Veg	0	0.0230	0.1095	0	0	0	**0.1095**
Veg_310	Veg	0	0.0117	0.1094	0	0	0	**0.1094**
Veg_313	Veg	0	−0.0001	0	0.0011	0	0	**0.0011**
Veg_314	Veg	0	0.0121	0.1095	0	0	0	**0.1095**
Veg_316	Veg	0	0.1361	0.0044	0	2.8547	0.0046	**2.8547**
Veg_319	Veg	0	−0.0357	0.1096	0	0	0	**0.1096**
Veg_335	Veg	0	−0.0046	0.1097	0	0	0	**0.1097**
Veg_39	Veg	−0.3157	0	0.3233	0	0	0.0531	**0.3233**
Veg_50	Veg	−0.0113	0	0.0001	0	0	0.0825	**0.0825**
Veg_53	Veg	−0.0635	0	0.0807	0	0	0.0348	**0.0807**
Veg_54	Veg	0	0	0	0	0	0.0006	**0.0006**
Veg_57	Veg	0.0003	0	0.0004	0	0	0.0015	**0.0015**
Veg_61	Veg	−0.0004	0	0.0005	0	0.0002	0.1013	**0.1013**
Veg_62	Veg	0	0	0.1097	0	0	0	**0.1097**
Veg_64	Veg	0	0	0	0	0	0.0006	**0.0006**
Veg_66	Veg	0	0	0	0	0	0.0006	**0.0006**
Veg_68	Veg	0	0.0143	0.1093	0	0	0	**0.1093**
Veg_69	Veg	0	−0.0115	0.1096	0	0	0.0003	**0.1096**
Veg_73	Veg	0	−0.0016	0.1097	0	0	0	**0.1097**
Veg_79	Veg	0	0.0088	0.1097	0	0	0	**0.1097**
Veg_83	Veg	0	0.0001	0	0	0	0.0006	**0.0006**
Veg_84	Veg	0	0.0859	0.0022	0	3.1369	0	**3.1369**
Veg_87	Veg	0	−0.0003	0.0017	0	0	0.1247	**0.1247**
Veg_88	Veg	0	0	0	0	0	0.0006	**0.0006**
Veg_92	Veg	0	0	0	0	0	0.0006	**0.0006**
Veg_96	Veg	0	0.0001	0	0	0	0.2027	**0.2027**
Veg_97	Veg	0	0.0001	0	0	0	0.0025	**0.0025**
WOCg101	WL	−0.0319	0	0.0003	0	0	0.2932	**0.2932**
WOCg103	WL	−0.0202	0	0.0002	0	0	0.2618	**0.2618**
WODg27	WL	−0.0609	0	0.0047	0	0	0.4919	**0.4919**
WODg28	WL	−0.0612	0	0.0047	0	0	0.4945	**0.4945**
WODg30	WL	−0.1277	0	0.0060	0	0	0.1533	**0.1533**
WODg32	WL	−0.0640	0	0.0104	0	0	0.0599	**0.0640**
WODg34	WL	0	0.0003	0	0	0	0.0730	**0.0730**
WODg36	WL	0	0	0	0	0	0.0002	**0.0002**
WOEf29	WL	0	0	0	0	0	0.0007	**0.0007**
WOEf31	WL	0	0.0003	0	0	0	0.0002	**0.0003**
WOEf33	WL	0	0	0	0	0	0.0002	**0.0002**
WOEf35	WL	0	0	0	0	0	0.0002	**0.0002**
WOEf37	WL	0	0.0752	0	0	1.3114	0	**1.3114**
WOFf12	WL	0	0	0.0505	0	0	0	**0.0505**
|Max|		**0.3157**	**0.5263**	0.3233	0.1134	3.6135	0.4945	

References Cited

Anderson, M.P., and Woessner, W.W., 1992, Applied groundwater modeling—Simulation of flow and advective transport: San Diego, Calif., Academic Press, 381 p.

Bakker, M., Schaars, F., Hughes, J.D., Langevin, C.D., and Dausman, A.M., 2013, Documentation of the seawater intrusion (SWI2) package for MODFLOW: U.S. Geological Survey Techniques and Methods, book 6, chap. A46, 47 p., accessed on December 15, 2014, at https://doi.org/10.3133/tm6A46.

Banks, W.S.L., Masterson, J.P., and Johnson, C.D., 2012, Well network installation and hydrogeologic data collection, Assateague Island National Seashore, Worcester County, Maryland, 2010: U.S. Geological Survey Scientific Investigations Report 2012–5079, 20 p., accessed on December 15, 2014, at https://doi.org/10.3133/sir20125079.

Cooley, R.L., Konikow, L.F., and Naff, R.L., 1986, Nonlinear-regression groundwater flow modeling of a deep regional aquifer system: Water Resources Research, v. 22, no. 13, p. 1759–1778, accessed on January 15, 2017, at https://doi.org/10.1029/WR022i013p01759.

D'Agnese, F.A., Faunt, C.C., Hill, M.C., and Turner, A.K., 1999, Death Valley regional ground-water flow model calibration using optimal parameter estimation methods and geoscientific information systems: Advances in Water Resources, v. 22, no. 8, p. 777–790, accessed on January 15, 2017, at https://doi.org/10.1016/S0309-1708(98)00053-0.

Dausman, A.M., Doherty, J., Langevin, C.D., and Sukop, M.C., 2010, Quantifying data worth toward reducing predictive uncertainty: Ground Water, v. 48, no. 5, p. 729–740, accessed on January 15, 2017, at https://doi.org/10.1111/j.1745-6584.2010.00679.x.

Dillow, J.J.A., Banks, W.S.L., and Smigaj, M.J., 2002, Groundwater quality and discharge to Chincoteague and Sinepuxent Bays adjacent to Assateague Island National Seashore, Maryland: U.S. Geological Survey Water-Resources Investigations Report 02–4029, 42 p., accessed on December 15, 2014, at https://doi.org/10.3133/wri024029.

Faunt, C.C., Blainey, J.B., Hill, M.C., D'Agnese, F.A., and O'Brien, G.M., 2004, Transient numerical model, Chapter F of Belcher, W.R., ed., Death Valley regional ground-water flow system, Nevada and California—Hydrogeologic framework and transient ground-water flow model: U.S. Geological Survey Scientific Investigations Report 2004–5205, 27 p., accessed on January 15, 2017, at https://doi.org/10.3133/sir20045205.

Fienen, M.N., Doherty, J.E., Hunt, R.J., and Reeves, H.W., 2010, Using prediction uncertainty analysis to design hydrologic monitoring networks—example applications from the Great Lakes Water Availability Pilot Project: U.S. Geological Survey Scientific Investigations Report 2010–5159, 44 p., accessed on January 15, 2017, at https://doi.org/10.3133/sir20105159.

Ghyben, W.B., 1889, Nota in verband met de voorgenomen putboring nabij Amsterdam: Tijdschrift van het Koninklijk Instituut van Ingenieurs, p. 8–22.

Harbaugh, A.W., Banta, E.R., Hill, M.C., and McDonald, M.G., 2000, MODFLOW-2000, the U.S. Geological Survey modular ground-water model—User guideto modularization concepts and the ground-water flow process: U.S. Geological Survey Open-File Report 00–92, 121 p., accessed on January 15, 2017, at https://doi.org/10.3133/ofr200092.

Harbaugh, A.W., 2005, MODFLOW—2005, the U.S. Geological Survey modular ground-water model—The ground-water flow process: U.S. Geological Survey Techniques and Methods, book 6, chap. A16, 17 p., accessed on December 15, 2015, at https://doi.org/10.3133/tm6A16.

Herzberg, A., 1901, Die Wasserversorgung einiger Nordseebäüüder: Journal für Gasbeleuchtung und Wasserversorgung, v. 44, p. 815–819.

Hill, M.C., 1998, Methods and guidelines for effective model calibration: U.S. Geological Survey Water-Resources Investigations Report 98–4005, 90 p., accessed on January 15, 2017, at https://doi.org/10.3133/wri984005.

Hill, M.C., Banta, E.R., Harbaugh, A.W., and Anderman, E.R., 2000, MODFLOW-2000, the U.S. Geological Survey modular ground-water model—User guide to the observation, sensitivity, and parameter-estimation processes and three post-processing programs: U.S. Geological Survey Open-File Report 00–184, 209 p., accessed on January 15, 2017, at https://doi.org/10.3133/ofr00184.

Hill, M.C., and Tiedeman, C.R., 2007, Effective groundwater model calibration—With analysis of data, sensitivities, predictions, and uncertainty: Hoboken, N.J., John Wiley & Sons, 455 p., also available at https://doi.org/10.1002/0470041080.

Krantz, D.E., 2009, A hydrogeomorphic map of Assateague Island National Seashore, Maryland and Virginia, accessed on February 29, 2016, at http://www.eeescience.utoledo.edu/Faculty/Krantz/download_files/NPS_Report.Assateague_Hydrogeomorphology.pdf.

Langevin, C.D., Thorne, D.T., Jr., Dausman, A.M., Sukop, M.C., and Gou, W., 2008, SEAWAT Version 4—A computer program for simulation of multi-species solute and heat transport: U.S. Geological Survey Techniques and Methods, book 6, chap. A22, 39 p., accessed on December 15, 2015, at https://doi.org/10.3133/tm6A22.

Masterson, J.P., Fienen, M.N., Gesch, D.B., and Carlson, C.S., 2013, Development of a numerical model to simulate groundwater flow in the shallow aquifer system of Assateague Island, Maryland and Virginia: U.S. Geological Survey Open-File Report 2013–1111, 34 p., accessed on December 15, 2014, at https://doi.org/10.3133/ofr20131111.

Niswonger, R.G., Panday, S., and Ibaraki, M., 2011, MODFLOW-NWT, A Newton formulation for MODFLOW-2005: U.S. Geological Survey Techniques and Methods 6–A37, 44 p., accessed on January 15, 2017, at https://doi.org/10.3133/tm6A37.

Niswonger, R.G., Prudic, D.E., and Regan, R.S., 2006, Documentation of the Unsaturated-Zone Flow (UZF1) Package for modeling unsaturated flow between the land surface and the water table with MODFLOW-2005: U.S. Geological Survey Techniques and Methods 6–A19, 74 p., accessed on January 15, 2017, at https://doi.org/10.3133/tm6A19.

Poeter, E.P., and Hill, M.C., 1997, Inverse models—A necessary next step in ground-water modeling: Ground Water, v. 35, no. 2, p. 250–260, also available at https://doi.org/10.1111/j.1745-6584.1997.tb00082.x.

Poeter, E.P., Hill, M.C., Banta, E.R., Mehl, S., and Christensen, S., 2005, UCODE_2005 and six other computer codes for universal sensitivity analysis, calibration, and uncertainty evaluation: U.S. Geological Survey Techniques and Methods 6–A11, 283 p., accessed on January 15, 2017, at https://doi.org/10.3133/wri984080.

Poeter, E.P., Hill, M.C., Lu, D., Tiedeman, C.R., and Mehl, S., 2014, UCODE_2014, with new capabilities to define parameters unique to predictions, calculate weights using simulated values, estimate parameters with SVD, evaluate uncertainty with MCMC, and more: Integrated Groundwater Modeling Center GWMI Report 2014–02, 172 p.

San Juan, C.A., Belcher, W.R., Laczniak, R.J., and Putnam, H.M., 2004, Hydrologic components for model development, Chapter C of Belcher, W.R., ed., Death Valley regional ground-water flow system, Nevada and California—Hydrogeologic framework and transient ground-water flow model: U.S. Geological Survey Scientific Investigations Report 2004–5205, 136 p., accessed on January 15, 2017, at https://doi.org/10.3133/sir20045205.

Sanford, W.E., Plummer, L.N., McAda, D.P., Bexfield, L.M., and Anderholm, S.K., 2004, Hydrochemical tracers in the middle Rio Grande Basin, USA—2. Calibration of a groundwater-flow model: Hydrogeology Journal, v. 12, no. 4, p. 389–407, accessed on January 15, 2017, at https://doi.org/10.1007/s10040-004-0326-4.

Sneddon, L., Menke, J., Berdine, A., Largay, E., and Gawler, S., 2017, Vegetation classification and mapping of Assateague Island National Seashore: National Park Service, Natural Resource Report NPS/ASIS/NRR—2017/1422, accessed on June 28, 2021, at https://irma.nps.gov/DataStore/DownloadFile/575367.

Tonkin, M.J., Tiedeman, C.R., Ely, D.M., and Hill, M.C., 2007, OPR-PPR, a computer program for assessing data importance to model predictions using linear statistics: U.S. Geological Survey Techniques and Methods TM–6E2, 115 p., accessed on January 15, 2017, at https://doi.org/10.3133/tm6E2.

Walter, D.A., McCobb, T.D., Masterson, J.P., and Fienen, M.N., 2016, Potential effects of sea-level rise on the depth to saturated sediments of the Sagamore and Monomoy flow lenses on Cape Cod, Massachusetts: U.S. Geological Survey Scientific Investigations Report 2016–5058, 55 p., accessed on January 15, 2016, at https://doi.org/10.3133/sir20165058.

Zheng, C., and Wang, P.P., 1999, MT3DMS—A modular three-dimensional multispecies transport model for simulation of advection, dispersion, and chemical reactions of contaminants in groundwater systems—Documentation and user's guide: U.S. Army Corps of Engineers Contract Report SEDRP-99–1, 169 p.

For more information, contact:
Director, Maryland-Delaware-D.C. Water Science Center
U.S. Geological Survey
5522 Research Park Drive
Catonsville, MD 21228

or visit our website at
https://www.usgs.gov/centers/md-de-dc-water/

Publishing support provided by the
West Trenton Publishing Service Center.

ISSN 2328-0328 (online)
https://doi.org/10.3133/sir20205104